STM JOURNALS

Journal of
Polymer & Composites

ISSN: 2321-2810 (Online)
ISSN: 2321-8525 (Print)
Volume 13, Special Issue 2, 2025
DOI (Journal): 10.37591/JoPC

https://journals.stmjournals.com/jopc

Review JoPC

Aerodynamic Analysis of Foliage Stimulated Airfoil Design for Enhanced Strength with Carbon Fibre-reinforced Polymer

S.L. Pradeep Kumar[1,*], J. Suguna Yuvasri[2], B. Priyadharsani[3], Shaik Athik Ahamad[4], T. Karthik[5]

Abstract

Ever since the beginning of aviation, there has been an unwavering desire to improve airfoil design in order to improve aircraft performance. This insatiable desire for improvement has driven innumerable aerodynamicists to create a diverse range of revolutionary airfoils. This research investigates a revolutionary method to airfoil design, inspired by the complicated structures and aerodynamic qualities of natural leaves. Using biomimicry, the project seeks to increase the performance and efficiency of standard airfoil forms by modifying and incorporating leaf-like elements. The leaf's coordinates are retrieved using image processing techniques and then loaded into the ANSYs design modeller. Computational fluid dynamics (CFD) simulations are performed using ANSYs Fluent to investigate the complex fluid motion of leaf-based airfoils made of Carbon Fibre Reinforced Polymer (CFRP). Velocity, pressure, and turbulence contours are presented for various leaves, and metrics such as lift coefficient, drag coefficient, and lift-to-drag ratio are calculated at different angles of attack. The comparison of the leaves shows promising improvements in lift-to-drag ratio and performance, implying possible applications in aircraft and wind turbine technology. The results conclude with implications of this bio-inspired CFRP airfoil has optimizing aerodynamic performance, reducing the impact of non-Newtonian fluid boundary layer effects and minimizing the flow separation with greater shear strength.

Keywords: Carbon fibre-reinforced polymer**,** Non-newtonian fluid characteristics, foliage airfoil, flow visualization, turbulence

INTRODUCTION

Airfoil

An airfoil, also known as an airfoil, is a carefully designed shape that plays a pivotal role in the generation of lift and control of aerodynamic forces when an object moves through a fluid, such as air. The term "airfoil" typically refers to the cross-sectional shape of an object, like an aircraft wing, that interacts with the fluid [1]. Airfoils are essential components in various applications, most notably in aviation, where they form the basis of aircraft wings, but they are also utilized in wind turbines, hydrofoils, and even in the design of certain automotive components [4]. This research not only helps in optimizing the aerodynamic performance of airfoils but also has broader implications. Understanding the aerodynamic effects of different airfoil shapes, pressures, and velocity distributions, much like how leaves are influenced by their shapes and surface

***Author for Correspondence**
S.L. Pradeep Kumar
Email: pradeepzero1991@gmail.com

[1]Assistant Professor, Department of Aeronautical Engineering, KIT-Kalaignarkarunanidhi Institute of Technology, Coimbatore, Tamil Nadu, India
[2–5]Students, Department of Aeronautical Engineering, KIT-Kalaignarkarunanidhi Institute of Technology, Coimbatore, Tamil Nadu, India

Received Date: July 02, 2024
Accepted Date: September 27, 2024
Published Date: February 21, 2025

Citation: S.L. Pradeep Kumar, J. Suguna Yuvasri, B. Priyadharsani, Shaik Athik Ahamad, T. Karthik. Aerodynamic Analysis of Foliage Stimulated Airfoil Design for Enhanced Strength with Carbon Fibre-reinforced Polymer. 2025; 13(Special Issue 2): S560–S616p.

characteristics, is essential. This knowledge is especially valuable in the field of airfoil design, where efficiency and performance are key factors [2]. In essence, this research contributes to a deeper understanding of the intricate aerodynamic principles that underlie airfoil performance and has the potential to significantly enhance their design and selection for various applications [2].

Nomenclature

To describe and analyze airfoils accurately, specific nomenclature is used to denote their key features

1. *Chord Line:* This is a straight line that connects the leading edge (the front) and the trailing edge (the rear) of the airfoil [3]. The length of this chord line is referred to as the chord length, an important parameter in airfoil design.
2. *Leading Edge:* The leading edge is the foremost part of the airfoil where it first encounters the oncoming airflow. It plays a crucial role in the initial interaction between the airfoil and the fluid [7].
3. *Trailing Edge:* The trailing edge is located at the rear of the airfoil and marks the endpoint of both upper and lower surfaces. It signifies the final point where the fluid interacts with the airfoil [7].
4. *Upper Surface:* The upper surface of the airfoil is typically curved and longer than the lower surface. It is the primary region where lift is generated [4].
5. *Lower Surface:* In contrast to the upper surface, the lower surface of the airfoil is flatter and situated underneath [4]. It generally exhibits a smaller curvature compared to the upper surface.
6. *Camber:* Camber refers to the curvature of the upper surface of the airfoil. It can be either positively cambered (having an upward curve) or negatively cambered (having a downward curve). Camber significantly affects the airfoil's lift characteristics [3].
7. *Thickness:* The thickness of an airfoil is the measurement of the distance between its upper and lower surfaces. Thickness varies along the length of the chord, influencing the airfoil's drag and structural properties [1].

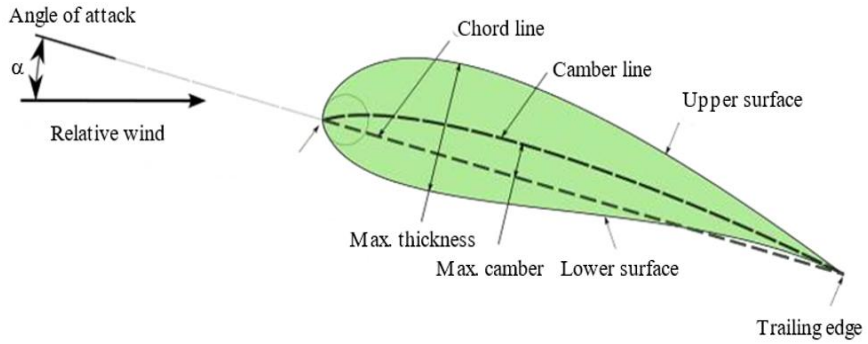

Figure 1. Nomenclature of Airfoil.

Figure 1 shows the leading edge, trailing edge, upper surface, lower surface, chord line, camber line, etc., of an airfoil.

Characteristics

Airfoils exhibit several key characteristics that are crucial for their operation

1. *Lift Generation:* The primary function of an airfoil is to generate lift. This is achieved by creating a difference in pressure between the upper and lower surfaces. The curved upper surface results in lower pressure, while the lower surface generates higher pressure, producing lift [4].
2. *Drag Production:* While lift is generated, airfoils also produce drag, which is the aerodynamic resistance to forward motion caused by the interaction of the fluid with the airfoil's surfaces [4].
3. *Angle of Attack (AOA):* The angle at which the airfoil meets the oncoming airflow is known as the angle of attack. The AOA significantly influences the airfoil's lift and drag production. Pilots can adjust the AOA to control an aircraft's lift and descent [5].

4. *Aspect Ratio:* The aspect ratio is the ratio of the wingspan to the mean chord length of the airfoil. A higher aspect ratio is associated with more efficient wings, reducing induced drag.

The various types of airfoil geometries along with their geometrical description and characteristics are given in Table 1.

Table 1 Types of airfoil.

Types of Airfoil Geometry	Geometrical Description	Geometrical Characteristics
Symmetric airfoils	Has zero camber, upper and lower surfaces are mirror images	* Lift at zero degrees of attack *Used in some aerobatic and high-speed aircraft
Cambered airfoils	Have curvature along the upper surface, which can be positively or negatively cambered	*Lift at various angles of attack *Used in general aviation and commercial airliners
Unsymmetric airfoils	Lack symmetry about the chord line, upper and lower surfaces are not mirror images	*Asymmetric lift generation *Used in rotor blades on helicopters and rotary-wing aircraft

LITERATURE REVIEW

This study examines the aerodynamic performance of a new horizontal axis wind turbine airfoil design that was influenced by the shape of a banana leaf midrib. The innovative airfoil was created to maximize wind energy conversion efficiency and capitalize on the advantages of natural biomimicry. A horizontal axis wind tunnel was used for several studies to evaluate its performance. The results demonstrated the potential of the banana leaf midrib-inspired airfoil to enhance the energy capture capabilities of wind turbines. This paper presents the findings of these experiments, offering insights into the aerodynamic properties and potential advantages of this innovative design and motivates us to use natural things as inspiration [1].

Engineers and researchers have long looked to nature for inspiration when trying to improve the performance and efficiency of airplanes, particularly when designing more efficient airfoils. In recent years, bio-inspired airfoils have become more and more popular. These airfoils derive their design ideas from the aerodynamic properties of birds, insects, and marine organisms. This essay examines the idea of bio-inspired airfoils, their design ideas, and the possible improvements in aerodynamic efficiency, noise reduction, and environmental sustainability that they may provide. Bio-inspired airfoils have the potential to transform the aviation sector and contribute to a more sustainable future by mimicking the clever designs [2].

From wind energy generation to aviation, the aerodynamic performance of airfoils is critical to many applications. Many studies have been carried out in an effort to improve the performance of airfoils by altering their surface over time. This article offers a thorough examination of research on the aerodynamic behavior of airfoils with altered surfaces. An overview of the major conclusions, approaches, and developments in the subject of airfoil surface alterations and their effects on performance is the main goal of this paper [3].

The design and aerodynamic performance of airfoils have changed dramatically throughout time due to developments in testing, materials, and computer approaches. For the continuous development of wind turbines, airplanes, and other aerospace applications that are more ecologically friendly, research in this area is still essential. Airfoil design will continue to be shaped in the future by interdisciplinary cooperation and using cutting-edge technologies [4].

A comparison between NACA 4412 and NACA 0012 airfoils demonstrates their unique qualities and applicability in fields. With its symmetrical design, NACA 0012, which is appropriate for small and soaring UAVs, offers reduced drag and predictable stall behavior. The cambered shape of NACA 4412

offers increased lift capacity, which makes it more suitable for wind turbines and light aircraft. The selection of an appropriate airfoil for a given application in aeronautical engineering and beyond is crucial, as it is ultimately determined by specific design requirements, performance, and Reynolds number considerations [5].

In order to guarantee aircraft performance and safety, nonlinear aeroelastic behavior in damped elastic airfoil systems must be studied. The capacity to precisely model and forecast the nonlinear response of such systems is becoming more and more important as aircraft design advances. Aeroelasticity, structural mechanics, and aerodynamics experts working together to drive progress in this subject will ultimately shape aviation's future by enabling the construction of safer, more flexible, and more efficient aircraft [6].

Aerodynamics' study of unstable lift for high-amplitude airfoils is essential and has broad applications in wind energy, aeronautics, and other domains. Significant progress has been made by researchers in the areas of theoretical frameworks, experimental methods, and real-world applications. To address the remaining issues and improve our knowledge of unstable lift phenomena for high- amplitude airfoils, more study is necessary. This will eventually result in safer and more effective aerodynamic systems [7].

Numerous factors, such as airfoil geometry, Reynolds number, angle of attack, Mach number, surface roughness, and flow control methods, affect the S833 airfoil's aerodynamic performance. It's critical to comprehend how these factors combine to maximize the performance of the S833 airfoil in applications like small wind turbines and unmanned aerial vehicles (UAVs). To further improve our view of these factors, more research is required [8].

Aerospace engineering and related fields rely heavily on the design and analysis of airfoils. Our grasp of and capacity to create highly customized and efficient airfoils has greatly increased because to the study of aerodynamics of airfoils, computational approaches, and optimization techniques. We may anticipate even more ground-breaking discoveries that will improve the efficiency and sustainability of airfoil-based technology as this field of study continues to advance [9].

The investigation of form parametrization techniques for optimizing airfoils is an essential facet of aerodynamics and aerospace engineering. Though the discipline is fast evolving with the introduction of new techniques like genetic algorithms, spline-based methods, and deep learning approaches, traditional methods like NACA profiles and Bézier curves are still helpful. The choice of parametrization technique should be in line with the particular objectives of the airfoil optimization project, taking into account variables like computing capacity, shape complexity, and intended aerodynamic properties. It is conceivable that further studies in this area will provide creative answers to problems with airfoil optimization and design [10].

An essential component of wind turbine design and the wind energy sector overall is airfoil optimization. Conventional optimization methods such as CFD simulations and genetic algorithms are still quite useful. But the combination of advances in manufacturing technology and artificial Intelligence/machine learning techniques has created new and intriguing opportunities for the creation of highly specialized and efficient airfoil designs. With the increasing significance of wind energy, scientists will probably concentrate on customizing airfoils for certain operating environments, increasing the effectiveness and economy of wind turbines. The dynamic and inventive nature of this field of study will continue to reflect the changing demands for new types and modifications of airfoil in the wind energy sector [11].

Aerospace engineering is a dynamic and developing field, and multi-level CFD-based airfoil shape optimization with automated low-fidelity model selection is one of them. Scholars are tackling the problems of accuracy and processing cost by creating novel algorithms that choose the best fidelity

level for assessing airfoil designs on the fly. These techniques facilitate effective design space exploration, which eventually improves airfoil performance for a range of applications. Multi-level optimization techniques will become more important in determining the direction of airfoil design as technology and computer power grow [12].

One important area of wind energy research is the computational fluid dynamics (CFD) analysis of wind turbine airfoils at different angles of attack. Optimizing wind turbine performance and efficiency necessitates a thorough understanding of airfoil behavior under various wind conditions. CFD simulations will become more important in the design and study of wind turbine airfoils as computational tools and methodologies advance, which will help to increase the production of sustainable energy [13].

Using computational fluid dynamics (CFD) to compare the aerodynamic performances of airfoils from various families is a crucial field of research for wind turbine, aeroplane, and other application efficiency optimization. CFD simulations are becoming more important in airfoil design and analysis as computing power increases. Precise comparisons offer perspectives to designers, aiding in the creation of high-performing airfoils for a range of uses [14].

To inform airfoil design and analysis, comparative investigations of XFOIL and CFD performance estimates for high lift low Reynolds number airfoils are crucial. Although XFOIL is a useful tool for exploratory studies, CFD simulations provide a more thorough understanding of the flow physics. To assure dependable results and support the creation of effective and high-performance airfoils for a variety of aeronautical applications, researchers must consider the advantages and disadvantages of each tool and validate the predictions [15].

Turbulence-Interaction When it comes to aviation noise reduction, noise is a major concern. Important elements impacting TIN have been found to be the airfoil design and the angle of attack. Tin levels can be considerably reduced by utilizing airfoil designs intended for noise reduction and lowering AOA during take-off and landing. The combined effects of AOA and changes to the form of the airfoil offer encouraging directions for further study in the quest for quieter aircraft. Targeting TIN, noise reduction technology is always improving to make flying less harmful to the environment and less disturbing to the communities that near airports [16].

The design of airfoils for turbulent flows over unstructured grids has advanced significantly in the last several years. More effective and high-performing airfoil designs have been made possible by the combination of unstructured grids, sophisticated turbulence modelling, high-performance computation, optimization methods, and transition/separation control. This field of research will continue to be a hub for innovation and development as the wind energy and aerospace sectors strive for ever-higher levels of efficiency and performance. The process of designing airfoils may be sped up and our understanding of turbulent flows may be further enhanced by the incorporation of AI and machine learning techniques [17].

Aerodynamic performance can be improved in aviation by the use of tension-morphing airfoils, which show great potential. Many benefits are available when tensegrity principles, cutting-edge materials, and complex control techniques are combined. These benefits include improved efficiency, load management, and flexibility. Notwithstanding current obstacles, research in this area has the potential to completely transform the aerospace sector by giving aeroplanes the capacity to instantly adjust and optimize their shape, increasing safety and fuel efficiency which is more essential to be considered at this stage of growth and inventions [18].

The design of morphing wings that can adjust to changing flight conditions requires a strong emphasis on parametric optimization. It is essential for enhancing the performance, efficiency, and adaptability of aircraft. Future aircraft design could benefit from further optimizing morphing structures through the

continuous development of parametric optimization techniques and the integration of cutting-edge technology, which have the potential to completely transform the aerospace industry. The fusion of established optimization techniques with cutting-edge technologies opens the door to more advanced, effective, and versatile morphing wings that perform well in a range of operating settings [19].

The aviation and aerospace industries continue to have serious concerns about stall-induced noise from airfoils close to stall conditions. Developing practical noise reduction techniques requires an understanding of the principles driving this kind of noise. An overview of the main mechanisms involved, such as the function of leading-edge vortices, flow separation, and acoustic radiation, has been given by this survey of the literature. By combining computational and experimental methods, this field's ongoing study will help create aircraft designs that are greener and quieter, which will eventually lessen the negative effects that airfoil noise near stall conditions have on the environment and nearby communities [20].

The intricate relationship between aerodynamics and acoustics in transitional airfoils with feedback-loop interactions has been better understood because to recent developments in this field of study. Advanced experimental methods, computer simulations, and theoretical models combined have produced insightful results that help guide the creation of quieter and more effective airfoil designs. Advances in aero-acoustic engineering research are expected to amplify practical applications, particularly in aviation, automotive, and wind energy. Interdisciplinary collaboration will play a key role, fostering solutions to address noise-related challenges across diverse sectors and enable the future for more innovations [21].

Computed fluid dynamics (CFD) has been a vital tool in the study of the intricate aerodynamics of "Diamond Back" wings. CFD simulations help to understand complex fluid dynamics, which contributes to advancements in a variety of fields ranging from aeronautics to other fields. Aerospace technology cannot progress until it can study spanwise differences in aerodynamic properties and maximize wing performance. Numerical simulation will remain an indispensable tool for the continued investigation of novel wing designs such as the "Diamond Back" if computer resources and modelling approaches are developed further [22].

Which airfoil profile—NACA 0015 or NACA 4415—is best based on the requirements of the application. Since every airfoil has pros and cons, they can be used for a variety of tasks. The airfoils experienced a significant loss of lift between angles of attack at 10 and 15 degrees, where flow separation occurred on the suction side, leading to stall. To maximize the performance of their designs and engineering projects, designers and engineers need to pay close attention to these airfoils' aerodynamic properties. [23].

The importance of researching various airfoil shapes in aeronautics and aerospace engineering has been brought to light by this review of the literature. Over time, the design and analysis of airfoils have changed, having an impact on a variety of applications such as wind turbines, UAVs, and aeroplanes. Ongoing study will surely help optimize the design of airfoils and boost aeronautical and renewable energy technologies if it keeps progressing [24].

An important development in aviation design is the creation of a new family of airfoils specifically suited for wings with variable camber. Under a variety of operating situations, these airfoils have the ability to increase aerodynamic efficiency, decrease fuel consumption, and improve aircraft performance. As this field of study develops, it is evident that these advancements have the power to influence aviation's future by increasing aircraft's environmental friendliness, efficiency, and adaptability [25].

There is a great deal of interest under and research into the behavior of the NACA 4412 airfoil in ground effect. Numerical simulations combined with experimental research have yielded important

insights into this airfoil's intricate near-ground aerodynamics. The design and operation of vehicles that operate near surfaces require an understanding of these concepts, which present potential for innovation and optimization in the fields of aerospace and marine engineering. To solve the unanswered concerns in this subject, more study is required [26].

In aerospace engineering, the impact of recurring variations in the angle of attack on airfoil performance is a crucial subject. It is crucial to comprehend how airfoils react to changes in angle of attack while building effective and secure aircraft. The historical background, airfoil performance measurements, stall behavior, dynamic stall phenomena, and the contribution of cutting-edge research techniques to the advancement of our understanding of this intricate topic are all highlighted in this overview of the literature. Future studies in this sector will aid in the creation of more dependable airfoil designs for a range of aviation applications [27].

Enhancing aircraft and UAV performance and safety requires a complicated and varied research area the study of airfoil section properties at high angles of attack. Scholars are still examining how sophisticated flow control techniques, control surfaces, and airfoil shapes affect the performance of airfoils under these difficult circumstances. Our knowledge of airfoil performance at high angles of attack has greatly expanded thanks to developments in experimental testing, computational techniques, and numerical simulations. These developments have real-world implications for the aerospace and aviation industries. More studies in this area should result in aircraft designs that are safer and more effective [28].

Within a narrow angle of attack range, laminar, transitional, and turbulent flow regimes interact intricately in low Reynolds number airfoil aerodynamics. Although laminar flow performs well and has little drag, it is prone to flow separation. As the angle of attack increases, the flow becomes turbulent and occasionally separates and reattaches. Higher angles of attack are more likely to produce turbulent flow, which increases lift but increases drag. When designing and improving airfoil profiles for purposes, researchers and engineers dealing with low Reynolds number airfoils need to take these flow patterns into account. To maximize the benefits of flow separation and turbulence reduction and achieve the intended aerodynamic performance, precise management of variables such as airfoil geometry, Reynolds number, and surface roughness is necessary. Furthermore, current research in this area seeks to create approaches to enhance the control and efficiency of low Reynolds number airfoils [29].

The numerical optimization of airfoil design evaluation is a dynamic and developing area of aerodynamics. The historical background, numerical optimization techniques, objective functions, design variables, the function of CFD, uncertainty, resilient optimization, and case studies demonstrating the effectiveness of these methods are all highlighted in this overview of the literature. The use of numerical optimization in airfoil design is anticipated to become even more sophisticated and efficient as technology and processing power continue to grow, opening up new avenues for enhanced aerodynamic performance [30].

AERODYNAMIC PERFORMANCE PARAMETERS OF AN AIRFOIL

Lift

1. Lift is generated due to the pressure differential between the upper and lower surfaces of the airfoil. According to Bernoulli's principle, the air above the airfoil's curved upper surface has lower pressure compared to the air below, creating an upward force [2].
2. The lift coefficient (C_l) is a dimensionless number used to quantify the lift an airfoil generates. It is influenced by the angle of attack (AOA) and is typically depicted on a lift curve. C_{lmax} is the maximum lift coefficient an airfoil can achieve before stall [2].
3. To maximize lift, airfoil design factors such as camber, thickness distribution, and aspect ratio are crucial. These factors influence how smoothly the airfoil can generate lift, particularly at varying angles of attack [6, 8].

Drag

Drag is divided into two primary components profile drag and induced drag [6, 8].

1. *Profile Drag:* Profile drag, also known as parasitic drag, is associated with the friction and pressure differences along the surfaces of the airfoil. Engineers aim to minimize profile drag by improving surface finish, maintaining laminar flow, and reducing surface roughness [6].
2. *Induced Drag:* Induced drag is a consequence of generating lift. It occurs as vortices form at the wingtips, particularly at high angles of attack or low aspect ratios. Increasing the wingspan (higher aspect ratio) is a common strategy to reduce induced drag [5].

Wake Region

1. The wake region is the disturbed flow of air behind the airfoil. It is characterized by turbulent, low-velocity air. Turbulence in the wake leads to energy loss, affecting the efficiency and performance of the airfoil [26].
2. Airfoil design aims to minimize wake region disturbances. Winglet design, for example, reduces the strength of wingtip vortices and, consequently, the size of the wake, which can lead to improved aerodynamic efficiency.[8]

Stagnation Point

1. The stagnation point is located at the leading edge of the airfoil. It is the point where the fluid comes to a complete stop before splitting into the upper and lower surface flows [3].
2. This point is of paramount importance because it marks the region of maximum pressure on the airfoil. Pressure decreases as air flows over the upper and lower surfaces, ultimately creating lift [3].
3. Engineers use the concept of the stagnation point to determine lift, perform CFD (computational fluid dynamics) simulations, and optimize airfoil designs [4].

Boundary Layer Interactions

1. The boundary layer is a thin layer of air adjacent to the airfoil's surface. It is critical in airfoil performance as it influences both lift and drag [23].
2. Turbulent boundary layers, especially those that separate from the airfoil's surface, can lead to a significant increase in drag and a reduction in lift [8].
3. Engineers employ various techniques to control boundary layer interactions, such as laminar flow control, vortex generators, and active flow control systems. These methods are used to maintain attached, more efficient boundary layers and minimize turbulence and separation [8].

The aerodynamic performance parameters of an airfoil encompass crucial factors influencing its efficiency. Lift and drag coefficients, critical angle of attack, stall characteristics, and pressure distribution are key parameters. Lift coefficient determines the lift generated, while drag coefficient influences aerodynamic resistance. The critical angle of attack denotes maximum lift before stall. Stall characteristics involve abrupt lift loss. Pressure distribution on the airfoil's surfaces affects overall performance. These parameters are fundamental in airfoil design, ensuring optimal lift, minimized drag, and stable aerodynamic behavior across various operating conditions. Comprehensive understanding and control of these parameters are vital for efficient aircraft and wind turbine design [4].

LEAF STRUCTURE

The structure of a leaf is not inherently designed for aerodynamics, but it does have certain features and characteristics that can be related to aerodynamic principles. Leaves have evolved to capture sunlight for photosynthesis rather than for aerodynamic purposes, but we can still draw some parallels. Here is an overview of the structure of a leaf and how it relates to aerodynamics [7].

1. *Leaf Shape:* Leaves come in a wide variety of shapes, and some of these shapes can resemble airfoils to some extent. For example, certain leaves have a curved upper surface and a flatter lower surface, which can create lift, similar to the way an airfoil generates lift [10].
2. *Camber:* The curvature of a leaf, known as camber, can be compared to the camber of an airfoil. Camber creates pressure differences between the upper and lower surfaces of the leaf, potentially contributing to lift, though not as effectively as an engineered airfoil [31, 32].
3. *Surface Texture:* The surface texture of a leaf is typically not smooth, and it may have irregularities like tiny hairs or wax coatings. These features can influence the flow of air over the leaf's surface and may affect drag, much like the surface roughness on an engineered airfoil can impact its performance [26].
4. *Thickness Distribution:* Leaves have a varying thickness from the midrib to the edges. This thickness distribution can influence how air flows around the leaf and creates lift, similar to how the thickness distribution on an airfoil affects its aerodynamic properties [26].
5. *Stomata and Pores:* Leaves have small openings called stomata and pores on their surfaces. These structures can create localized turbulence and influence the boundary layer, which can impact the overall aerodynamic performance of the leaf, albeit in a very different way than an airfoil [21].
6. *Flexibility:* Leaves are flexible and can change their orientation and shape in response to environmental conditions. This adaptability is unlike engineered airfoils, which typically maintain a fixed shape [19].
7. *Natural Imperfections:* Leaves are not designed for optimal aerodynamic performance, and they have natural imperfections that can disrupt airflow. These imperfections can lead to turbulence and decreased aerodynamic efficiency compared to a purpose-built airfoil [15].

It is crucial to acknowledge that while there exist certain loose parallels between the structural features of leaves and aerodynamics, leaves fundamentally serve biological functions, notably photosynthesis and transpiration. In contrast, engineered airfoils undergo precision design, adhering to specific aerodynamic principles meticulously crafted to maximize lift and minimize drag. These airfoils find applications in diverse fields, including aircraft wings and wind turbine blades [22].

In essence, though there may be loose associations between leaf structure and aerodynamics concerning aspects like shape, camber, and surface characteristics, leaves lack the optimization for aerodynamic performance that is characteristic of engineered airfoils. The differences in scale, intended purpose, and evolutionary pressures render the aerodynamic characteristics of leaves and engineered airfoils distinctly unique [2].

In a deeper context, we should understand that the existing models of inventions has gone through several phases of modifications periodically from time to time. These modifications were mostly inspired by nature. This takes our study to the next level and gave us inspiration to do this from naturally obtained leaves of trees [1].

MODELLING OF AN AIRFOIL

Leaves chosen for analysis

Leaves are chosen for analysis based on their shape, which is similar to an airfoil. The leaves chosen are Javaplum leaf, Sapota leaf, Custard apple leaf, Ixora plant leaf, Mango leaf, Pumpkin ash leaf, Antiaris toxicaria (Upas) leaf, Curry leaf, and Adadhoda leaf. The list of leaves chosen are shown in Table 2.

Table 2. Leaves chosen for analysis

S.N.	Leaf	Scientific name of plant	Image
1	Javaplum	Syzygium cumini	
2	Sapota	Manilkara zapota	
3.	Custard apple	Annona squamosa	
4.	Ixora live	Ixora coccinea	
5.	Mango	Mangifera indica	
6.	Pumpkin Ash	Fraxinis profunda	
7.	Upas tree	Antiaris toxicaria	
8.	Curry	Murraya koenigii	
9.	Adadhoda	Justicia adhatodas	

Extraction of coordinates using Mobilefish

Mobilefish is a free web service that allows you to upload an image and capture all XY mouse coordinates by mouse clicks. By clicking the leaf's outline, the following XY mouse coordinates were captured as shown in Figure 2.

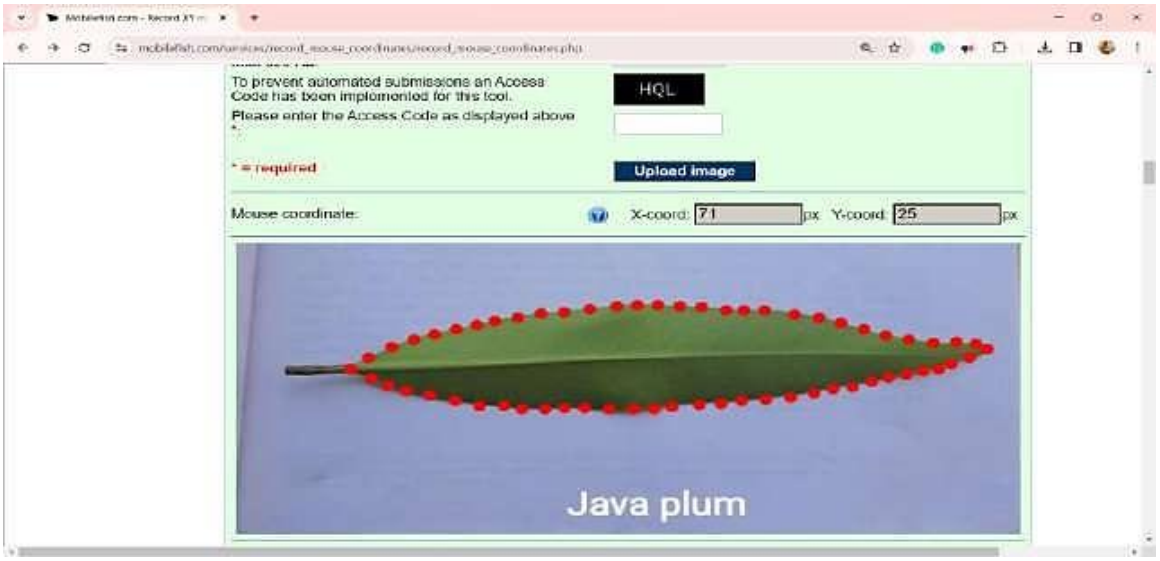

Figure 2. Coordinate extraction.

The images of the 9 leaves are imported into the Mobilefish website and the coordinates are extracted.

Analysis Using Ansys

ANSYS is a popular engineering simulation software that is used to model, analyze, and solve complex engineering and scientific problems. It provides a robust set of tools for structural, thermal, fluid dynamics, electromagnetic, and other simulations, allowing engineers and researchers to obtain essential insights into system behavior, improve designs, and make knowledgeable choices.

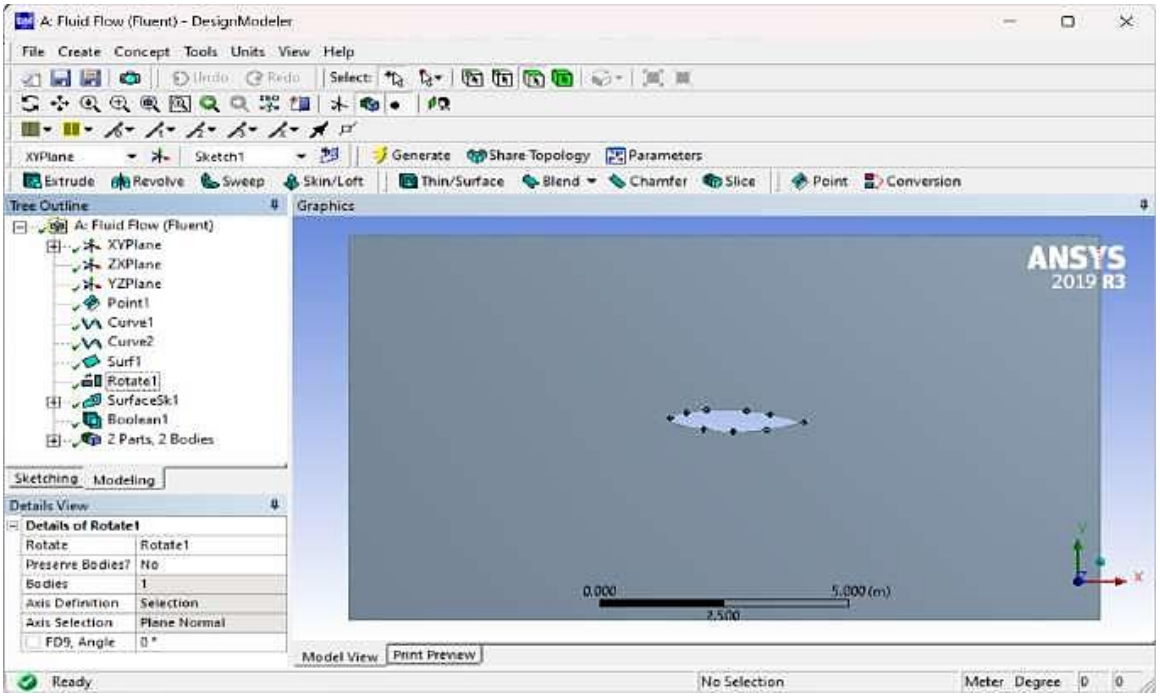

Figure 3. Importing coordinates and generating surface.

ANSYS Workbench is a platform incorporated into ANSYS that simplifies the setup, execution, and post-processing of numerous simulation tasks.

The extracted coordinates are fed into the ANSYs software and a 2D model of the leaf is made.

A boundary is made to incorporate the required conditions. These are shown in Figure 3.

The meshing is done for the same and the boundaries are defined as shown in Figure 4.

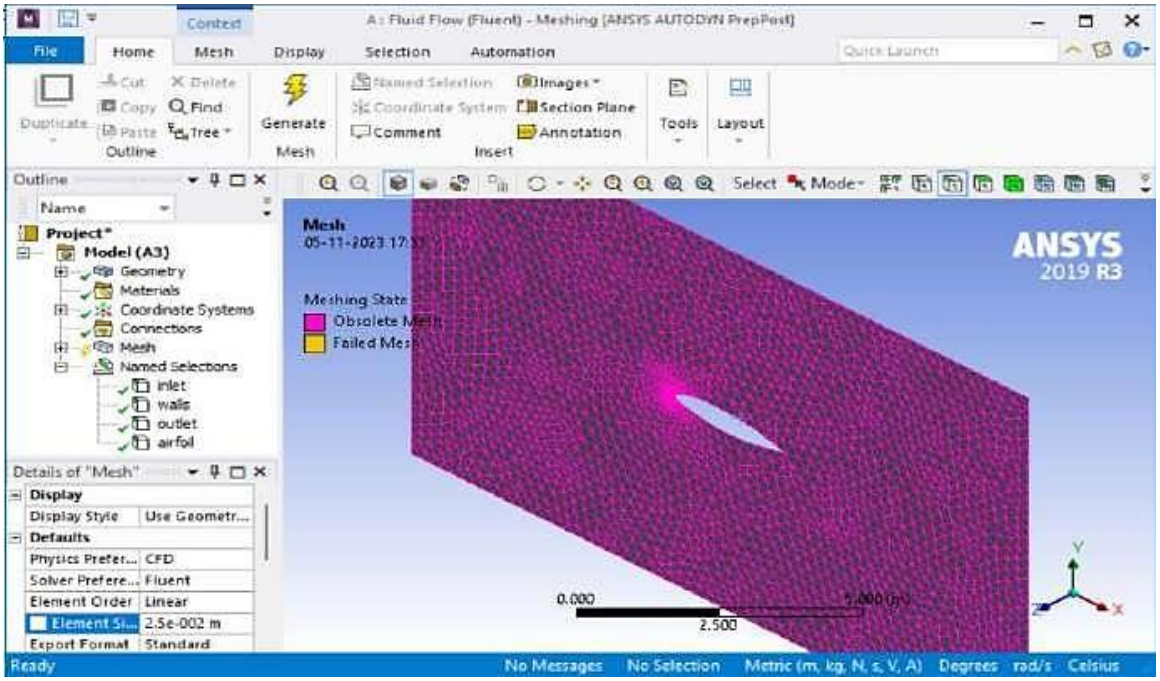

Figure 4. Meshing

The analysis is done by setting k-ω (SST) model. The values of C_l and C_d is observed and tabulated for all the 9 leaves for inlet velocities 10 m/s and 37 m/s for varying angle of attacks ($\boldsymbol{\alpha}$ = 0°, 4°,8°, 12°).

We selected to use the Shear-Stress Transport (SST) model, which is a typical turbulence model in Computational Fluid Dynamics (CFD). This model incorporates properties from both the (k-omega) and (k-epsilon) models, giving it versatility in addressing varied flow conditions. The SST model is well-suited for simulations including adverse pressure gradients and separated flows because it was specifically built for reliable predictions in near-wall turbulent flows. Its thorough handling of boundary layer interactions increases its dependability. In systems like as ANSYS Fluent, we use the SST model by providing boundary conditions, mesh details, and solver parameters. The versatility of this model makes it a beneficial choice, allowing us to acquire complete insights into fluid dynamics and aerodynamics across different situations in our study.

We chose speeds of 10 and 37 meters per second, which are typically utilized in wind tunnel testing of airfoils. Wind tunnels are aerodynamic and engineering instruments used to model the effects of air on things. Our study tries to simulate conditions relevant to real-world situations by using wind tunnel testing speeds. Wind tunnel testing provides practical insights that may be used to a variety of engineering applications by helping us understand how our airfoil operates in the presence of airflow. This choice assures that our investigation closely matches with industry norms and that our conclusions are applicable to real-world settings.

Also, we chose the angle of attacks ($\boldsymbol{\alpha}$) = 0°, 4°,8°, 12°, just to study the possible lift generation in the leaves considering take-off conditions.

We chose ANSYS software, over other software because of its adaptability to our specific conditions. Despite the lengthy analysis, ANSYS produced the expected results for each leaf. The adaptability of the software allowed us to incorporate specific conditions necessary for our study, ensuring a thorough and accurate analysis of the aerodynamic performance of the leaves.

CFD ANALYSIS

The analysis was done for all the nine leaves in the ANSYs software and the C_l and C_d values of the leaves were compared among one another. Among the nine leaves tested, four leaves (Javaplum, Ixora, Custard apple and Sapota) were shown to have the highest C_l/C_d ratio.

Pressure, velocity, and turbulence contours were obtained and compared for these four leaves.

Pressure contours

Pressure contours illustrate the distribution of pressure around the airfoil. The pressure contours of the four leaves are shown below in Figure 5:

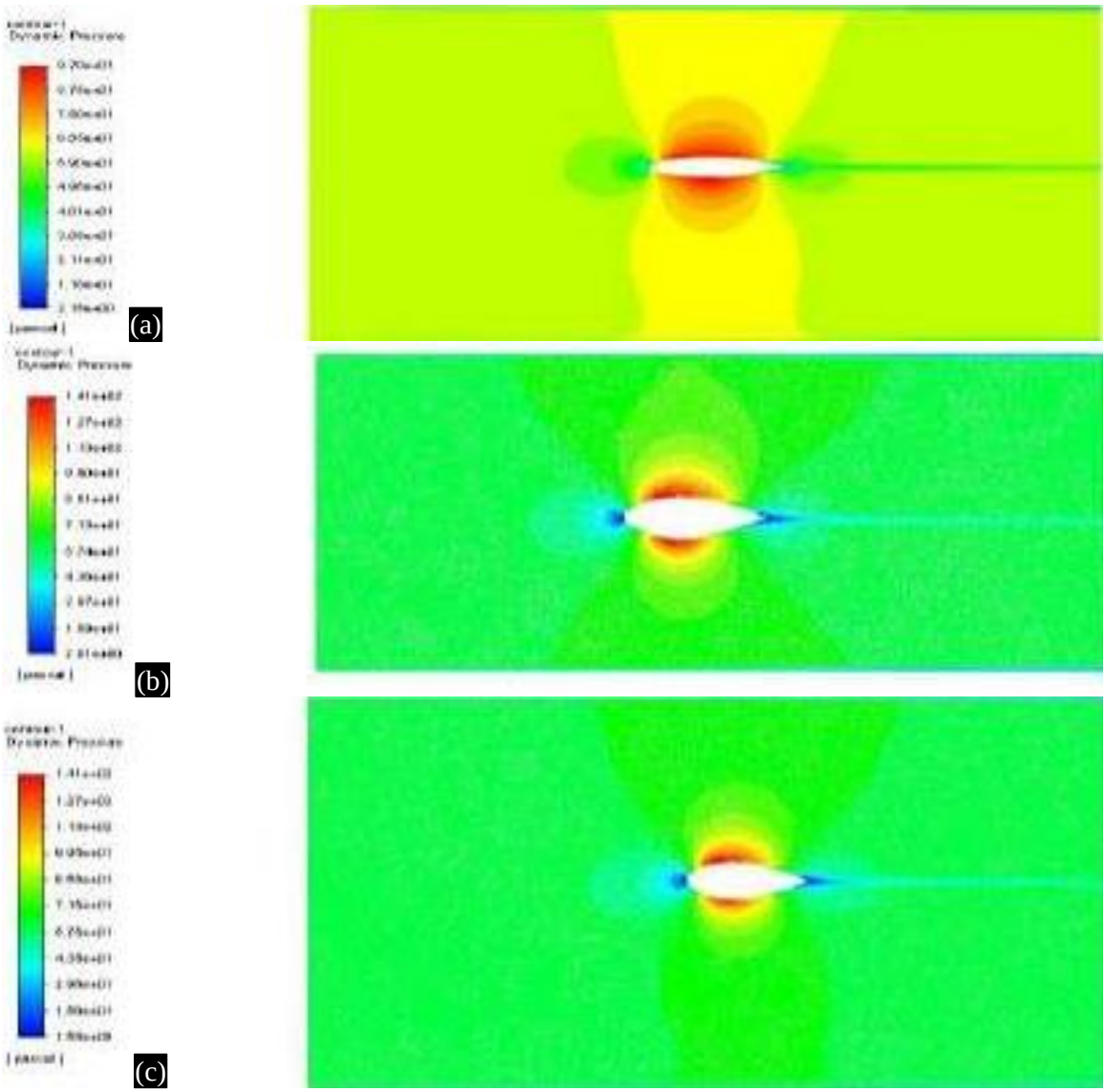

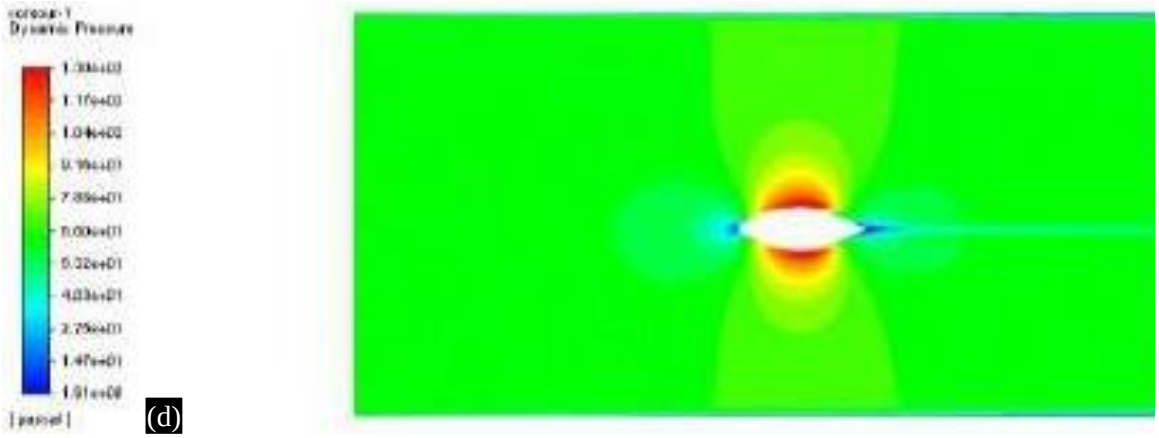

Figure 5. Pressure contour at 0° angle of attack (at 10m/s). (a) Javaplum leaf, (b) Ixora leaf, (c) Custard apple leaf, and (d) Sapota leaf.

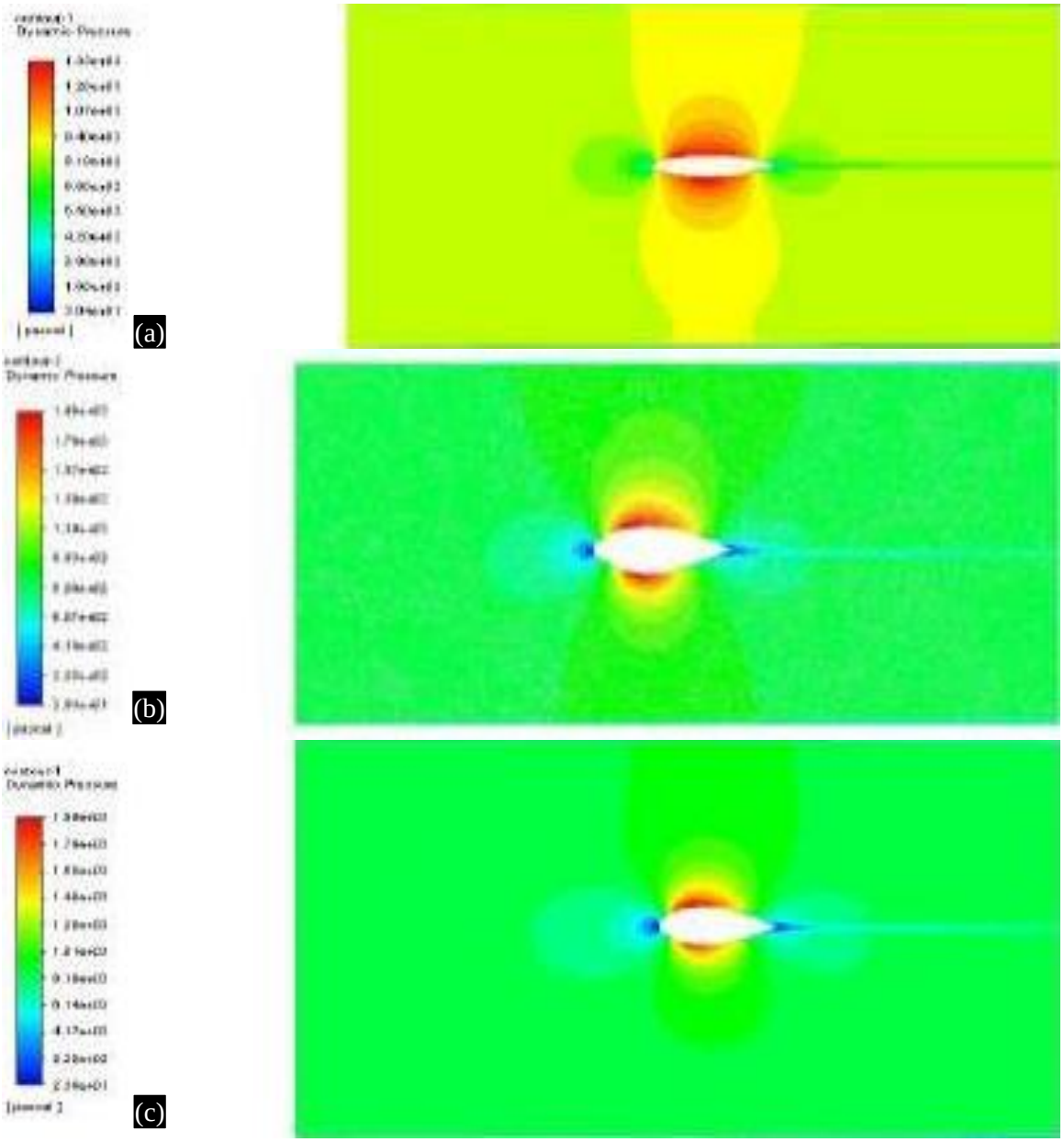

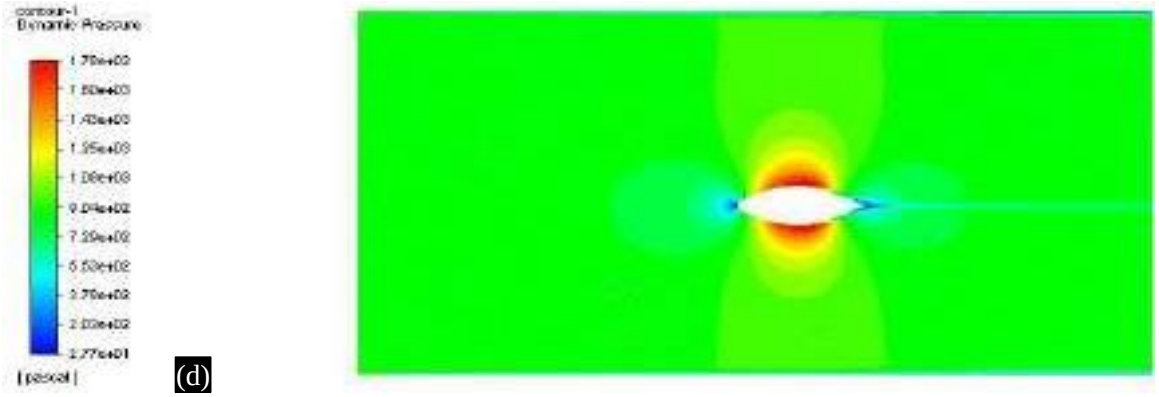

Figure 6. Pressure contour at 0° angle of attack (at 37m/s). (a) Javaplum leaf, (b) Ixora leaf, (c) Custard apple leaf, (d) Sapota leaf.

By observing Figures 5 and 6, the values of the pressure have increased diligently from 10m/s to 37m/s. But the contours look the same. The Javaplum leaf (Figure 6(a) and Figure 7(a)) has variable pressure around the whole boundary. All the four leaves are observed to have high pressure on both the upper and lower surfaces.

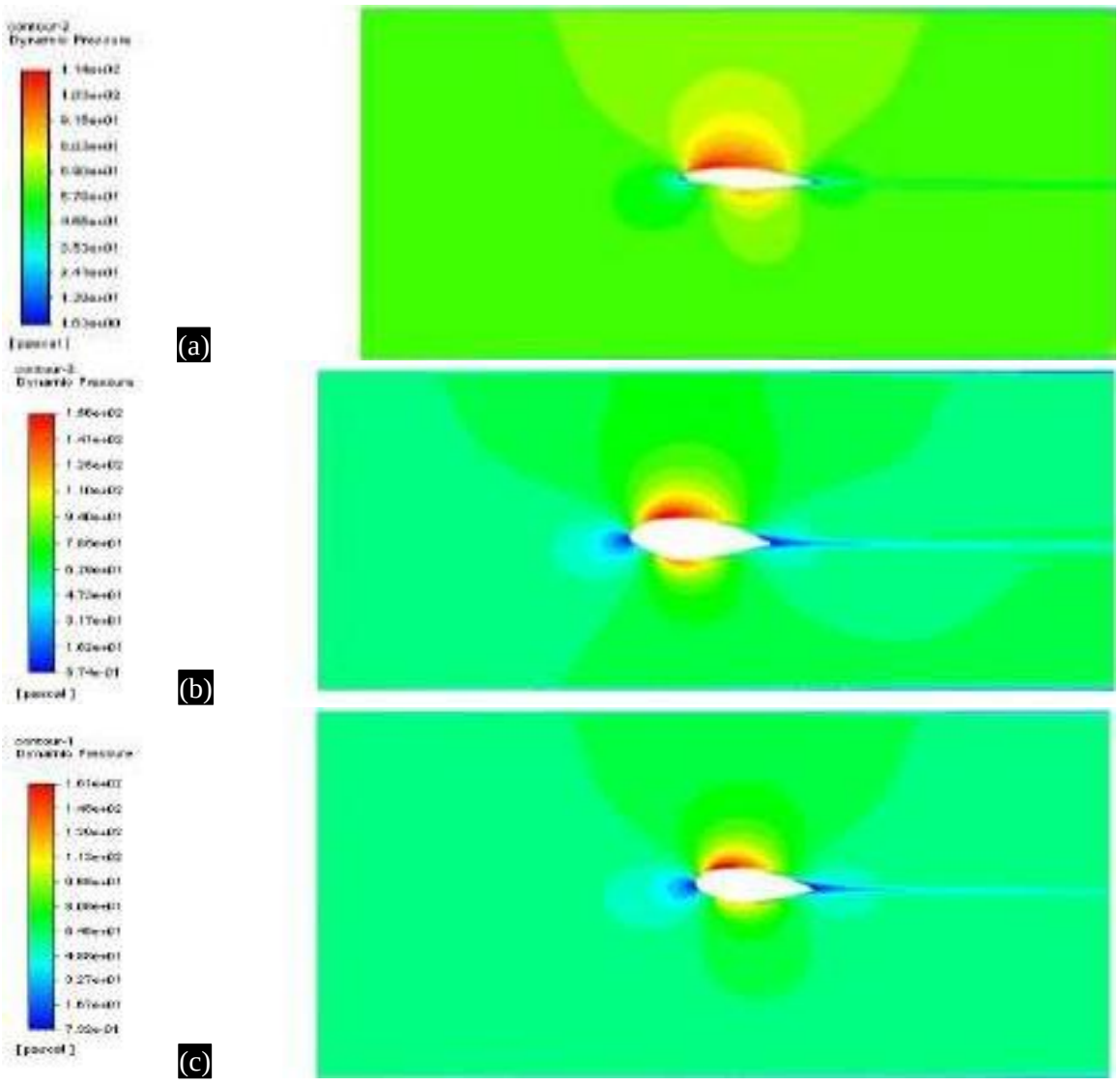

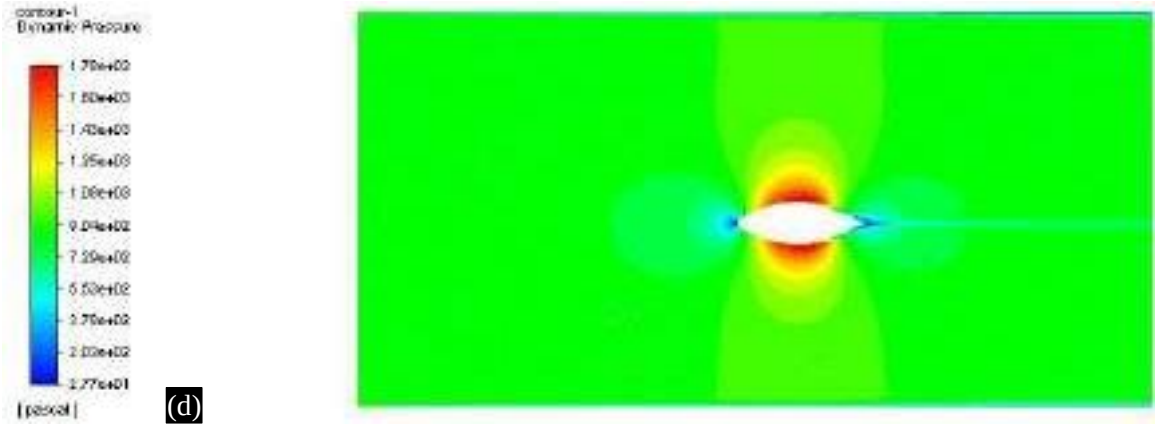

Figure 7. Pressure contour at 4° angle of attack (at 10m/s). (a) Javaplum leaf, (b) Ixora leaf, (c) Custard apple leaf, (d) Sapota leaf

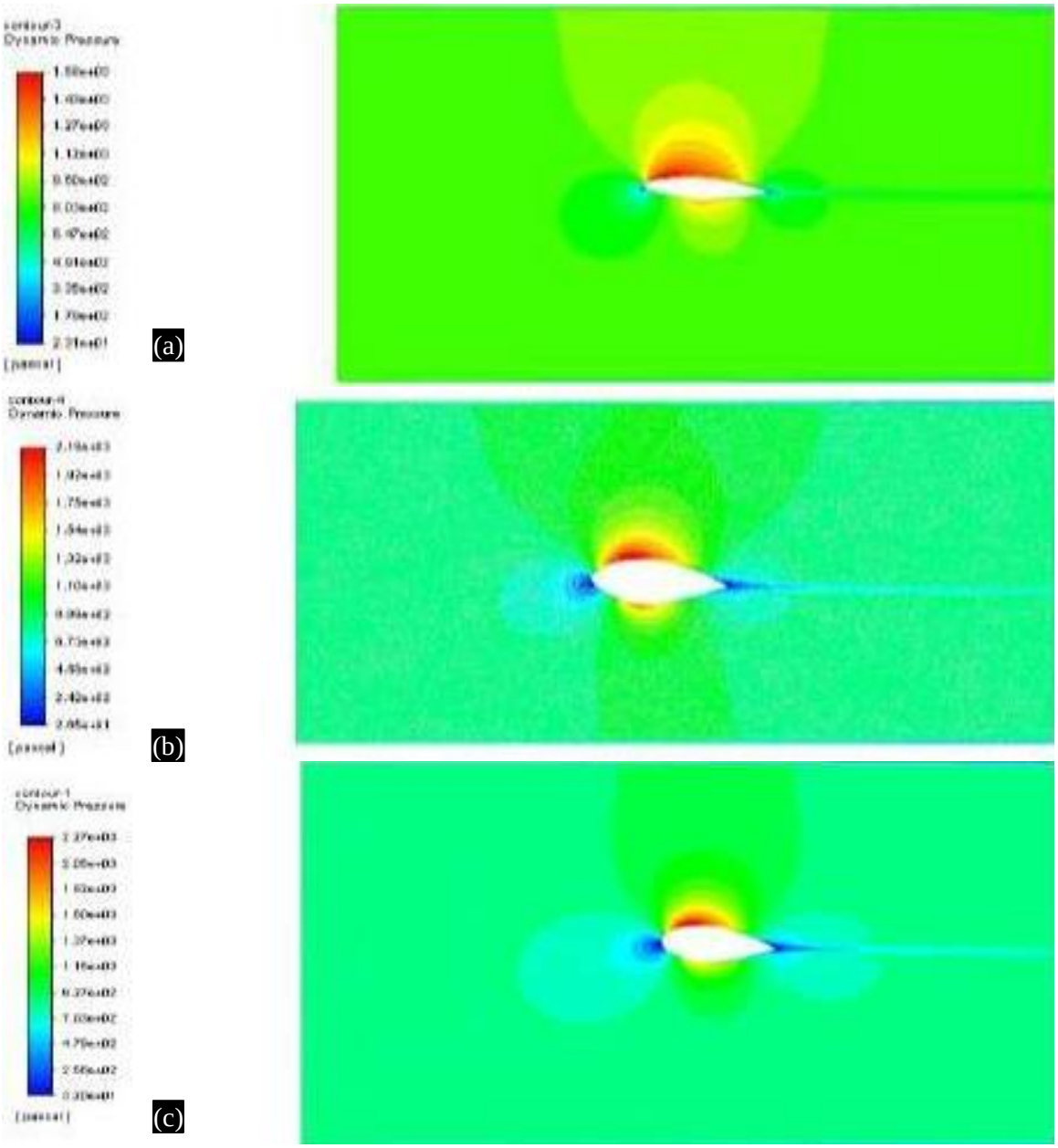

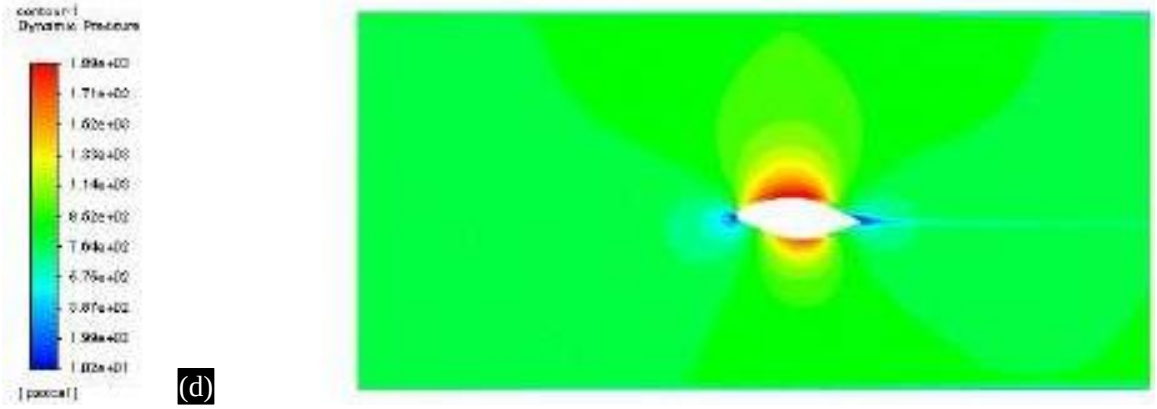

Figure 8. Pressure contour at 4° angle of attack (at 37m/s). (a) Javaplum leaf, (b) Ixora leaf, (c) Custard apple leaf, (d) Sapota leaf

By observing Figures 7 and 8, there is low pressure points on leading and trailing edges of all the leaves. The pressure values have increased diligently. There is comparatively low value of pressure on the lower surface for custard apple leaf (Figure 7(c) and Figure 8(c)).

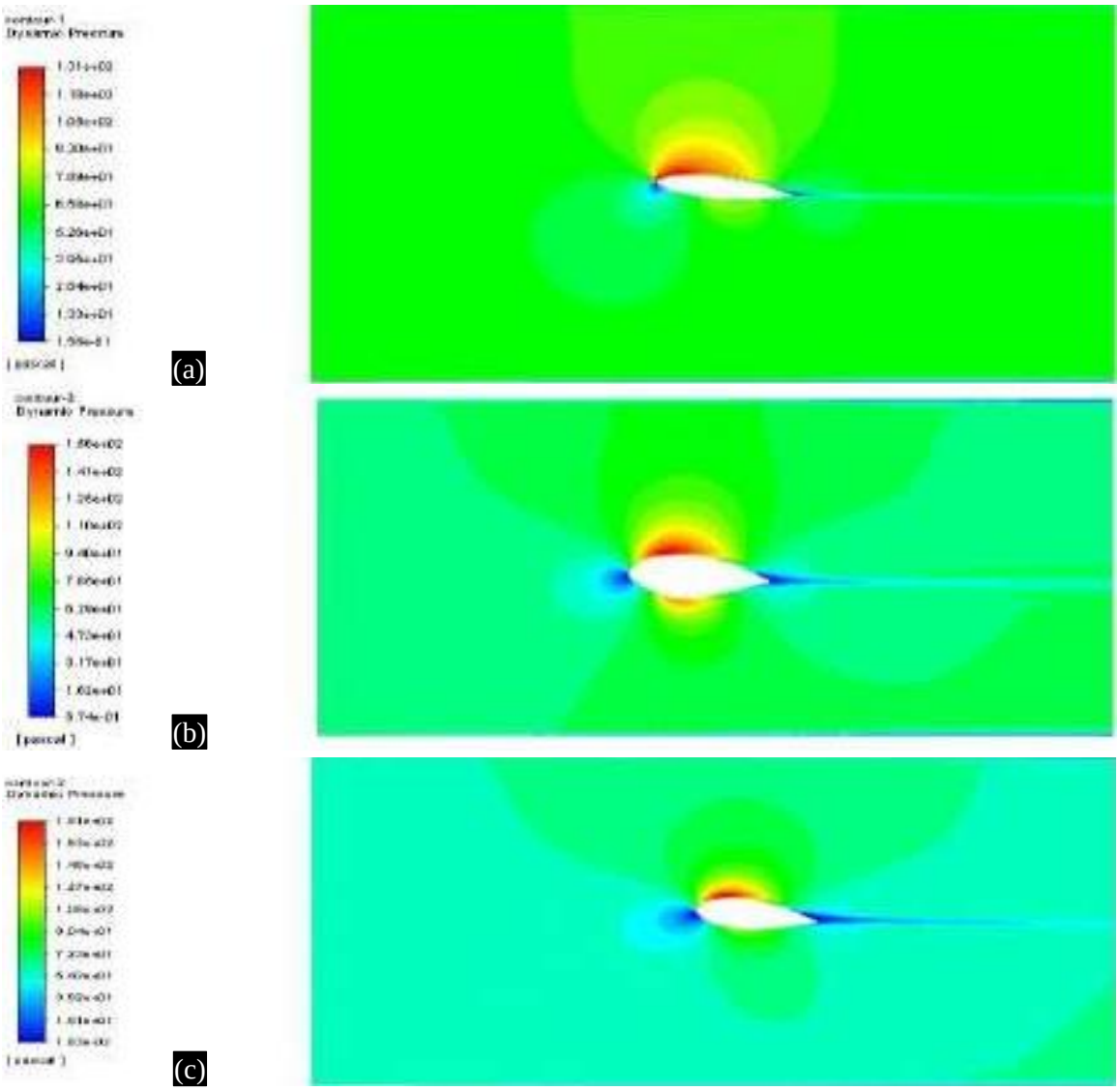

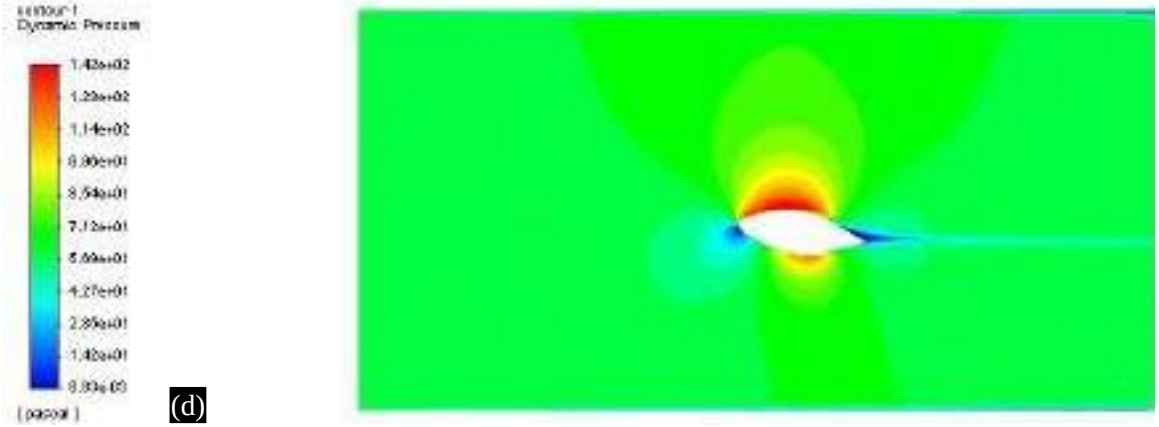

Figure 9. Pressure contour at 8° angle of attack (at 10m/s). (a) Javaplum leaf, (b) Ixora leaf, (c) Custard apple leaf, (d) Sapota leaf

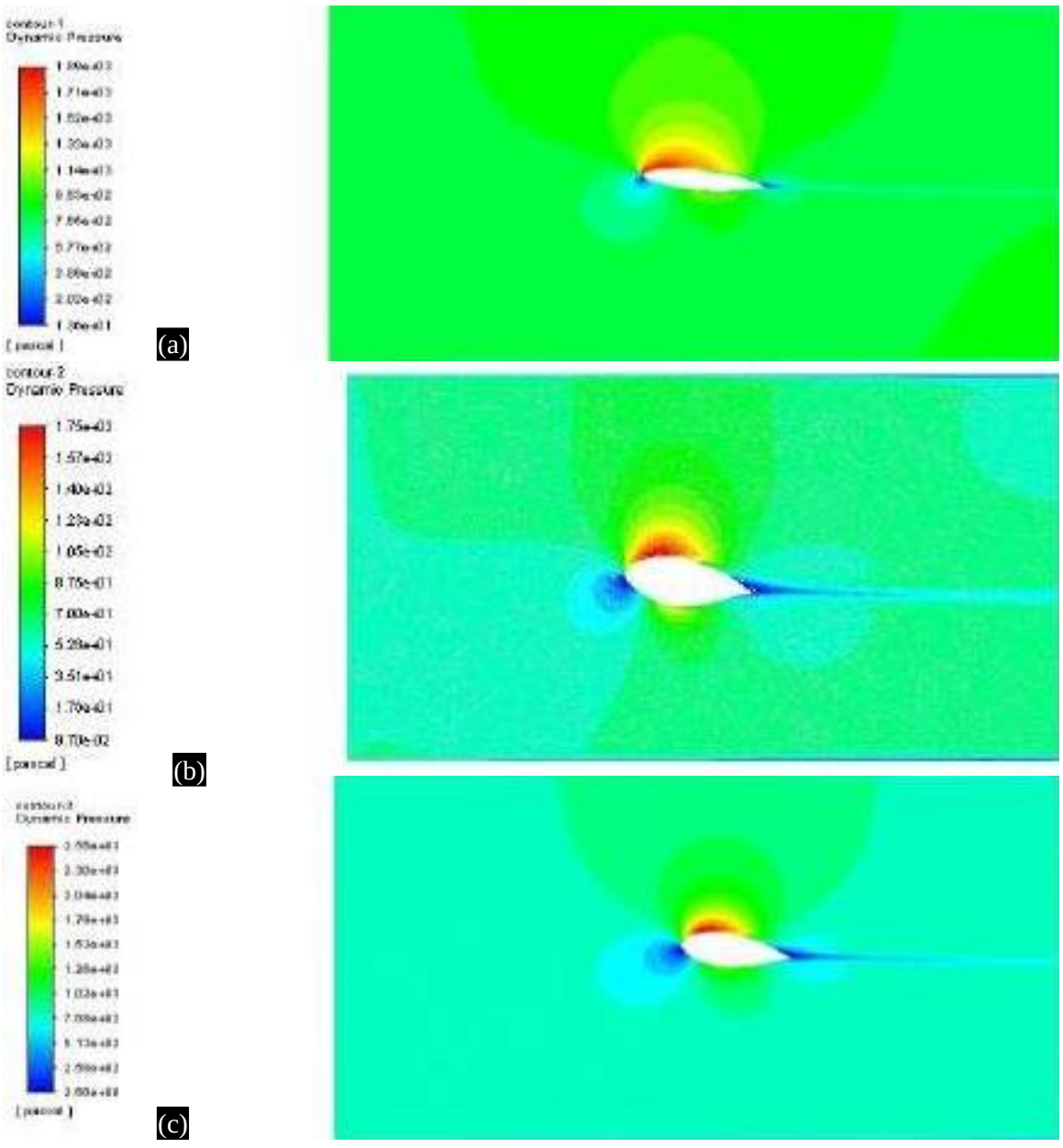

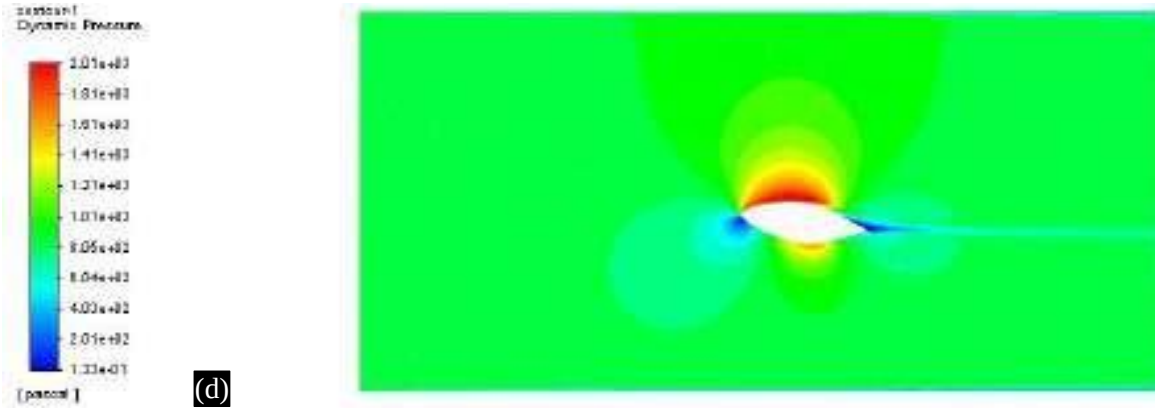

Figure 10. Pressure contour at 8° angle of attack (at 37 m/s). (a) Javaplum leaf, (b) Ixora leaf, (c) Custard apple leaf, (d) Sapota leaf

By observing Figures 9 and 10, the pressure values have increased diligently from 10m/s to 37 m/s. In all the leaves, there is high pressure on the top surface which is contradictory to the normal behavior of airfoils.

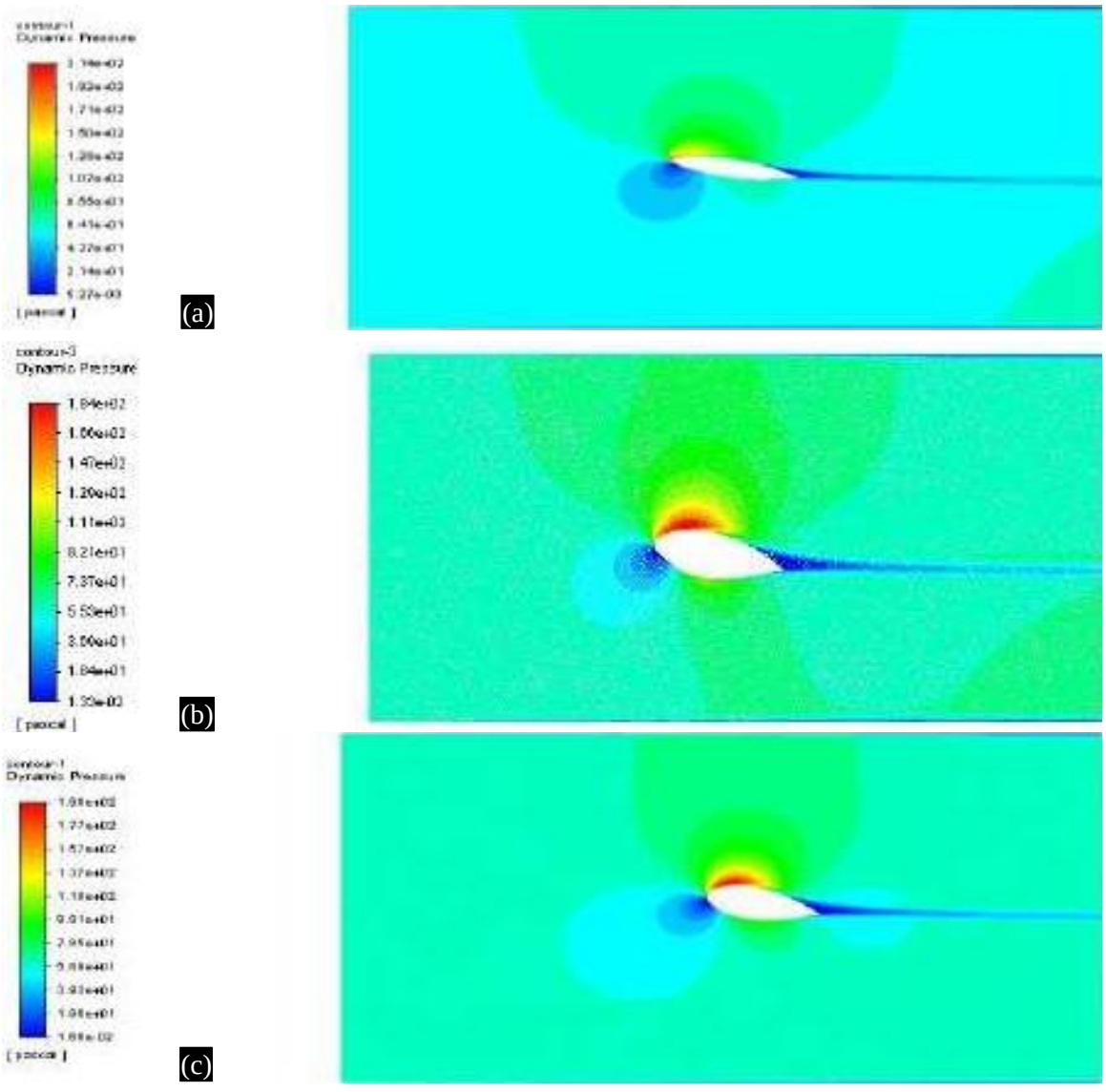

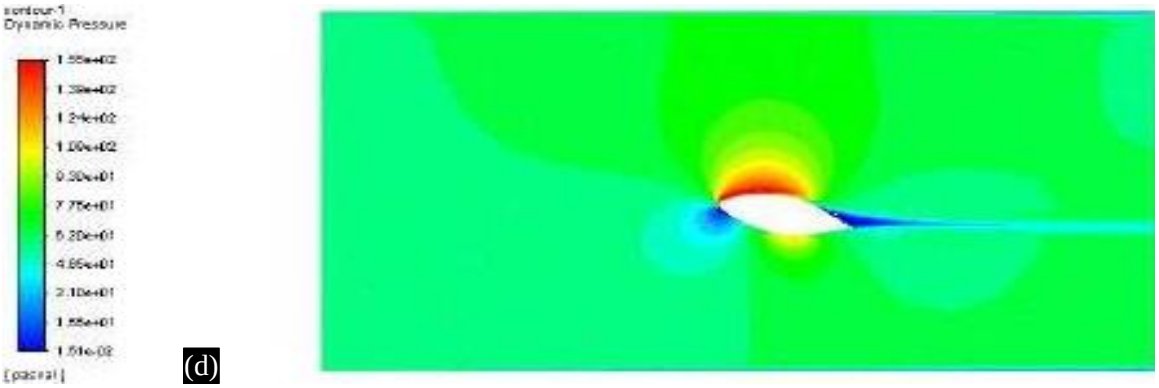

Figure 11. Pressure contour at 12° angle of attack (at 10m/s). (a) Javaplum leaf, (b) Ixora leaf, (c) Custard apple leaf, (d) Sapota leaf

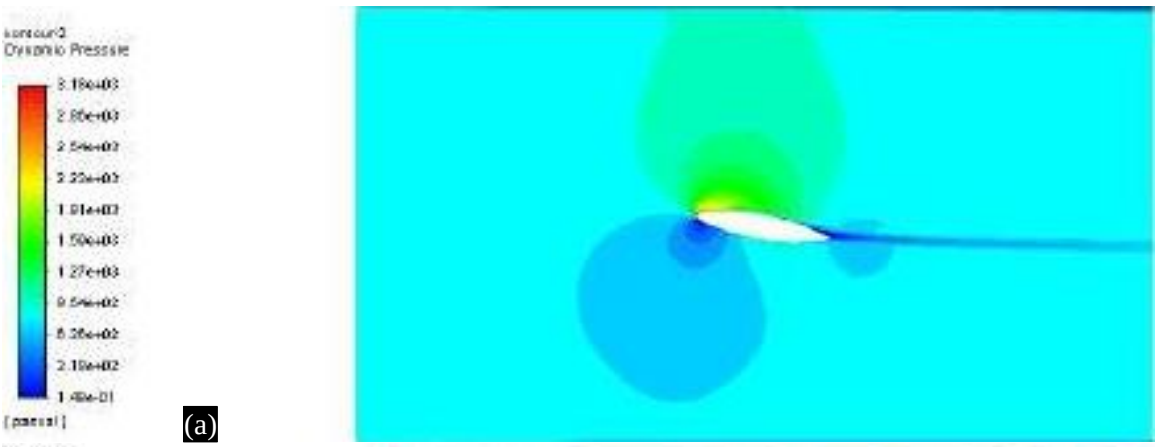

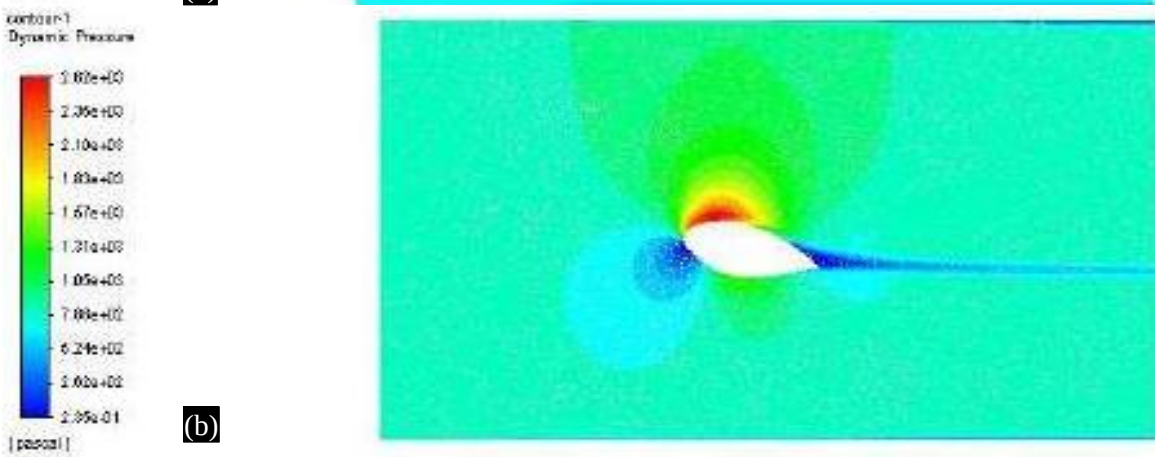

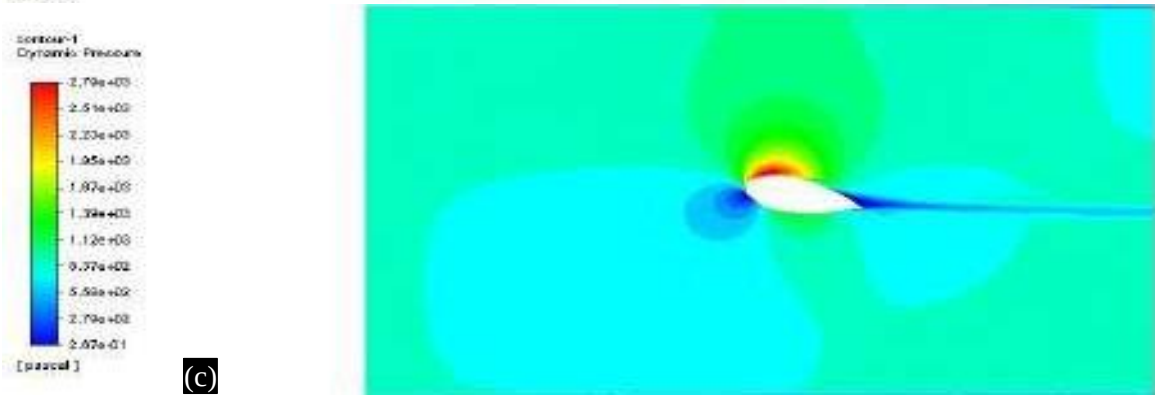

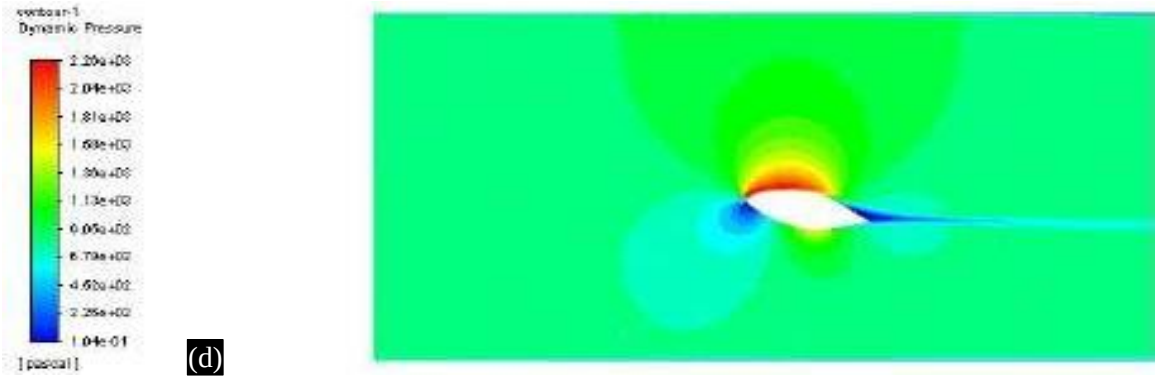

Figure 12. Pressure contour at 12° angle of attack (at 37m/s). (a) Javaplum leaf, (b) Ixora leaf, c) Custard apple leaf, (d) Sapota leaf

By observing Figure 11(a) and Figure 12(a), Javaplum leaf has a high pressure point near the leading edge. The high-pressure point at an airfoil's leading edge is strategically employed to generate lift. Air accelerates as it flows over the curved upper surface, causing a pressure difference with the lower surface. So, this key point is noted.

As a summary, from Figures 5-12 we can observe the increase in the pressure distribution along the top and bottom of the leaf. The pressure increases with increasing velocity through varying angle of attacks. Among the four leaves, Javaplum leaf has the maximum pressure value at 12° angle of attack (37 m/s) which is discussed in Table 3. But we should also note that the pressure in the upper surface is equally higher to that of the lower surface. This is contrast to the behavior of airfoil where low pressure is generated at the top.

Velocity Contour

Velocity contours illustrate the distribution of velocity around the airfoil. It is crucial to conduct velocity tests around the airfoil and determine the maximum and minimum values. Velocity contours of the four leaves are shown below:

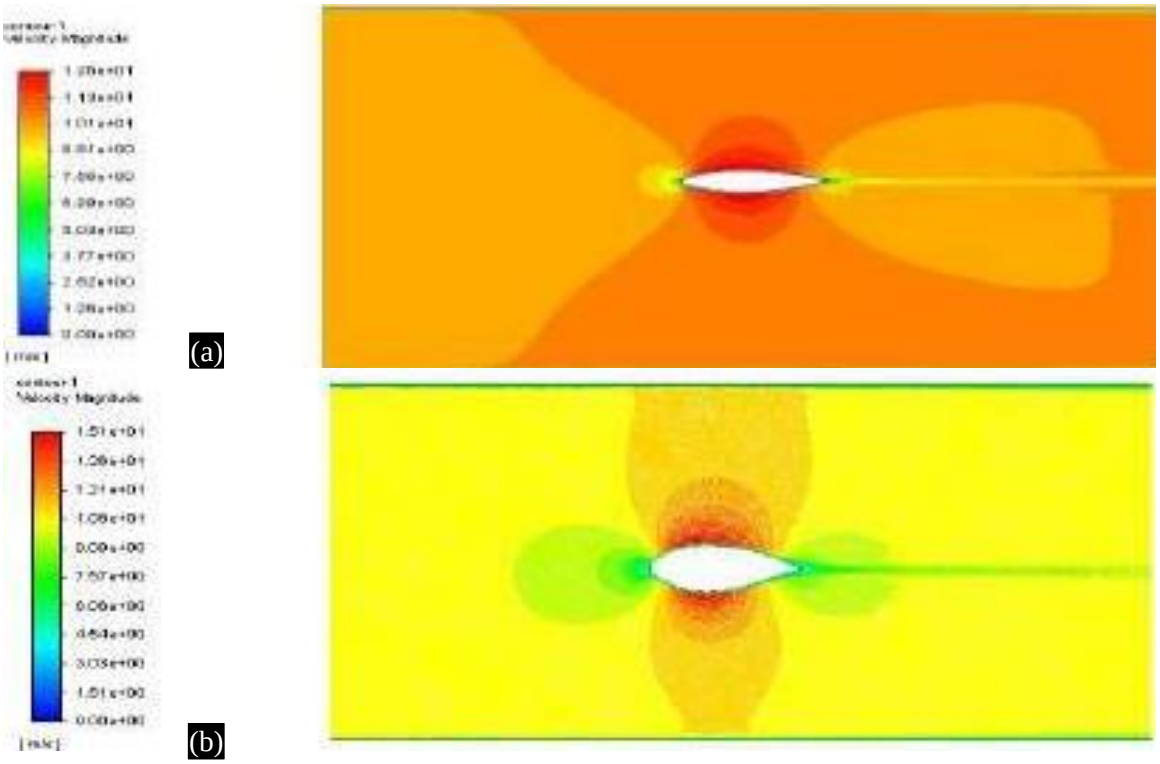

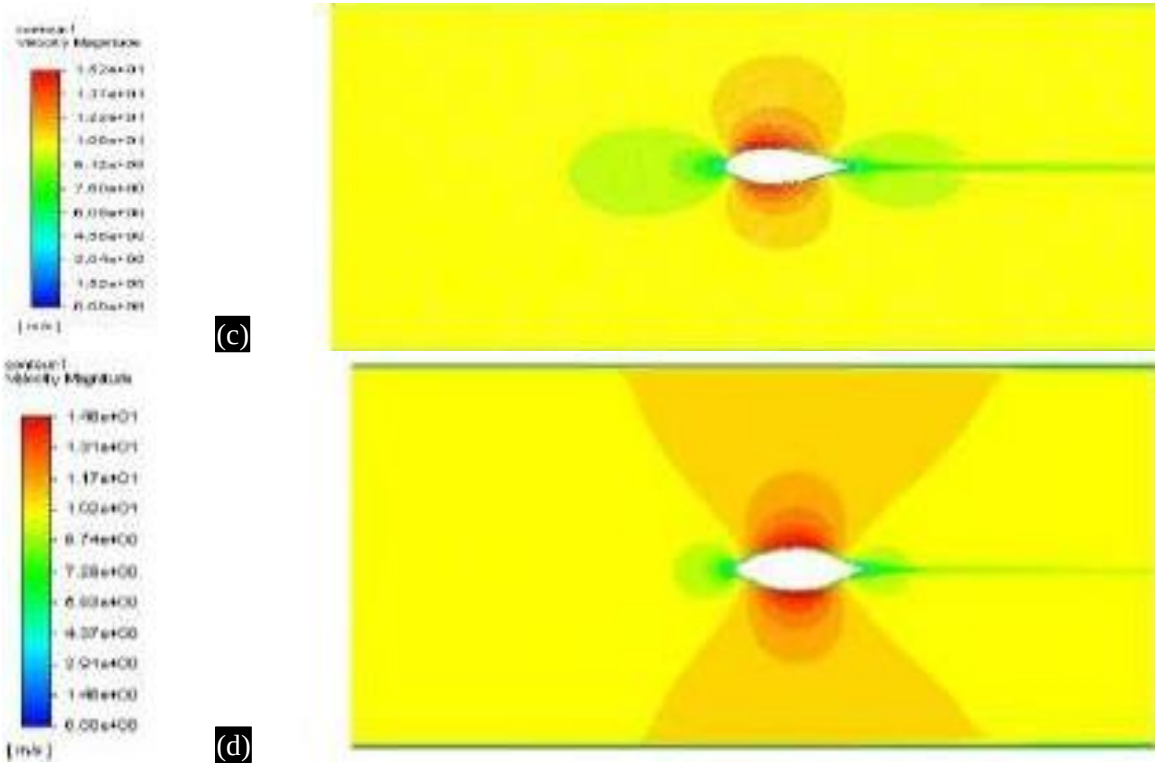

Figure 13. Velocity contour at 0° angle of attack (at 10m/s). (a) Javaplum leaf, (b) Ixora leaf, (c) Custard apple leaf, (d) Sapota leaf

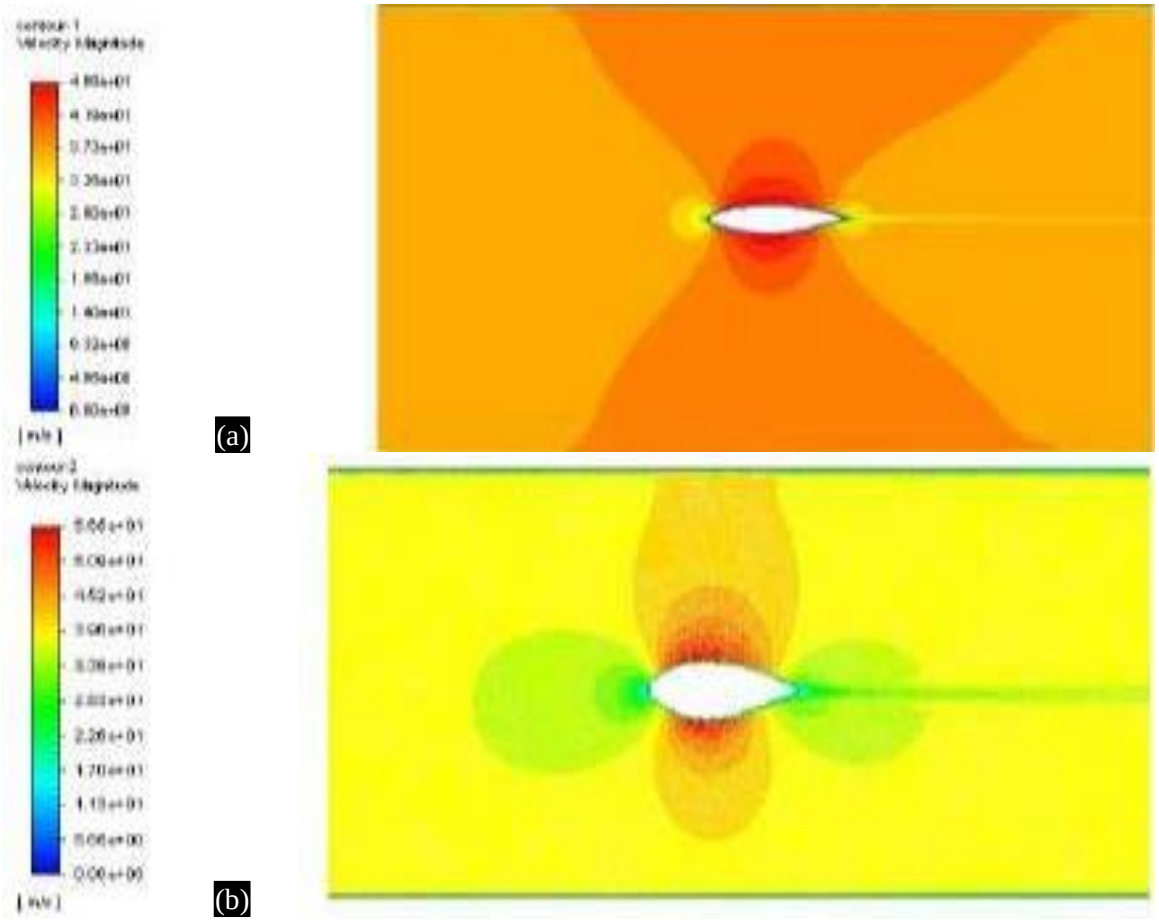

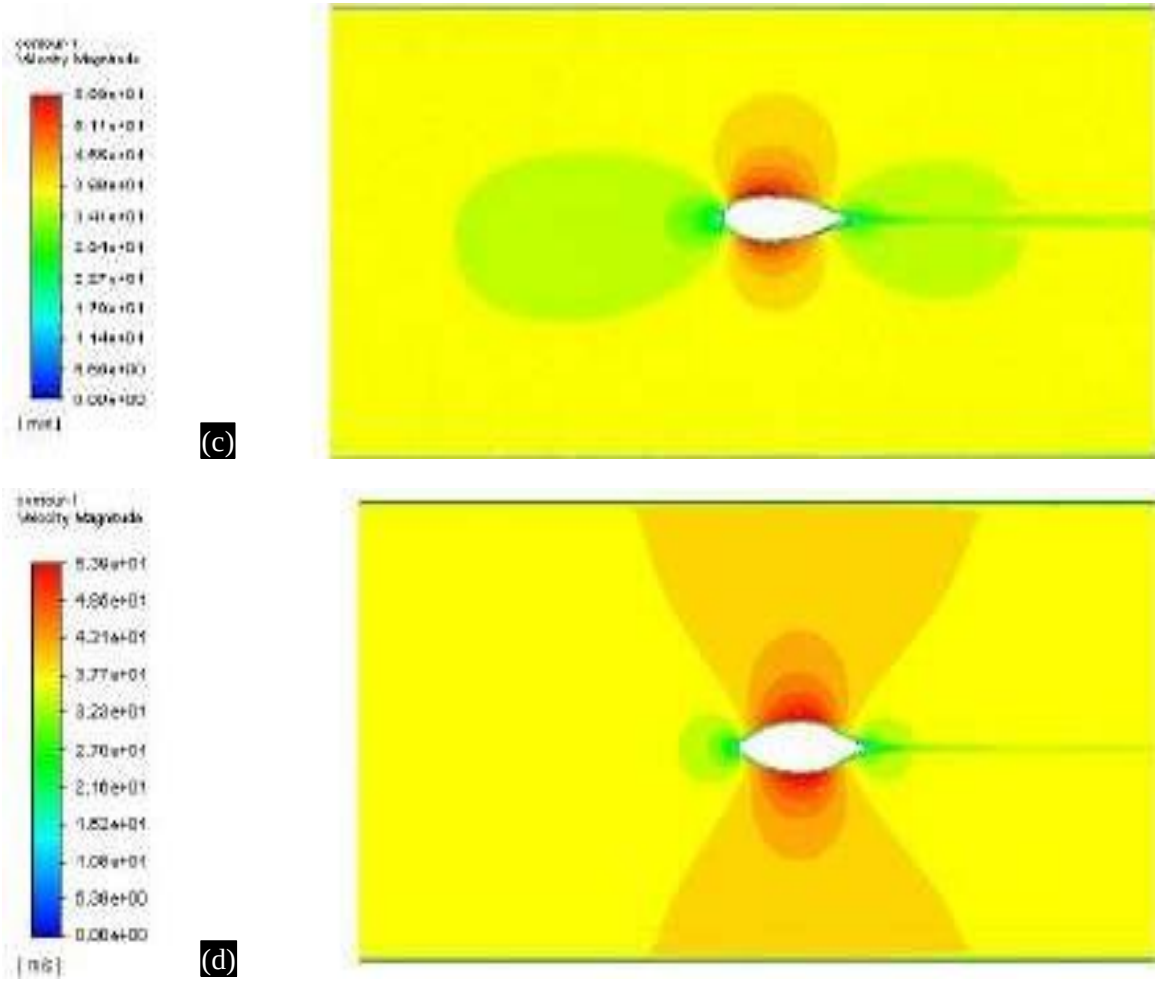

Figure 14 Velocity contour at 0° angle of attack (at 37m/s). (a) Javaplum leaf, (b) Ixora leaf, (c) Custard apple leaf, (d) Sapota leaf

From Figure 13 and Figure 14, we can observe stagnation points occurring through the outline of the leaf.

The upper and lower surface of all the leaves has relatively high velocities than the leading and trailing edges.

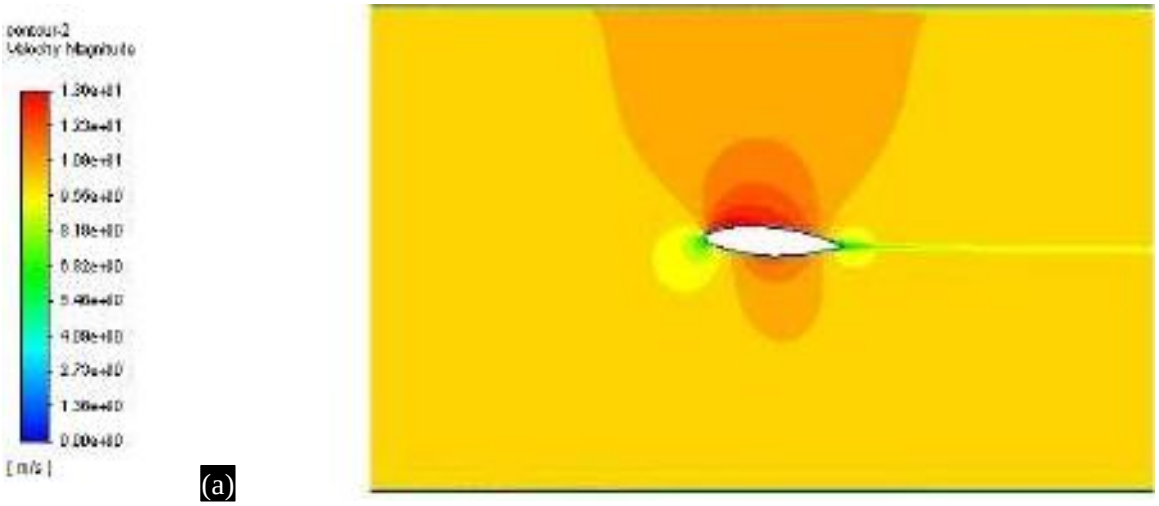

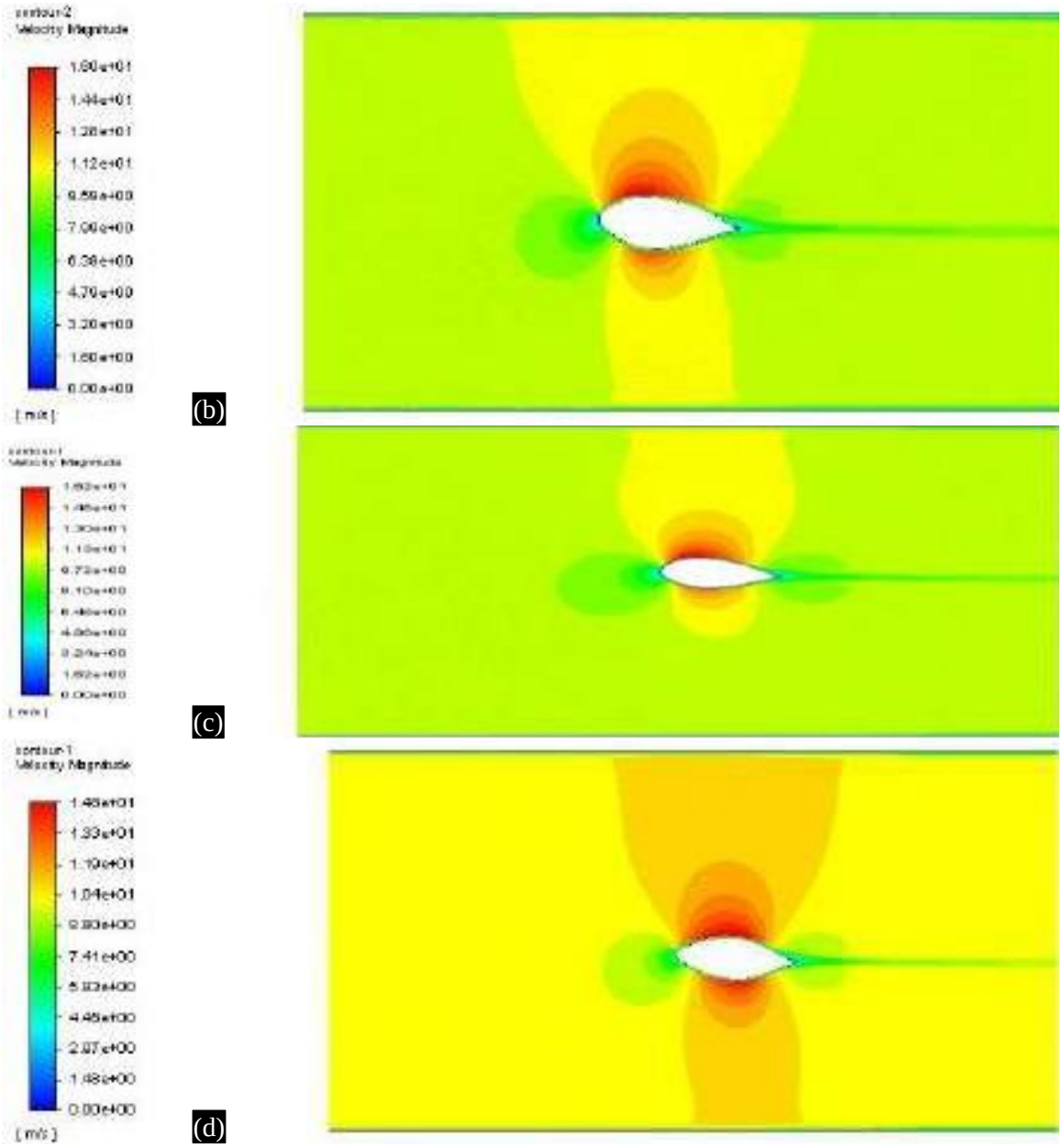

Figure 15. Velocity contour at 4° angle of attack (at 10m/s). (a) Javaplum leaf, (b) Ixora leaf, (c) Custard apple leaf, (d) Sapota leaf

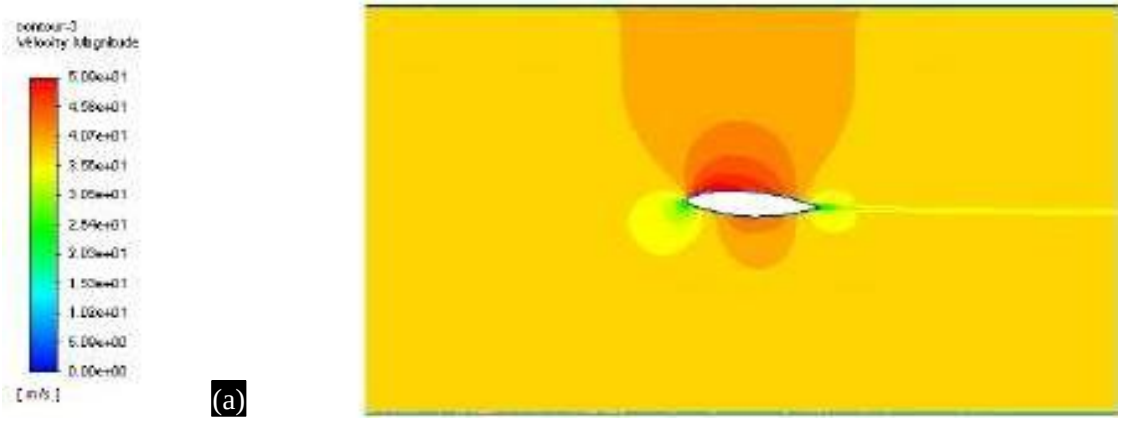

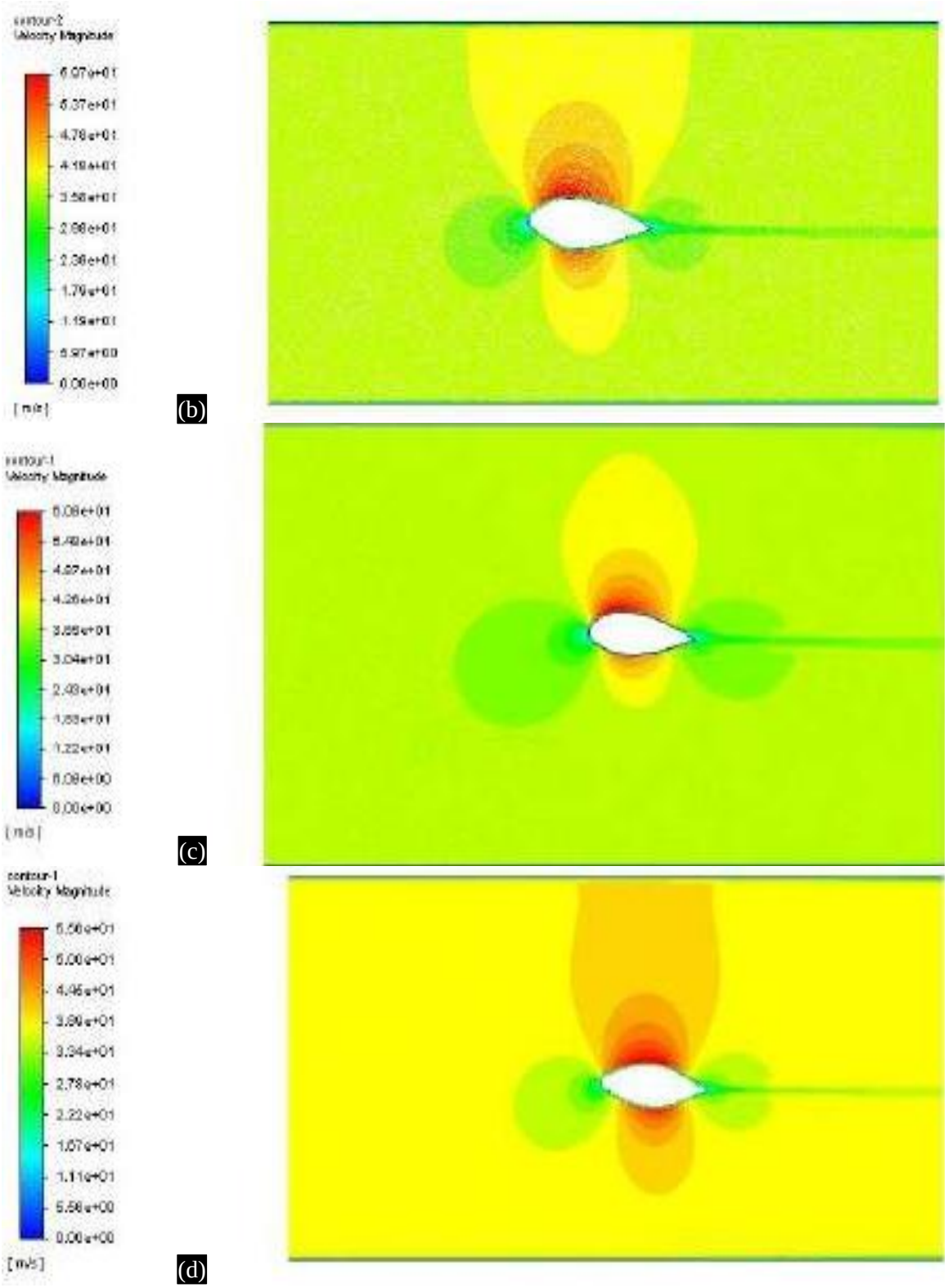

Figure 16. Velocity contour at 4° angle of attack (at 37m/s), (a) Javaplum leaf, (b) Ixora leaf, (c) Custard apple leaf, (d) Sapota leaf

From Figure 15 and Figure 16, yet again, we can observe stagnation points occurring through the outline of the leaf. The velocity around the Javaplum leaf (Figure 15(a) and Figure 16(a)) is noticed to be reduced by a large value when compared with the velocities at 0° angle of attack.

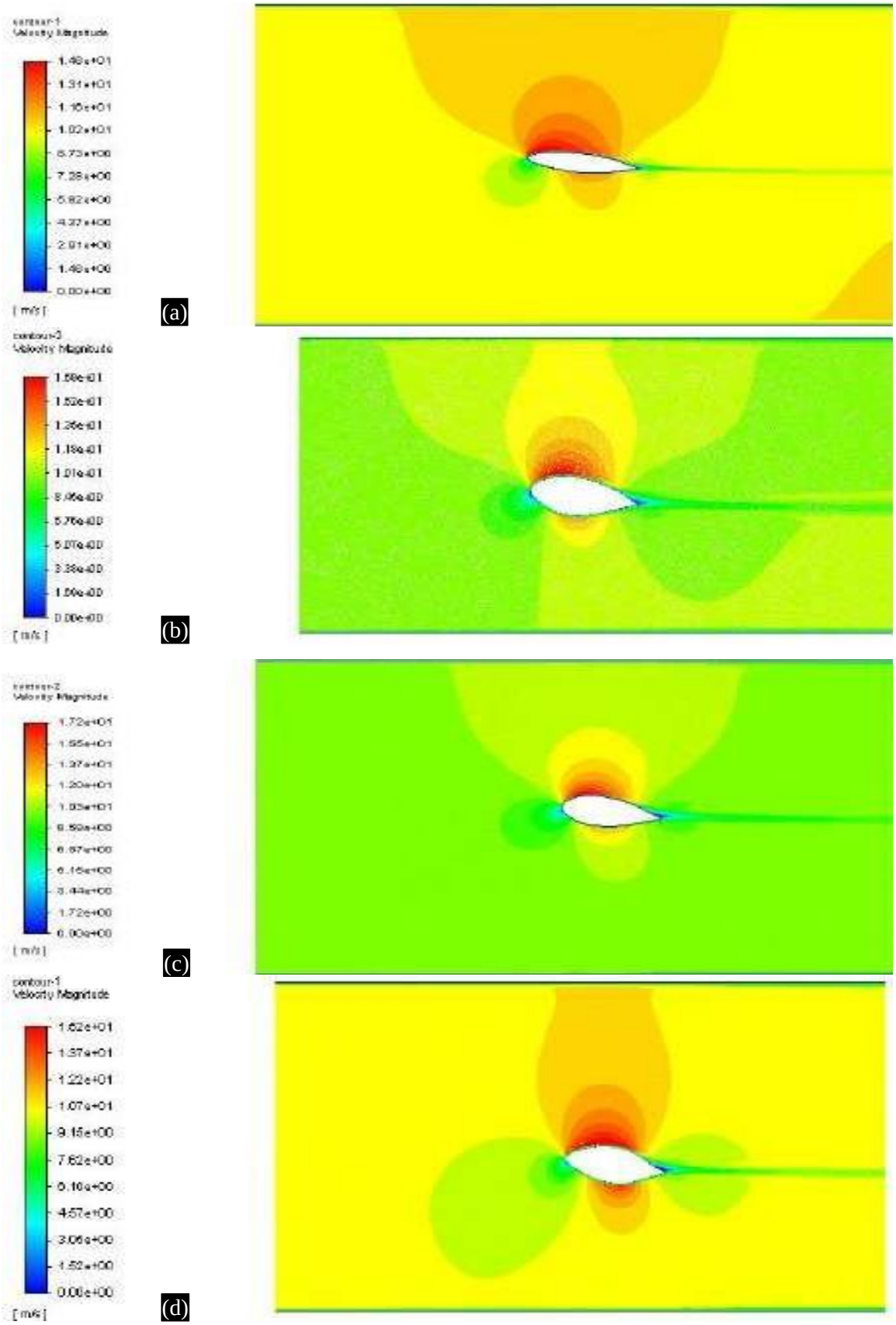

Figure 17. Velocity contour at 8° angle of attack (at 10m/s). (a) Javaplum leaf, (b) Ixora leaf, (c) Custard apple leaf, (d) Sapota leaf

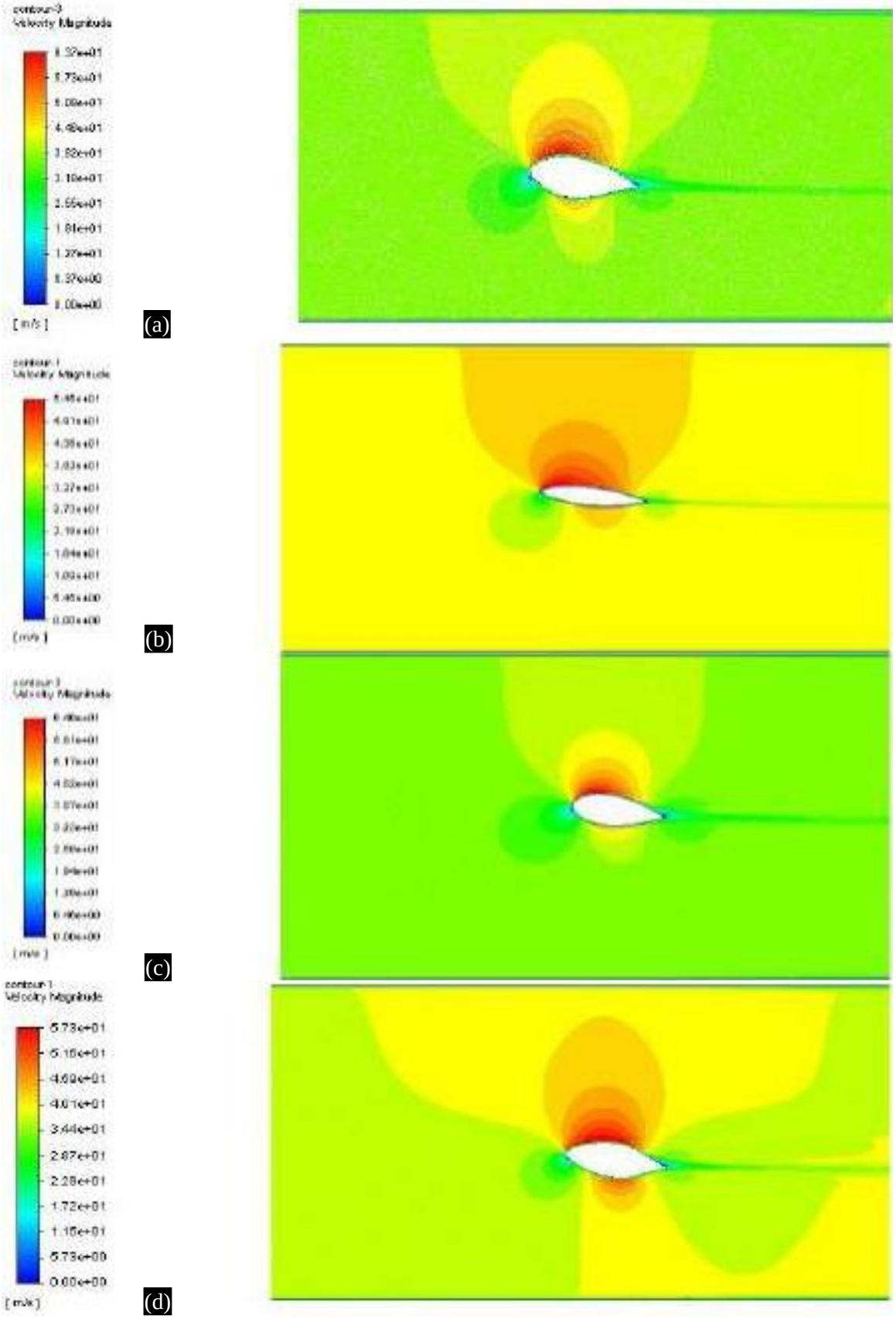

Figure 18. Velocity contour at 8° angle of attack (at 37m/s). (a) Javaplum leaf, (b) Ixora leaf, (c) Custard apple leaf, (d) Sapota leaf

From Figure 17 and Figure 18, yet there is comparatively high velocity on the upper surface than the low surface. It should be noted that high velocities on the upper surface contribute to lift, they also play a role in minimizing pressure drag.

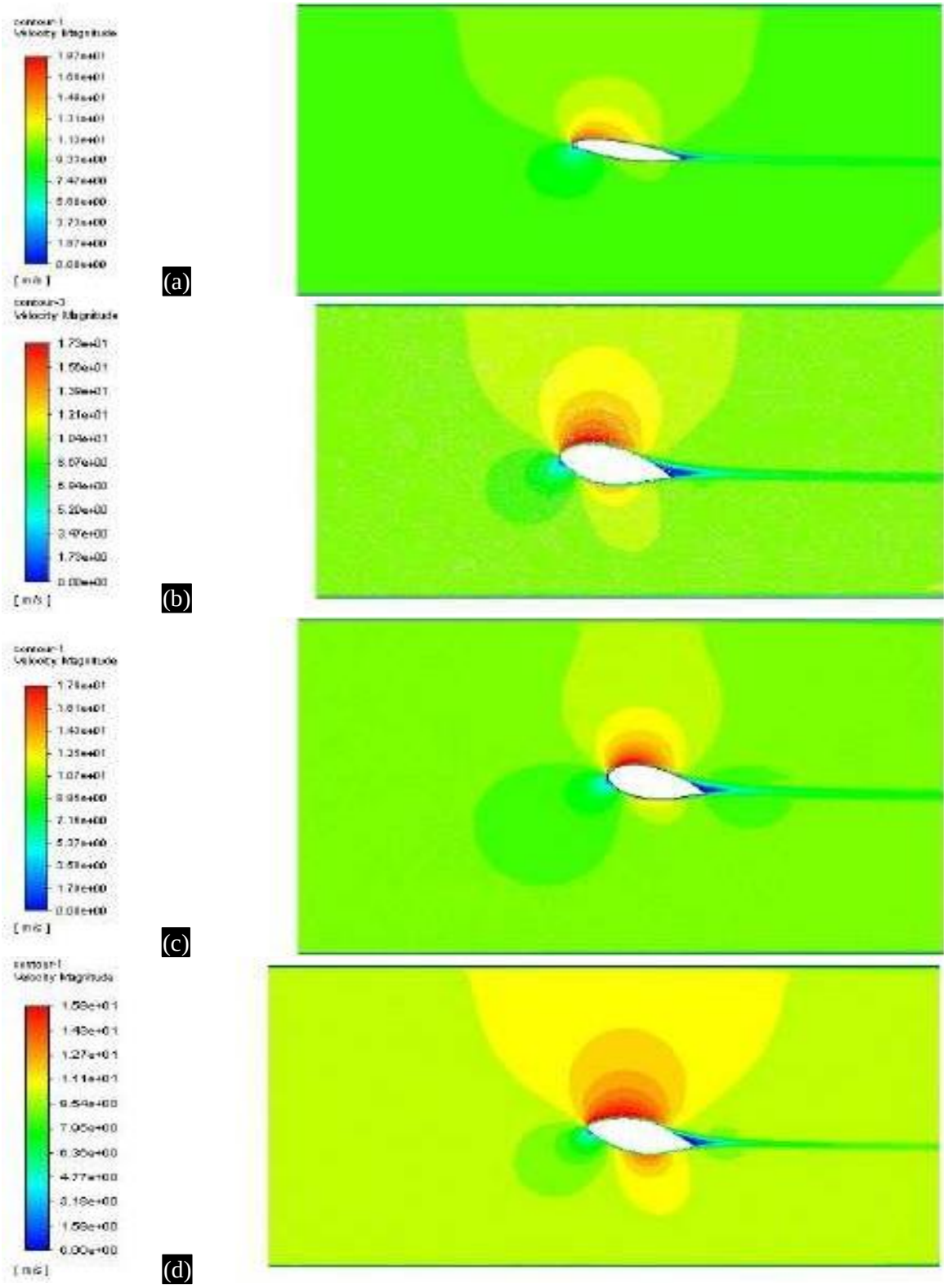

Figure 19. Velocity contour at 12° angle of attack (at 10m/s), (a) Javaplum leaf, (b) Ixora leaf, (c) Custard apple leaf, (d) Sapota leaf

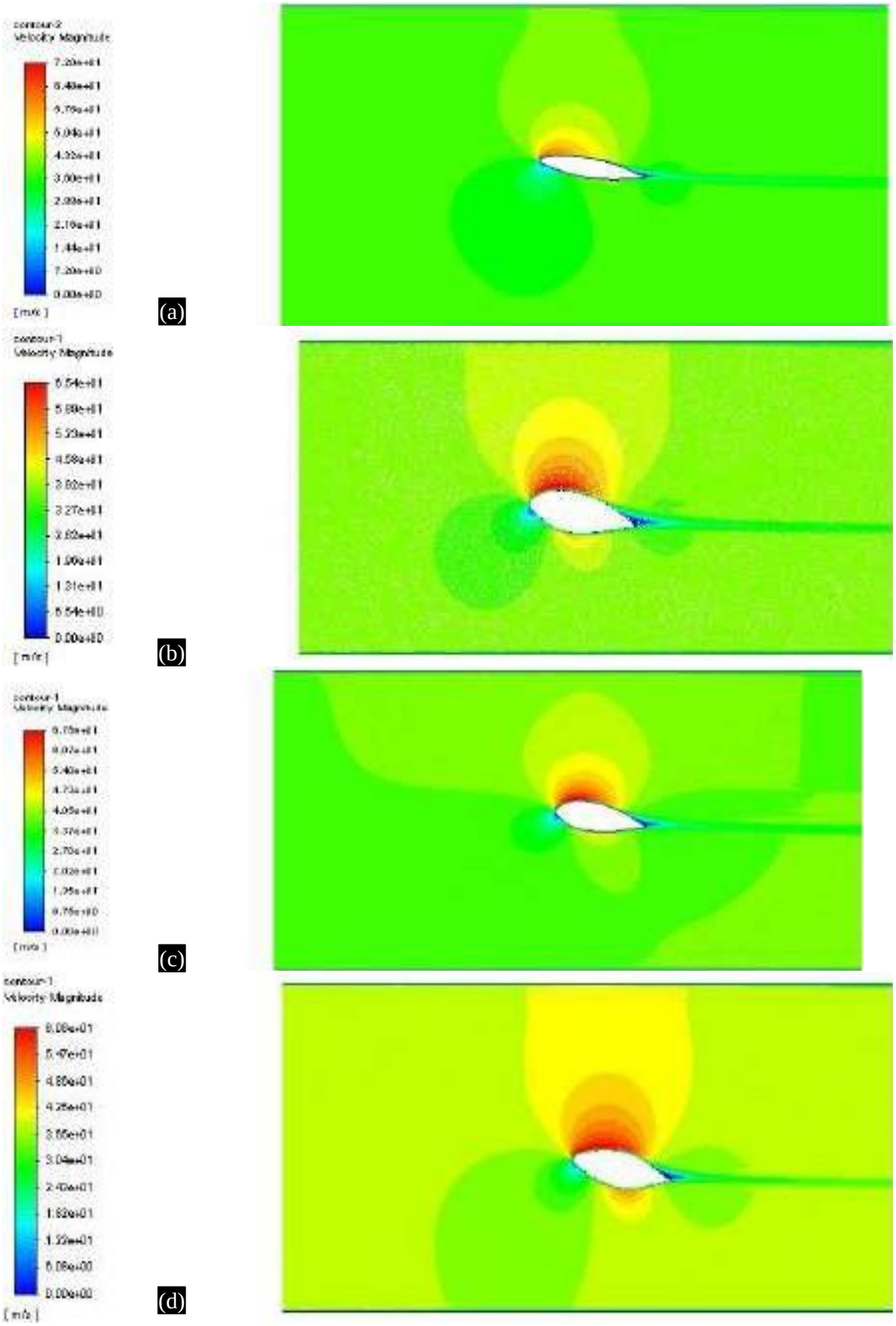

Figure 20. Velocity contour at 12° angle of attack (at 37m/s), (a) Javaplum leaf, (b) Ixora leaf, (c) Custard apple leaf, (d) Sapota leaf

From Figure 19 and Figure 20, we can observe that the velocity at around the outline of leaf is zero which indicates a stagnation point and there is high velocity on the upper surface.

As a summary, observing Figures 13-20, there lift generation and an overall increase in aerodynamic performance as we increase the angle of attack.

Turbulence Contours

The turbulence contour shows the distribution and intensity of turbulence around the airfoil.

Turbulence contours of the four leaves are shown below

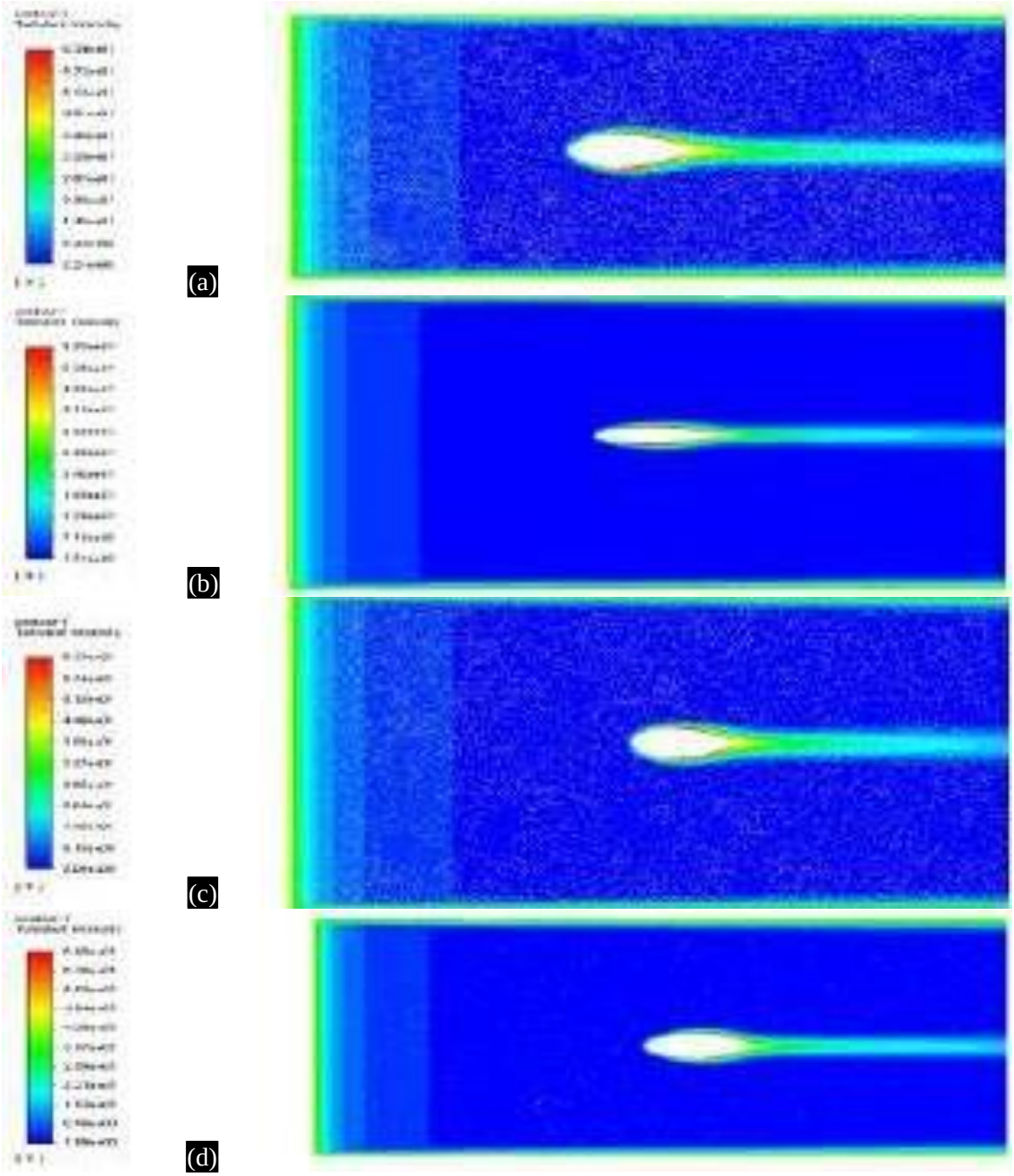

Figure 21. Turbulence contour at 0° angle of attack (at 10m/s). (a) Javaplum leaf, (b) Ixora leaf, (c) Custard apple leaf, (d) Sapota leaf

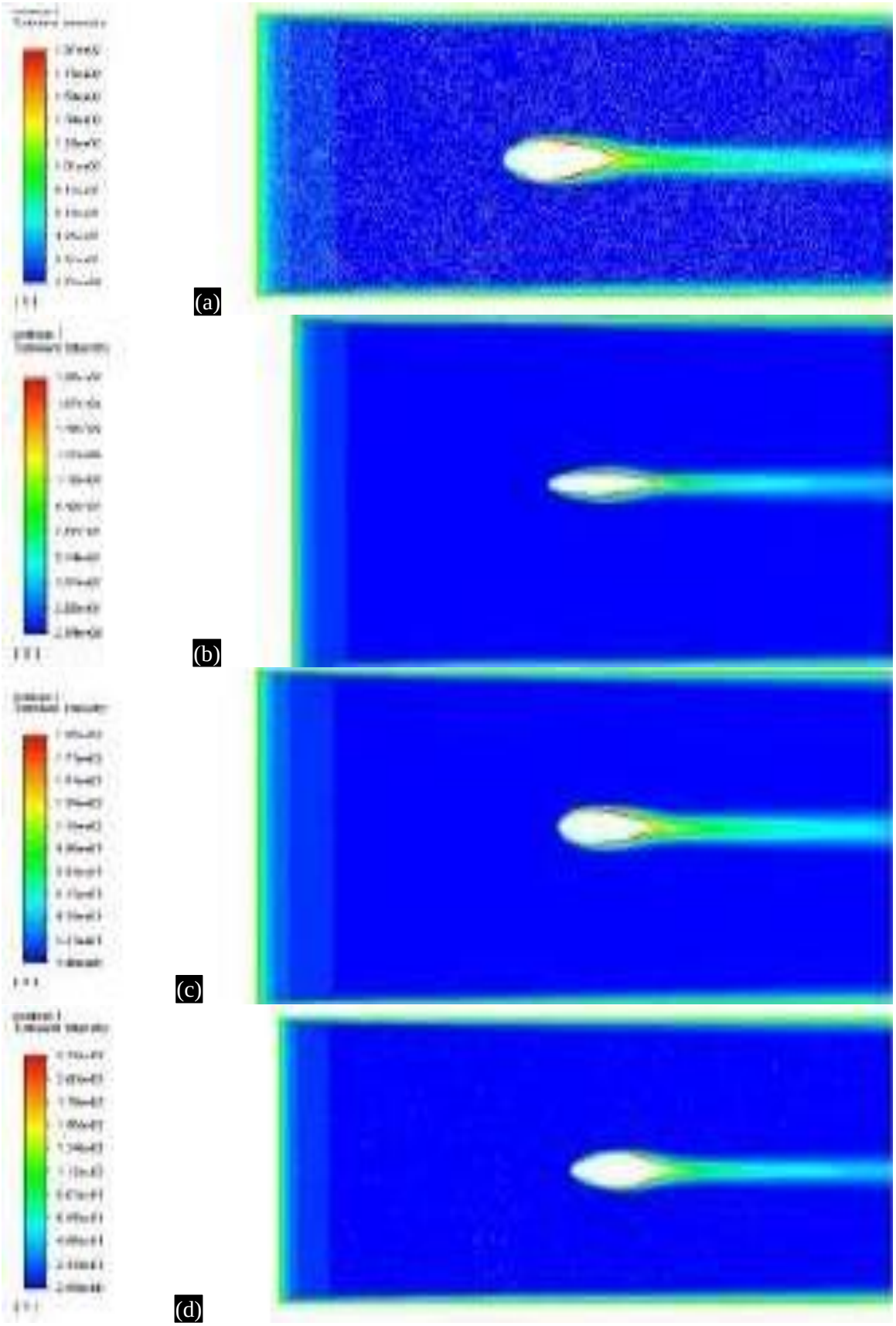

Figure 22. Turbulence contour at 0° angle of attack (at 37m/s). (a) Javaplum leaf, (b) Ixora leaf, (c) Custard apple leaf, (d) Sapota leaf

By observing Figure 21 and Figure 22, the turbulence intensity is even around all the values and the contours look similar for all the leaves for different velocities.

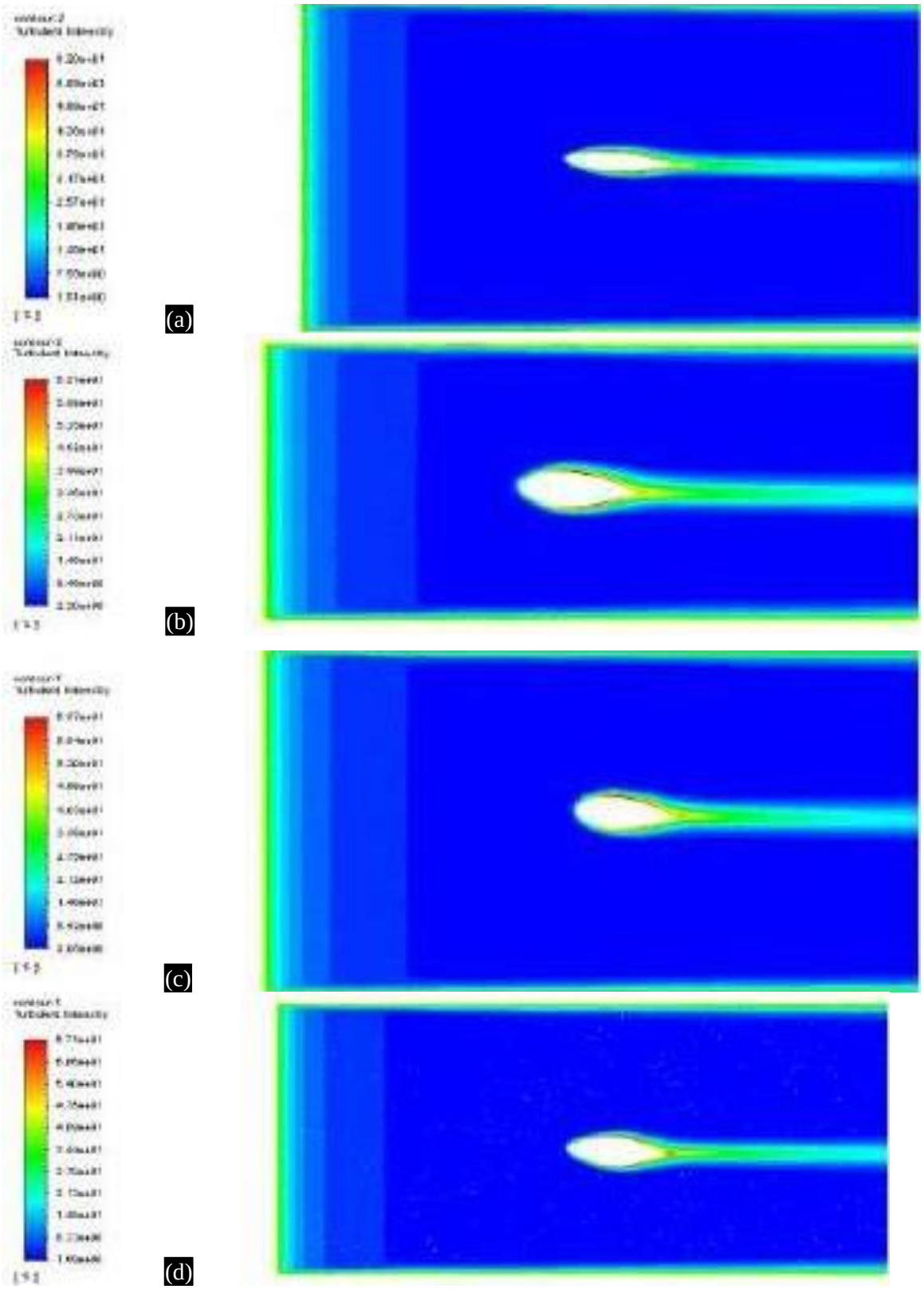

Figure 23. Turbulence contour at 4° angle of attack (at 10m/s). (a) Javaplum leaf, (b) Ixora leaf, (c) Custard apple leaf, (d) Sapota leaf

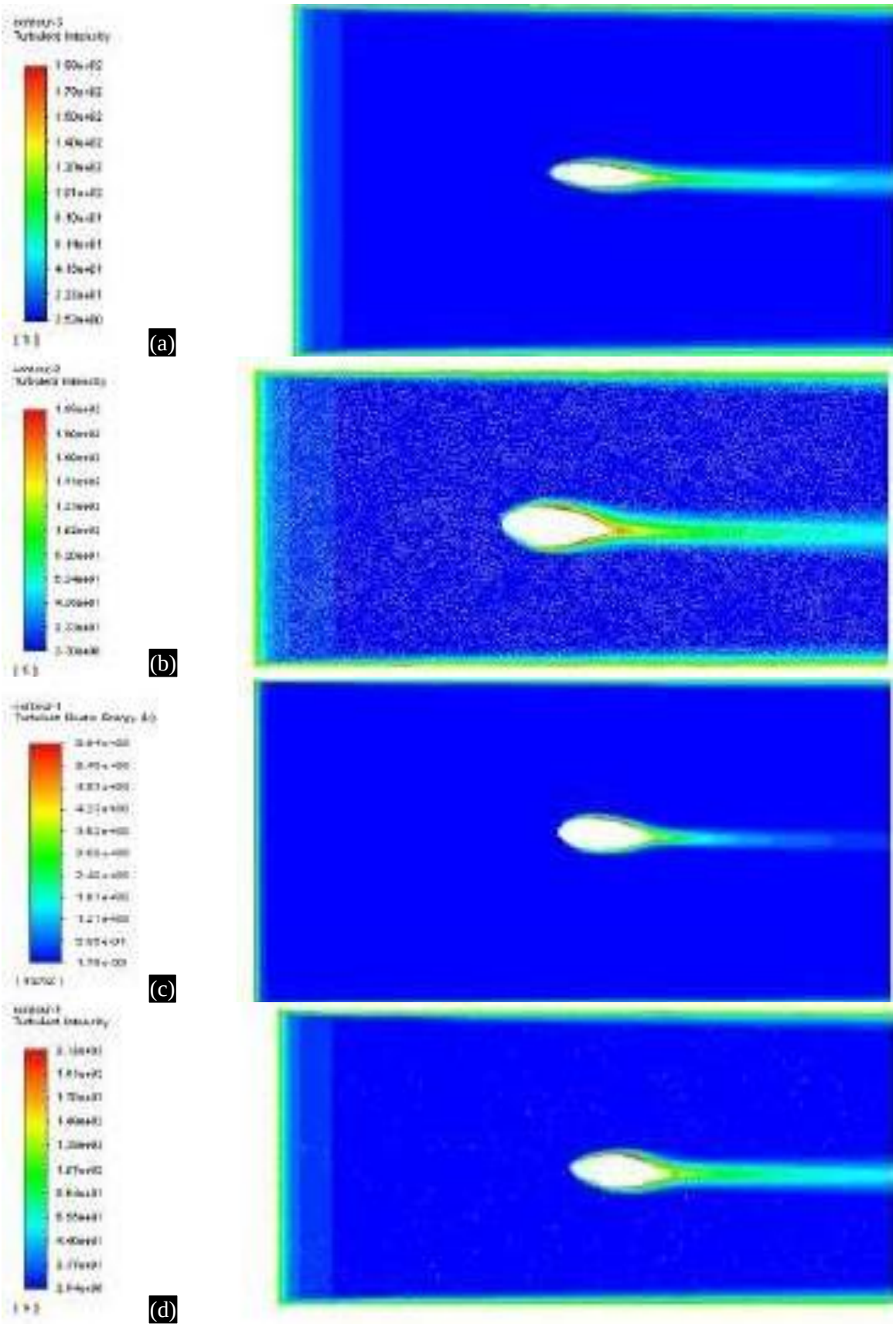

Figure 24. Turbulence contour at 4° angle of attack (at 37m/s). (a) Javaplum leaf, (b) Ixora leaf, (c) Custard apple leaf, (d) Sapota leaf

By observing Figure 23 and Figure 24, the turbulence intensity is found to be higher near the trailing edge for all the leaves.

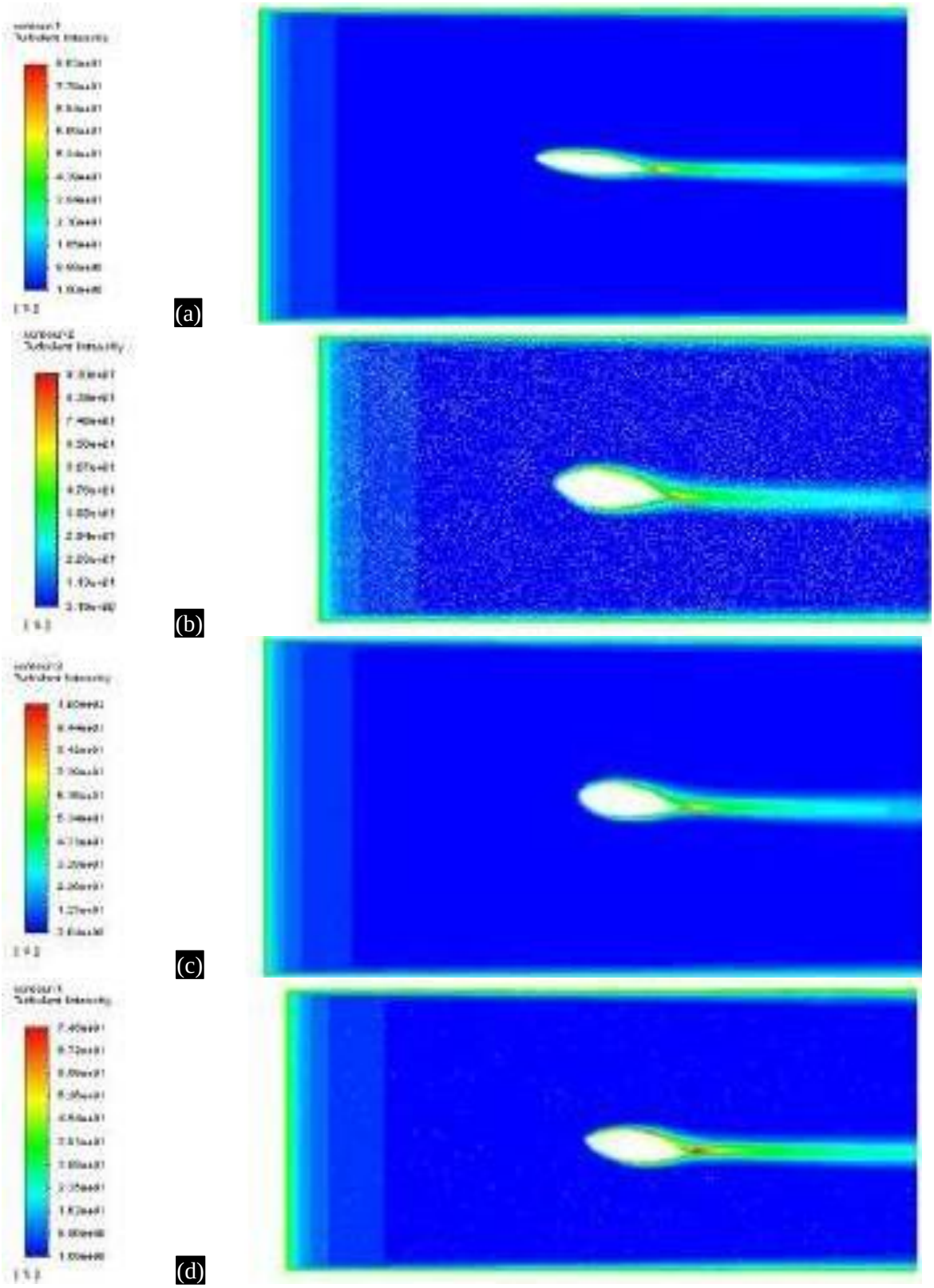

Figure 25. Turbulence contour at 8° angle of attack (at 10m/s). (a) Javaplum leaf, (b) Ixora leaf, (c) Custard apple leaf, (d) Sapota leaf

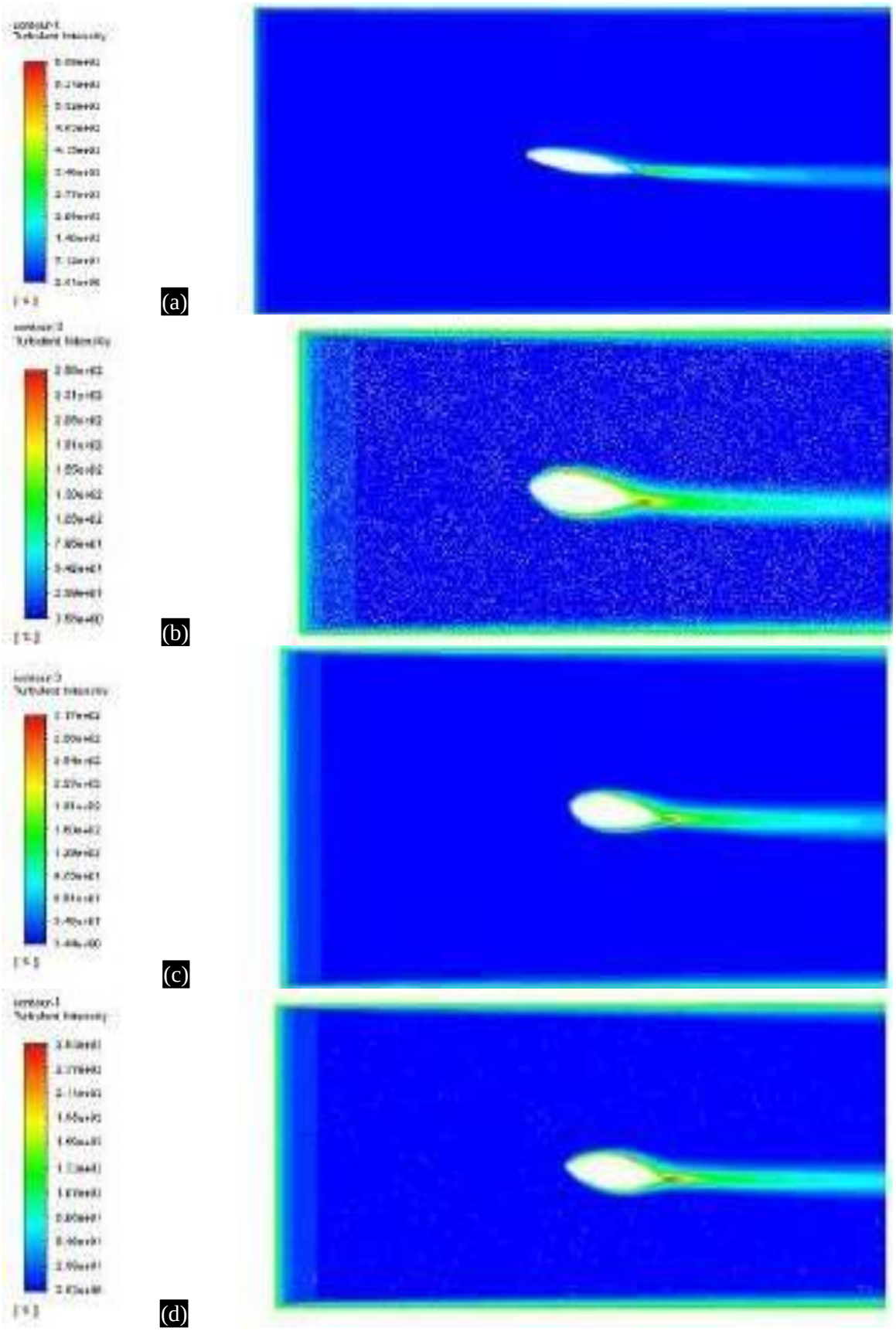

Figure 26. Turbulence contour at 8° angle of attack (at 37m/s). (a) Javaplum leaf, (b) Ixora leaf, (c) Custard apple leaf, (d) Sapota leaf

By observing Figure 25 and Figure 26, the turbulence intensity is found to be higher near the trailing edge for all the leaves like the before case. And the value has increased gradually from 4° angle of attack to 8° angle of attack.

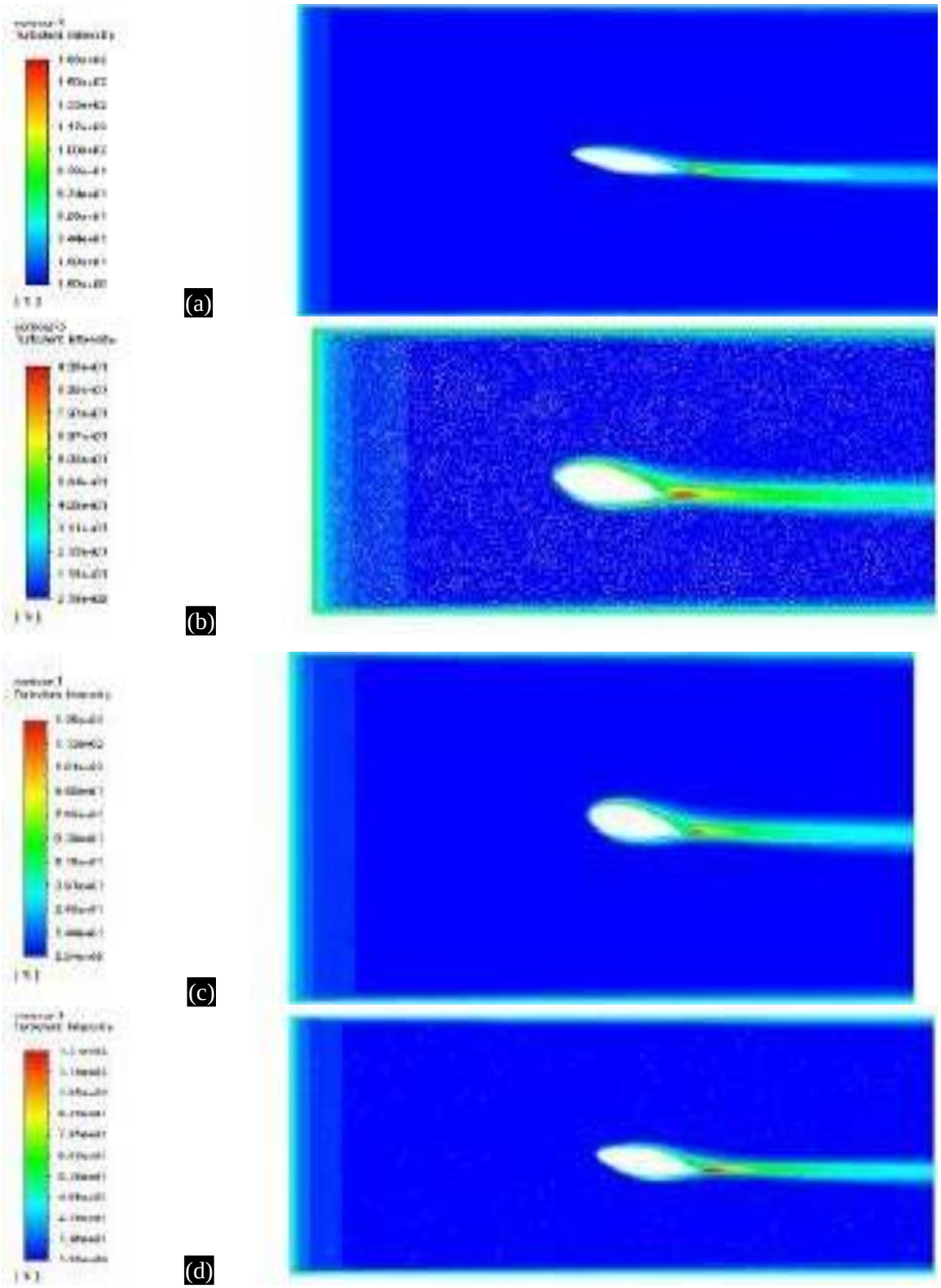

Figure 27. Turbulence contour at 12° angle of attack (at 10m/s). (a) Javaplum leaf, (b) Ixora leaf, (c) Custard apple leaf, (d) Sapota leaf

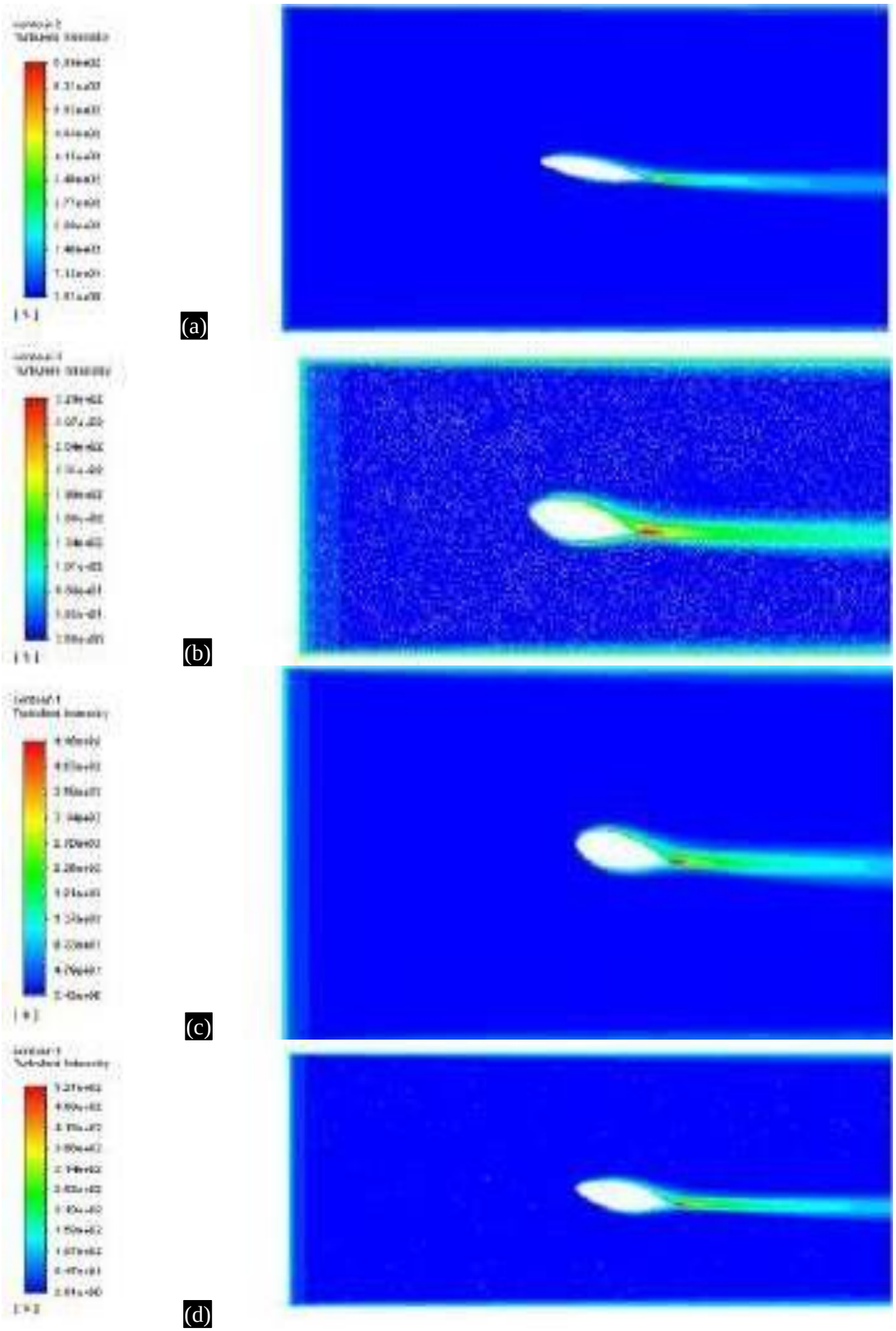

Figure 28. Turbulence contour at 12° angle of attack (at 37m/s). (a) Javaplum leaf, (b) Ixora leaf, (c) Custard apple leaf, (d) Sapota leaf

By observing Figure 27 and Figure 28 the turbulence has increased abruptly for all leaves.

As a summary referring to all the 8 Figures (Figures 21-28), we can notice that the turbulence is higher at the trailing edge of the leaf. Javaplum (Figure 28 (a)) has the highest turbulence percentage.

RESULTS AND DISCUSSION

Original Coordinate values

The leaves were analyzed with its original coordinates to give the following data.

Table 3. Pressure, velocity, turbulence, C_l and C_d values of Javaplum leaf.

Leaf	Velocity	AOA	Contours	min	max	C_l	C_d	C_l/C_d
Javaplum	10	0	static pressure(Pa)	-39.057	59.078	0.2645381	10.338237	0.02558832
			dynamic pressure(Pa)	2.149	96.96			
			velocity(m/s)	0	12.581			
			turbulence(%)	1.5118	58.274			
		4	static pressure(Pa)	-57.06	60.039	8.2742906	10.670967	0.77540214
			dynamic pressure(Pa)	1.631	113.97			
			velocity(m/s)	0	13.64			
			turbulence(%)	1.502	61.959			
		8	static pressure(Pa)	-101.82	59.83	13.42542	11.692517	1.14820616
			dynamic pressure(Pa)	0.157	131.38			
			velocity(m/s)	0	14.55			
			turbulence(%)	1.498	86.33			
		12	static pressure(Pa)	-231.64	61.217	18.349139	14.389885	1.27514146
			dynamic pressure(Pa)	0.00527	213.64			
			velocity(m/s)	0	18.668			
			turbulence(%)	1.4966	166.164			
	37	0	static pressure(Pa)	-536.65	805.226	4.3279609	112.73585	0.03839028
			dynamic pressure(Pa)	30.35	1329.96			
			velocity(m/s)	0	46.597			
			turbulence(%)	2.543	185.451			
		4	static pressure(Pa)	-806.51	820.48	128.40906	117.51157	1.09273546
			dynamic pressure(Pa)	23.12	1583.779			
			velocity(m/s)	0	50.85			
			turbulence(%)	2.531	198.75			
		8	static pressure(Pa)	-1495.63	816.248	203.144	131.00812	1.55062144
			dynamic pressure(Pa)	13.608	1893.004			
			velocity(m/s)	0	54.52			
			turbulence(%)	2.515	204.047			
		12	static pressure(Pa)	-3512.904	841.265	286.63779	168.42567	1.70186522
			dynamic pressure(Pa)	0.149	3180.37			
			velocity(m/s)	0	72.029			
			turbulence(%)	2.508	689.355			

Table 4. Pressure, velocity, turbulence, C_l and C_d values of Sapota leaf.

Leaf	Velocity	AOA	Contours	min	max	C_l	C_d	C_l/C_d
Sapota	10	0	static pressure(Pa)	-76.353	59.396	2.1466	9.8782	0.2173
			dynamic pressure(Pa)	1.909	130.033			
			velocity(m/s)	0	14.5704			
			turbulence(%)	1.6926	69.791			
		4	static pressure(Pa)	-79.027	59.617	5.6897	10.013	0.5682
			dynamic pressure(Pa)	0.0218	134.664			
			velocity(m/s)	0	14.827			
			turbulence(%)	1.6893	67.112			
		8	static pressure(Pa)	-88.297	60.964	10.216	10.886	0.9384
			dynamic pressure(Pa)	0.00883	142.329			
			velocity(m/s)	0	15.243			
			turbulence(%)	1.6806	74.489			
		12	static pressure(Pa)	-124.981	61.9294	13.858	12.4633	1.1119
			dynamic pressure(Pa)	0.0150	154.998			
			velocity(m/s)	0	15.9059			
			turbulence(%)	1.6760	131.390			
	37	0	static pressure(Pa)	-1045.83	807.816	27.584	106.0466	0.2601
			dynamic pressure(Pa)	27.7960	1779.96			
			velocity(m/s)	0	53.907			
			turbulence(%)	2.8470	221.589			
		4	static pressure(Pa)	-1140.14	808.875	100.588	107.94	0.9318
			dynamic pressure(Pa)	10.1936	1893.60			
			velocity(m/s)	0	55.602			
			turbulence(%)	2.8404	211.632			
		8	static pressure(Pa)	-1276.68	833.492	169.67	120.399	1.4092
			dynamic pressure(Pa)	0.1334	2012.42			
			velocity(m/s)	0	57.319			
			turbulence(%)	2.8201	262.720			
		12	static pressure(Pa)	-1941.85	850.232	221.452	142.044	1.5590
			dynamic pressure(Pa)	0.1043	2262.04			
			velocity(m/s)	0	60.764			
			turbulence(%)	2.81052	521.343			

Table 5. Pressure, velocity, turbulence, C_l and C_d values of Custard apple leaf.

Leaf	Velocity	AOA	Contours	min	max	C_l	C_d	C_l/C_d
Custard apple	10	0	static pressure(Pa)	-93.6	60	1.9477	8.0285	0.24259824
			dynamic pressure(Pa)	1.58	141			
			velocity(m/s)	0	15.2			
			turbulence(%)	2.05	63.3			
		4	static pressure(Pa)	-114	59.3	7.1308	8.1745	0.87232247
			dynamic pressure(Pa)	73.2	161			
			velocity(m/s)	0	16.2			

			turbulence(%)	2.05	65.7			
		8	static pressure(Pa)	137	60.7	11.8291	8.9874	1.31618711
			dynamic pressure(Pa)	0.0183	181			
			velocity(m/s)	0	17.2			
			turbulence(%)	2.04	105			
		12	static pressure(Pa)	-159	61.4	15.6882	10.184	1.54047526
			dynamic pressure(Pa)	0.0166	196			
			velocity(m/s)	0	17.9			
			turbulence(%)	3.42	448			
	37	0	static pressure(Pa)	-1310	815	38.087	86.544	0.44008828
			dynamic pressure(Pa)	23.6	1990			
			velocity(m/s)	0	56.8			
			turbulence(%)	3.46	196			
		4	static pressure(Pa)	-1620	812	121.191	88.412	1.37075284
			dynamic pressure(Pa)	32	2270			
			velocity(m/s)	0	60.9			
			turbulence(%)	3.44	201			
		8	static pressure(Pa)	-1970	832	191.95	98.81	1.94261714
			dynamic pressure(Pa)	2.66	2550			
			velocity(m/s)	0	64.6			
			turbulence(%)	2.04	105			
		12	static pressure(Pa)	-2300	839	249.44	114.922	2.17051565
			dynamic pressure(Pa)	-0.267	2790			
			velocity(m/s)	0	67.5			
			turbulence(%)	3.42	448			

Table 6. Pressure, velocity, turbulence, C_l and C_d values of Ixora leaf.

Leaf	Velocity	AOA	Contours	min	max	C_l	C_d	C_l/C_d
Ixora live plant	10	0	static pressure(Pa)	-89.2	60.1	2.3440082	7.6684251	0.305670
			dynamic pressure(Pa)	2.01	141			
			velocity(m/s)	0	15.1			
			turbulence(%)	2.21	63.4			
		4	static pressure(Pa)	-10.9	60.3	4.2097551	8.0112506	0.525480
			dynamic pressure(Pa)	57.4	156			
			velocity(m/s)	0	16			
			turbulence(%)	2.2	65.1			
		8	static pressure(Pa)	-131	62.2	6.6760486	8.6857284	0.768622
			dynamic pressure(Pa)	970	175			
			velocity(m/s)	0	16.9			
			turbulence(%)	2.19	93			
		12	static pressure(Pa)	-143	62.8	7.4357962	10.249361	0.725488
			dynamic pressure(Pa)	0.013	184			
			velocity(m/s)	0	17.3			
			turbulence(%)	2.19	98.6			

	37	0	static pressure(Pa)	-1240	816	36.136454	81.269164	0.444651
			dynamic pressure(Pa)	29.3	1960			
			velocity(m/s)	0	56.5			
			turbulence(%)	3.72	197			
		4	static pressure(Pa)	-1550	824	66.222454	86.159408	0.768603
			dynamic pressure(Pa)	26.5	2180			
			velocity(m/s)	0	59.7			
			turbulence(%)	3.7	199			
		8	static pressure(Pa)	-1870	848	103.88624	95.050101	1.09296
			dynamic pressure(Pa)	7.37	2480			
			velocity(m/s)	0	63.7			
			turbulence(%)	3.68	256			
		12	static pressure(Pa)	-2080	859	116.04162	115.55067	1.00424
			dynamic pressure(Pa)	23.5	2620			
			velocity(m/s)	0	65.4			
			turbulence(%)	3.68	329			

Table 7. Pressure, velocity, turbulence, C_l and C_d values of Mango leaf.

Leaf	**Velocity**	**AOA**	**Contours**	**min**	**max**	**C_l**	**C_d**	**C_l/C_d**
Mango	10	0	static pressure(Pa)	-67	60.4	-5.58311	12.3962	-0.45038883
			dynamic pressure(Pa)	1.84	12.3			
			velocity(m/s)	0	14.2			
			turbulence(%)	1.3	63.6			
		4	static pressure(Pa)	-66.6	60.6	-1.08271	12.5505	-0.08626828
			dynamic pressure(Pa)	1.33	109			
			velocity(m/s)	0	13.3			
			turbulence(%)	1.31	58.7			
		8	static pressure(Pa)	-180	61.4	1.10788	14.4273	0.07679053
			dynamic pressure(Pa)	0.00832	181			
			velocity(m/s)	0	17.1			
			turbulence(%)	1.31	86.7			
		12	static pressure(Pa)	-321	62.2	4.60873	16.6785	0.27632761
			dynamic pressure(Pa)	-0.00571	292			
			velocity(m/s)	0	21.8			
			turbulence(%)	1.31	129			
	37	0	static pressure(Pa)	-95.3	817	-88.736	136.523	-0.64997107
			dynamic pressure(Pa)	29.7	1710			
			velocity(m/s)	0	52.9			
			turbulence(%)	2.18	203			
		4	static pressure(Pa)	-900	827	-18.0337	138.802	-0.12992392
			dynamic pressure(Pa)	18.1	1500			
			velocity(m/s)	0	49			
			turbulence(%)	2.2	187			
		8	static pressure(Pa)	-2580	834	22.5439	164.417	0.13711417

			dynamic pressure(Pa)	-0.0216	2580			
			velocity(m/s)	0	64.3			
			turbulence(%)	2.2	278			
		12	static pressure(Pa)	-4730	851	74.138	192.094	0.38594646
			dynamic pressure(Pa)	0.155	4220			
			velocity(m/s)	0	83			
			turbulence(%)	2.19	526			

Table 8. Pressure, velocity, turbulence, C_l and C_d values of Pumpkin ash leaf.

Leaf	Velocity	AOA	Contours	min	max	C_l	C_d	C_l/C_d
Pumpkin ash	10	0	static pressure(Pa)	-116	61.7	-1.62477	12.27395	-0.132375
			dynamic pressure(Pa)	0.0094	167			
			velocity(m/s)	0	16.5			
			turbulence(%)	1.6	71.8			
		4	static pressure(Pa)	-103	62	3.39311	12.36727	0.274362
			dynamic pressure(Pa)	0.0035	155			
			velocity(m/s)	0	15.9			
			turbulence(%)	1.61	70.7			
		8	static pressure(Pa)	-115	62.1	6.78658	12.59276	0.538927
			dynamic pressure(Pa)	0.0112	165			
			velocity(m/s)	0	16.4			
			turbulence(%)	1.61	69.9			
		12	static pressure(Pa)	-119	63.2	10.2262	14.83234	0.689454
			dynamic pressure(Pa)	0.011	171			
			velocity(m/s)	0	16.7			
			turbulence(%)	1.62	142			
	37	0	static pressure(Pa)	-1700	829	-66.6488	131.9206	-0.505218
			dynamic pressure(Pa)	0.111	2400			
			velocity(m/s)	0	62.4			
			turbulence(%)	2.68	225			
		4	static pressure(Pa)	-1400	842	30.0133	132.0311	0.227319
			dynamic pressure(Pa)	2.3	2110			
			velocity(m/s)	0	58.8			
			turbulence(%)	2.7	220			
		8	static pressure(Pa)	-1680	848	127.2620	136.3326	0.933467
			dynamic pressure(Pa)	4.59	2340			
			velocity(m/s)	0	61.8			
			turbulence(%)	2.71	220			
		12	static pressure(Pa)	-1790	865	184.84901	164.2351	1.12551
			dynamic pressure(Pa)	0.2	2490			
			velocity(m/s)	0	63.7			
			turbulence(%)	2.7	677			

Table 9. Pressure, velocity, turbulence, C_l and C_d values of Upas tree leaf.

Leaf	Velocity	AOA	Contours	min	max	C_l	C_d	C_l/C_d
Upas tree	10	0	static pressure(Pa)	-101	56.2	-0.03446	1.70469	-0.02022
			dynamic pressure(Pa)	0.0000367	142			
			velocity(m/s)	0	15.2			
			turbulence(%)	2.35	57.1			
		4	static pressure(Pa)	-136	58.5	1.617401	5.17522	0.312528
			dynamic pressure(Pa)	0.000104	165			
			velocity(m/s)	0	16.3			
			turbulence(%)	1.59	63.1			
		8	static pressure(Pa)	-173	58.9	3.17151	5.7146	0.554985
			dynamic pressure(Pa)	0.000224	198			
			velocity(m/s)	0	17.8			
			turbulence(%)	1.57	70.2			
		12	static pressure(Pa)	-174	62.3	4.091724	7.1106827	0.575433
			dynamic pressure(Pa)	0.00669	199			
			velocity(m/s)	0	17.4			
			turbulence(%)	3.27	84.7			
	37	0	static pressure(Pa)	-1350	783	10.94048	58.630063	0.186602
			dynamic pressure(Pa)	0.0933	1970			
			velocity(m/s)	0	55			
			turbulence(%)	5.54	187			
		4	static pressure(Pa)	-1.65	787	22.7717	60.5741	0.375933
			dynamic pressure(Pa)	0.225	2.11			
			velocity(m/s)	0	58.2			
			turbulence(%)	5.57	183			
		8	static pressure(Pa)	-2390	798	43.49160	64.4536	0.674773
			dynamic pressure(Pa)	0.0336	2770			
			velocity(m/s)	0	62.7			
			turbulence(%)	6.86	209			
		12	static pressure(Pa)	-2430	848	57.9599	81.8272	0.708321
			dynamic pressure(Pa)	0.081	2800			
			velocity(m/s)	0	65.1			
			turbulence(%)	5.55	297			

Table 10. Pressure, velocity, turbulence, C_l and C_d values of Curry leaf.

Leaf	Velocity	AOA	Contours	min	max	C_l	C_d	C_l/C_d
Curry leaf	10	0	static pressure(Pa)	-96.4	59.1	-2.60897	9.939101	-0.26249
			dynamic pressure(Pa)	0.0365	145			
			velocity(m/s)	0	15.4			
			turbulence(%)	1.87	68.1			
		4	static pressure(Pa)	-104	59	-0.70316	10.094518	-0.0696
			dynamic pressure(Pa)	0.0499	153			
			velocity(m/s)	0	15.8			

			turbulence(%)	1.87	71			
		8	static pressure(Pa)	-121	61.3	2.92231	10.894639	0.268234
			dynamic pressure(Pa)	0.0063	170			
			velocity(m/s)	0	16.6			
			turbulence(%)	1.87	70.7			
		12	static pressure(Pa)	-144	62.7	10.4373	12.186685	0.856456
			dynamic pressure(Pa)	0.0152	191			
			velocity(m/s)	0	17.7			
			turbulence(%)	1.87	83			
	37	0	static pressure(Pa)	-1370	812	-70.029	107.23127	-0.65306
			dynamic pressure(Pa)	8.16	2050			
			velocity(m/s)	0	57.9			
			turbulence(%)	3.14	214			
		4	static pressure(Pa)	-1470	811	19.776	108.79093	0.181786
			dynamic pressure(Pa)	14.8	2150			
			velocity(m/s)	0	59.3			
			turbulence(%)	3.15	226			
		8	static pressure(Pa)	-1740	836	83.7025	119.3098	0.70155
			dynamic pressure(Pa)	0.273	2390			
			velocity(m/s)	0	62.4			
			turbulence(%)	3.15	219			
		12	static pressure(Pa)	-2070	859	184.8792	136.92	1.35027
			dynamic pressure(Pa)	0.0267	2700			
			velocity(m/s)	0	66.4			
			turbulence(%)	3.15	312			

Table 11. Pressure, velocity, turbulence, C_l and C_d values of Adadhoda leaf.

Leaf	**Velocity**	**AOA**	**Contours**	**min**	**max**	**C_l**	**C_d**	**C_l/C_d**
Adadhoda	10	0	static pressure(Pa)	-101	59.7	0.9092	10.094	0.09
			dynamic pressure(Pa)	1.26	150			
			velocity(m/s)	0	15.7			
			turbulence(%)	1.73	69.9			
		4	static pressure(Pa)	-105	60.4	4.4392	10.2182	0.4344
			dynamic pressure(Pa)	-0.0327	156			
			velocity(m/s)	0	16			
			turbulence(%)	1.73	71.4			
		8	static pressure(Pa)	-117	61.3	8.4116	10.9018	0.7715
			dynamic pressure(Pa)	0.00519	168			
			velocity(m/s)	0	16.6			
			turbulence(%)	1.72	116			
		12	static pressure(Pa)	-131	62.5	12.1308	12.3571	0.9816
			dynamic pressure(Pa)	0.0182	180			
			velocity(m/s)	0	17.1			
			turbulence(%)	1.72	124			

	37	0	static pressure(Pa)	-1360	811	16.3920	108.449	0.1511
			dynamic pressure(Pa)	27.2	2070			
			velocity(m/s)	0	58.2			
			turbulence(%)	2.92	219			
		4	static pressure(Pa)	-1500	825	83.7781	110.641	0.7572
			dynamic pressure(Pa)	12.7	2200			
			velocity(m/s)	0	59.9			
			turbulence(%)	2.91	226			
		8	static pressure(Pa)	-1680	844	141.434	119.857	1.180
			dynamic pressure(Pa)	-0.428	2380			
			velocity(m/s)	0	62.3			
			turbulence(%)	2.89	386			
		12	static pressure(Pa)	-1920	854	205.929	139.037	1.4811
			dynamic pressure(Pa)	0.121	2580			
			velocity(m/s)	0	64.9			
			turbulence(%)	2.89	477			

From Table 3, we can infer that the Javaplum leaf achieve higher lift along with increasing drag with elevated angles of attack and velocities. There are positive C_l/C_d ratios for Javaplum leaf noted to be as 1.148 and 1.275 at 8° and 12° angle of attacks respectively for 10 m/s and 1.092, 1.550 and 1.701 at

4°, 8° and 12° angle of attacks for 37 m/s.

From Table 4, we can infer that the Sapota leaf exhibits an ascending trend in both lift (C_l) and drag (C_d) coefficients as angles of attack and velocities increase. There are positive C_l/C_d ratios for Sapota leaf noted to be as 1.111 at 12° angle of attacks for 10 m/s and at 1.409 and 1.559 respectively at 8° and 12° angle of attacks for 37 m/s.

From Table 5, we can infer that the Custard apple leaf shows an increase in lift (C_l) and drag (C_d) with increasing angles of attack and velocities. The C_l/C_d ratio varies across different scenarios. There are positive C_l/C_d ratios for Custard apple leaf noted to be as 1.316 and 1.540 respectively at 8° and 12° angle of attacks for 10 m/s and 1.370, 1.942 and 2.170 respectively at 4°, 8° and 12° angle of attacks for 37 m/s.

From Table 6, Ixora leaf shows increased lift (C_l) and drag (C_d) with higher angles of attack and velocities. There are positive C_l/C_d ratios for Ixora live plant leaf noted to be as 1.092 and 1.004 respectively at 8° and 12° angle of attacks for 37 m/s.

From Table 7, we can infer that the Mango leaf's aerodynamics exhibit a transition from negative to positive lift (C_l) with increasing angles of attack. Concurrently, drag (C_d) rises with higher angles of attack, peaking at the same conditions. However, there is no value of C_l/C_d that is greater than one.

From the Table 8, we can infer that the Pumpkin ash shows a transition from negative to positive lift (C_l) as angles of attack increase. Correspondingly, drag (C_d) elevates with higher angles of attack and increasing velocity. There is a positive C_l/C_d ratio for Pumpkin ash leaf noted to be as **1.125** at 12° angle of attack for 37 m/s.

From Table 9, we can infer that the Upas tree leaf exhibits varying lift (C_l) and drag (C_d) across different angles of attack. Lift increases with angle and velocity, with increasing drag. The C_l/C_d ratio

fluctuates, indicating the leaf's dynamic lift-to-drag balance under changing wind conditions. However, there is no value of C_l/C_d that is greater than one.

From Table 10, we can infer that the Curry leaf shows increasing trend of lift and drag for increasing velocity and angle of attack. There is a positive C_l/C_d ratio for Curry leaf noted to be as 1.350 at 12° angle of attack for 37 m/s.

From the Table 11, we can infer that the Adadhoda leaf shows varying lift (C_l) and drag (C_d) across different angles of attack. There are positive C_l/C_d ratios for Adadhoda leaf noted to be as 1.180 and 1.481 respectively at 8° and 12° angle of attack for 37 m/s.

In general, the Tables 3-11 shows the values of pressure, velocity, turbulence, C_l and C_d values of the 9 leaves chosen. Of these Javaplum leaf (Table 3), Sapota leaf (Table 4), Custard apple leaf (Table 5) and Ixora leaf (Table 7) give higher values of lift and has a C_l/C_d ratio greater than one for both the velocities at least for one angle of attack. This indicates better lift generation. These 4 leaves are taken for further analysis.

Modified Values

Javaplum, Sapota, Custard apple and Ixora leaves are scaled to have a 1-metre chord length and the analysis was done again.

Table 12. C_l and C_d values of Modified Javaplum leaf.

Leaf	Velocity	AOA	C_l	C_d	C_l/C_d
Modified Javaplum	10	0	1.607798	4.642056	0.346355
		4	4.57006	4.83864	0.944493
		8	7.088265	5.535504	1.280509
		12	8.278254	6.730153	1.230025
	37	0	24.11607	48.86087	0.493566
		4	65.05724	51.46523	1.264101
		8	100.3892	60.69422	1.654015
		12	118.7785	76.61499	1.55033

Table 13. C_l and C_d values of Modified Ixora plant leaf.

Leaf	Velocity	AOA	C_l	C_d	C_l/C_d
Modified Ixora live plant	10	0	0.255275	6.75549	0.037788
		4	1.838907	6.901634	0.266445
		8	3.50773	7.161669	0.489792
		12	5.133913	8.165405	0.62874
	37	0	3.275747	74.02539	0.044252
		4	28.18634	76.44121	0.368732
		8	52.85224	76.56887	0.690257
		12	76.48647	92.67597	0.825311

Table 14. C_l and C_d values of Modified Custard apple leaf.

Leaf	Velocity	AOA	C_l	C_d	C_l/C_d
Modified Custard apple	10	0	0.846471	6.683716	0.126647
		4	0.96018	6.868567	0.139793
		8	3.277391	7.177195	0.45664
		12	5.306188	8.181655	0.648547
	37	0	9.166268	73.90224	0.124032
		4	17.58017	76.44031	0.229986
		8	54.07178	80.40015	0.672533
		12	82.44811	93.52023	0.881607

Table 15. C_l and C_d values of Modified Sapota leaf.

Leaf	Velocity	AOA	C_l	C_d	C_l/C_d
Modified Sapota	10	0	-0.76324	5.671213	-0.13458
		4	1.596083	5.803481	0.275022
		8	3.615009	6.141334	0.588636
		12	5.40684	6.746139	0.801472
	37	0	-9.99508	60.493	-0.16523
		4	25.65262	62.05738	0.413369
		8	53.73565	66.51038	0.807929
		12	79.21127	74.54065	1.062659

Tables 12-15 shows values of co-efficient of lift and co-efficient of drag values obtained for the Javaplum leaf, Ixora live plant leaf, Custard apple leaf, and Sapota leaf which is scaled to 1-metre chord length. The C_l/C_d ratio for the chosen 4 leaves is greater than 1 in this case also. These leaves are taken for further analysis.

Remodified values

Javaplum, Ixora live plant, Custard apple, and Sapota leaves are then reduced to 15% thickness (which is suggested to be optimum thickness of an airfoil) and the values of C_l and C_d are obtained by analysis.

Table 16 C_l and C_d values of Remodified Javaplum leaf.

Leaf	Velocity	AOA	C_l	C_d	C_l/C_d
Remodified Javaplum	10	0	0.323245	2.57621	0.125473
		4	2.399198	5.077675	0.472499
		8	7.811642	20.89149	0.373915
		12	9.772419	26.80807	0.364533
	37	0	4.561112	25.38637	0.179668
		4	32.75857	60.99067	0.537108
		8	38.46992	118.9012	0.323545
		12	130.8962	356.8663	0.366793

Table 17. C_l and C_d values of Remodified Ixora live plant leaf.

Leaf	Velocity	AOA	C_l	C_d	C_l/C_d
Remodified Ixora Live plant	10	0	0.130816	3.752563	0.03486
		4	2.265446	4.379502	0.517284
		8	2.273593	9.89947	0.229668
		12	3.997144	22.85892	0.174861
	37	0	1.888658	38.15645	0.049498
		4	30.35216	46.5624	0.65186
		8	27.1034	102.2463	0.265079
		12	53.63536	301.1048	0.178129

Table 18 C_l and C_d values of Remodified Custard apple leaf.

Leaf	Velocity	AOA	C_l	C_d	C_l/C_d
Remodified Custard apple	10	0	0.055721	2.740022	0.020336
		4	2.558535	3.051562	0.838435
		8	4.525758	4.514057	1.002592
		12	80.11957	107.5695	0.744817
	37	0	0.97094	27.28353	0.035587
		4	34.98665	31.21208	1.120933
		8	62.77099	49.3526	1.271888
		12	53.63636	301.1048	0.178132

Table 19. C_l and C_d values of Remodified Sapota leaf.

Leaf	Velocity	AOA	C_l	C_d	C_l/C_d
Remodified Sapota	10	0	-0.22527	2.956115	-0.07621
		4	2.817432	3.728382	0.755671
		8	5.616914	14.02782	0.400412
		12	14.63935	52.04795	0.281267
	37	0	-2.50587	29.28211	-0.08558
		4	38.98552	39.91668	0.976672
		8	67.33482	118.1917	0.569708
		12	159.7906	590.6357	0.27054

Tables 16-19 shows values of co-efficient of lift and co-efficient of drag values obtained for the Javaplum leaf, Ixora live plant leaf, Custard apple leaf, and Sapota leaf which has 15% thickness. The leaves of- Javaplum (Table 16), Ixora plant (Table 17), Sapota (Table 19) shows poor lift generation in this case and also has boundary layer separations. Custard apple seems to generate good amount of lift in this case. The contours of pressure, velocity, turbulence of Custard apple leaf with 15% thickness are taken.

Contours of 15% thickness Custard apple leaf

Redefining Custard apple leaves to 15% thickness shows increased lift without boundary layer separation. Figures 29-40 illustrate pressure, velocity, and turbulence contours for airspeeds of 10 m/s and 37 m/s at different angles of attack. These visual representations offer insights into the aerodynamic behaviour of the leaves under varying conditions, aiding in the understanding of how airflow, pressure, and turbulence affect lift for 15% thickness modified design.

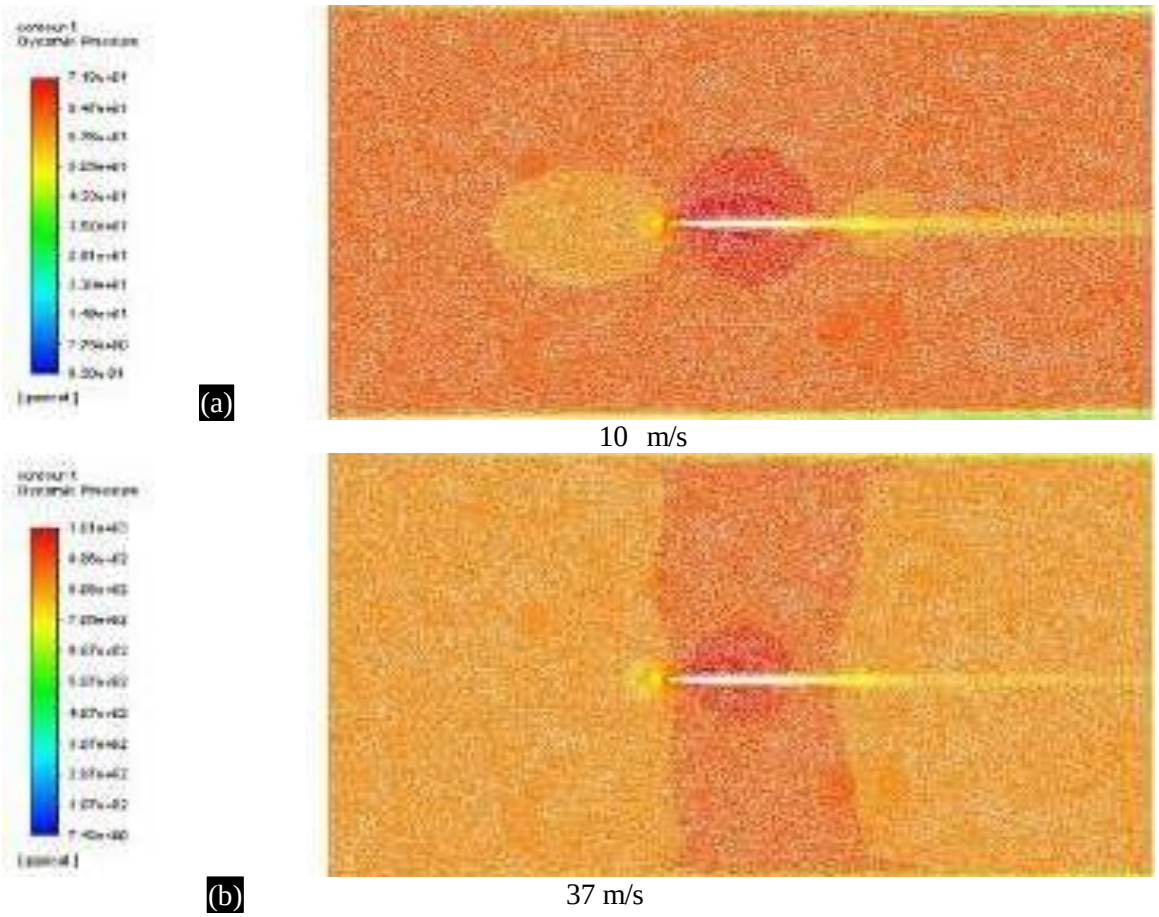

Figure 29. Pressure contour at 0° angle of attack.

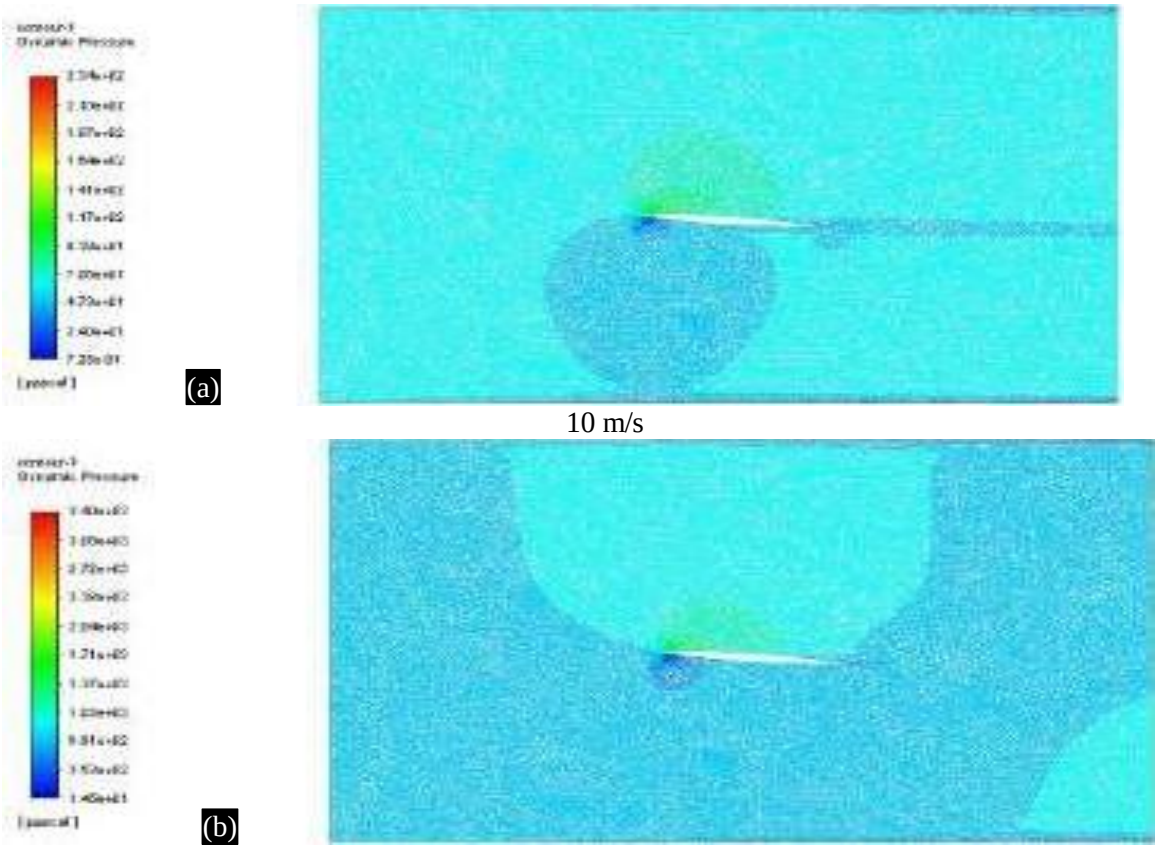

Figure 30. Pressure contour at 4° angle of attack.

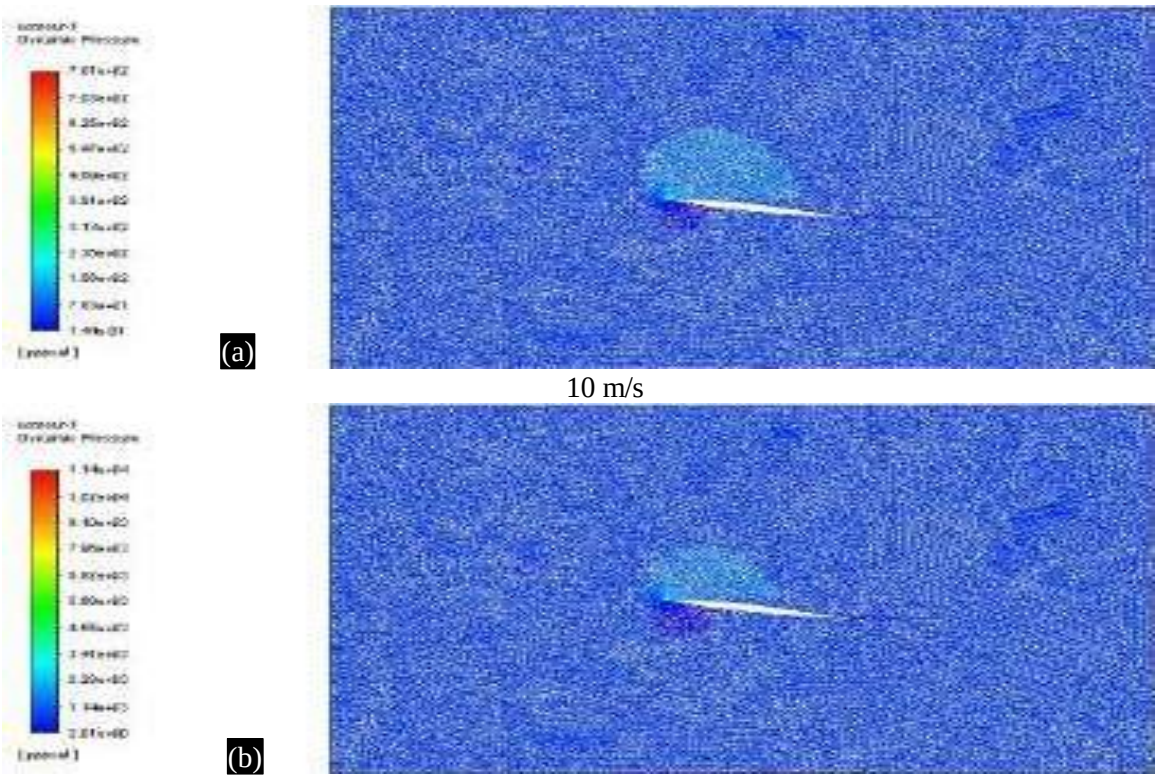

Figure 31. Pressure contour at 8° angle of attack.

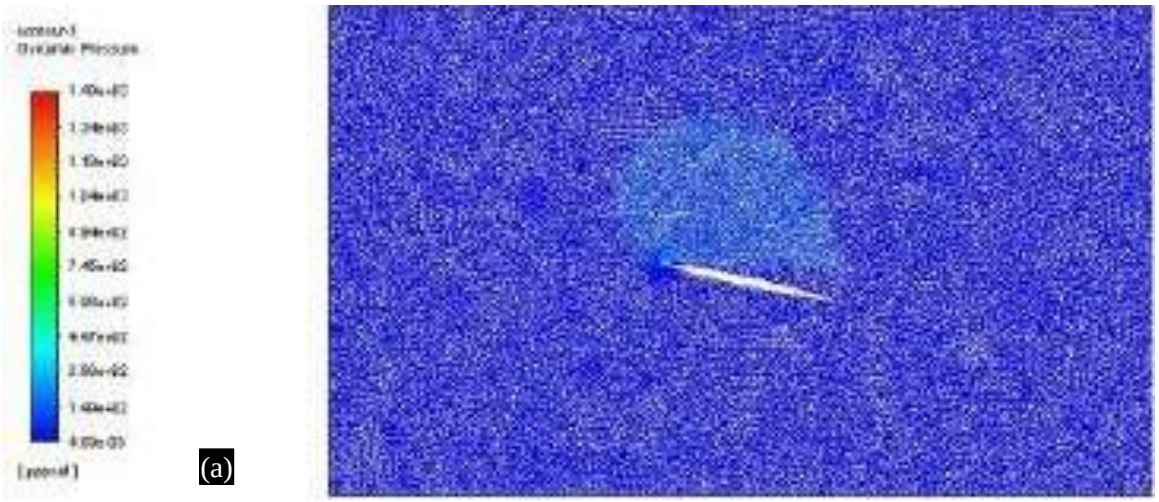

Figure 32. Pressure contour at 12° angle of attack

Figures 29 shows that the pressure distribution is high in the lower surface as well as in the upper surface. But as we raise the angle of attacks from 0° to 4°, 8° and 12° (figures 30-32), pressure distribution value is decreased and the pressure on the upper surface is somewhat higher than that of the lower surface.

Generation of high pressure on the upper surface obviously contradicts the behavior of a normal airfoil. But we can note that this high pressure on top has helped the 15% thickness remodified custard apple leaf to overcome stalling. This is a very crucial point to be noted. This is also proved by doing analysis for the same (Table 18).

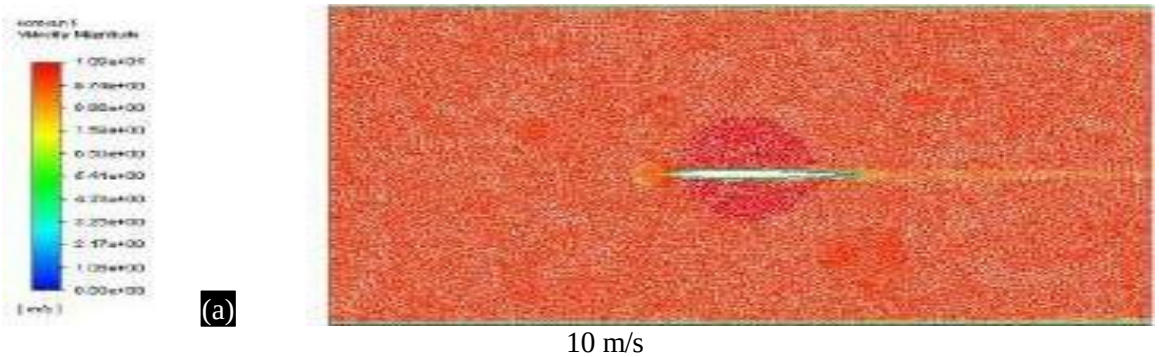

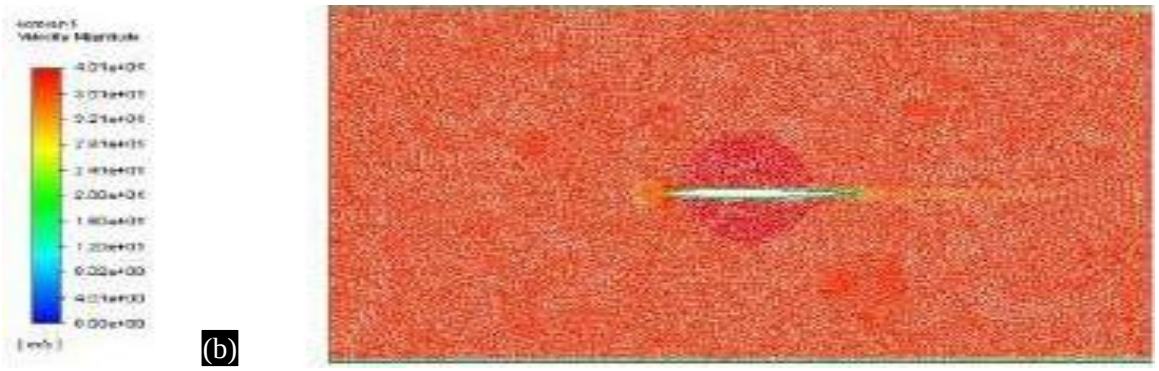

(b)

37 m/s

Figure 33. Velocity contour at 0° angle of attack.

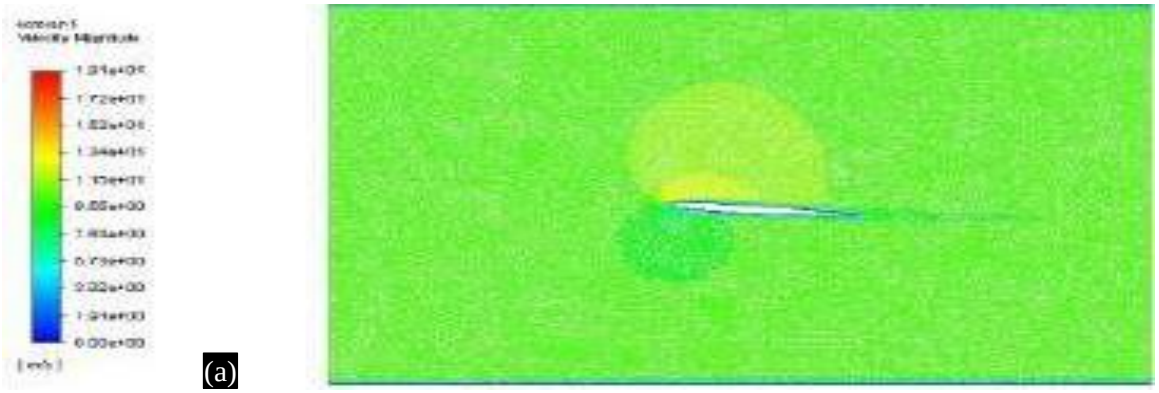

(a)

10 m/s

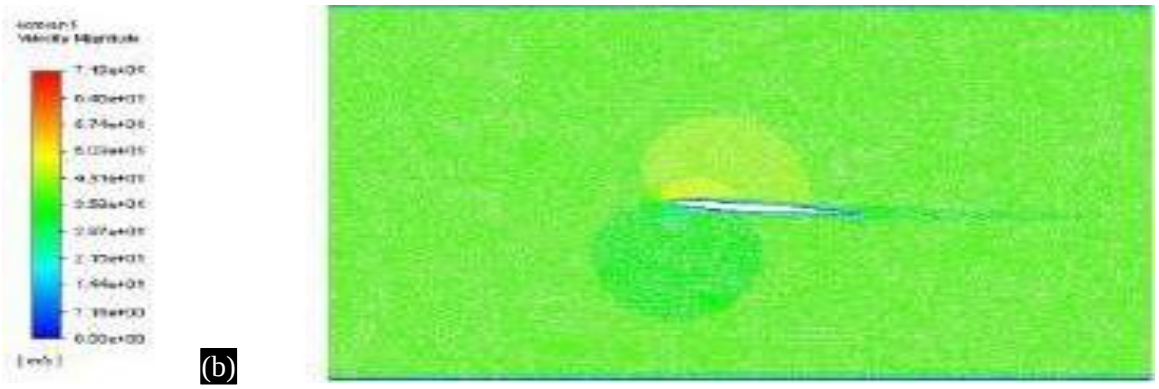

(b)

37 m/s

Figure 34. Velocity contour at 4° angle of attack.

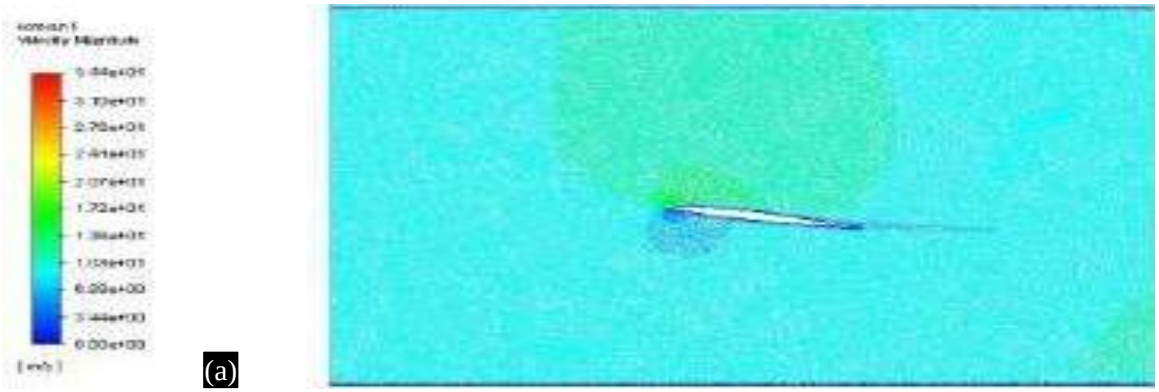

(a)

10 m/s

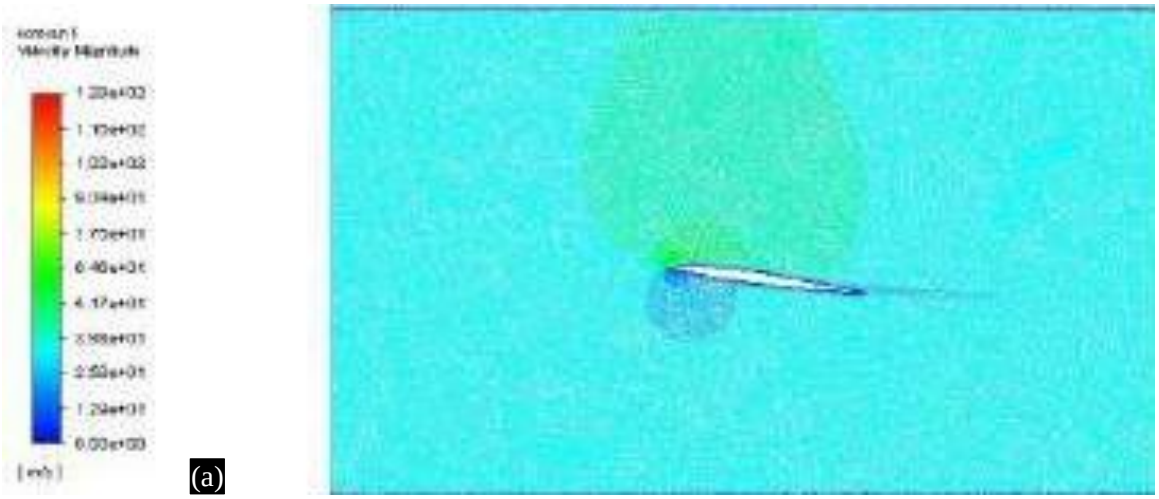

(a)

37 m/s

Figure 35. Velocity contour at 8° angle of attack.

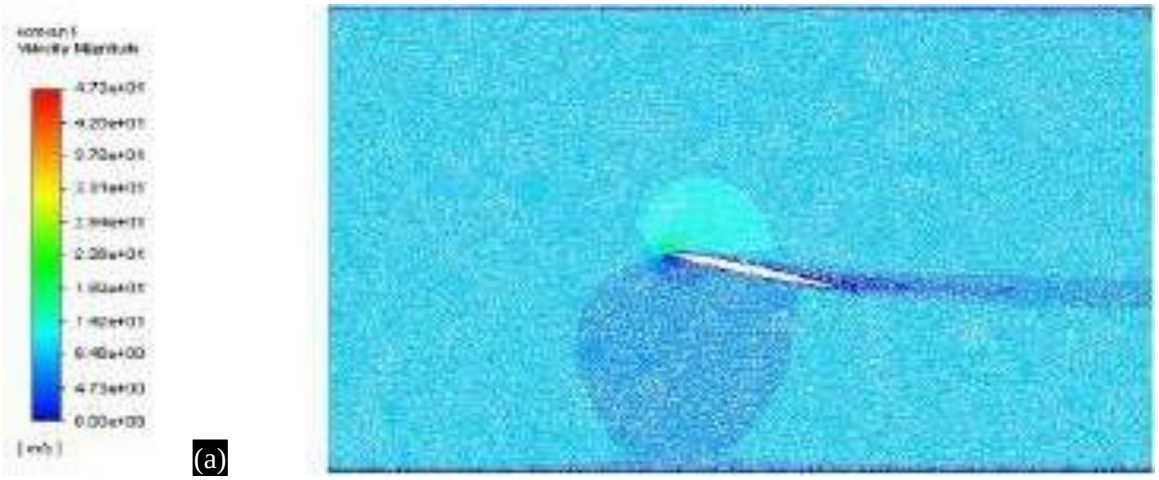

(a)

10 m/s

(b)

37 m/s

Figure 36. Velocity contour at 12° angle of attack.

Figure 33 shows that the velocity across the leaf (upper surface and lower surface) is equally very high. But as we increase the angle of attack (Figures 34-36), the velocity value is decreased around the leaf.

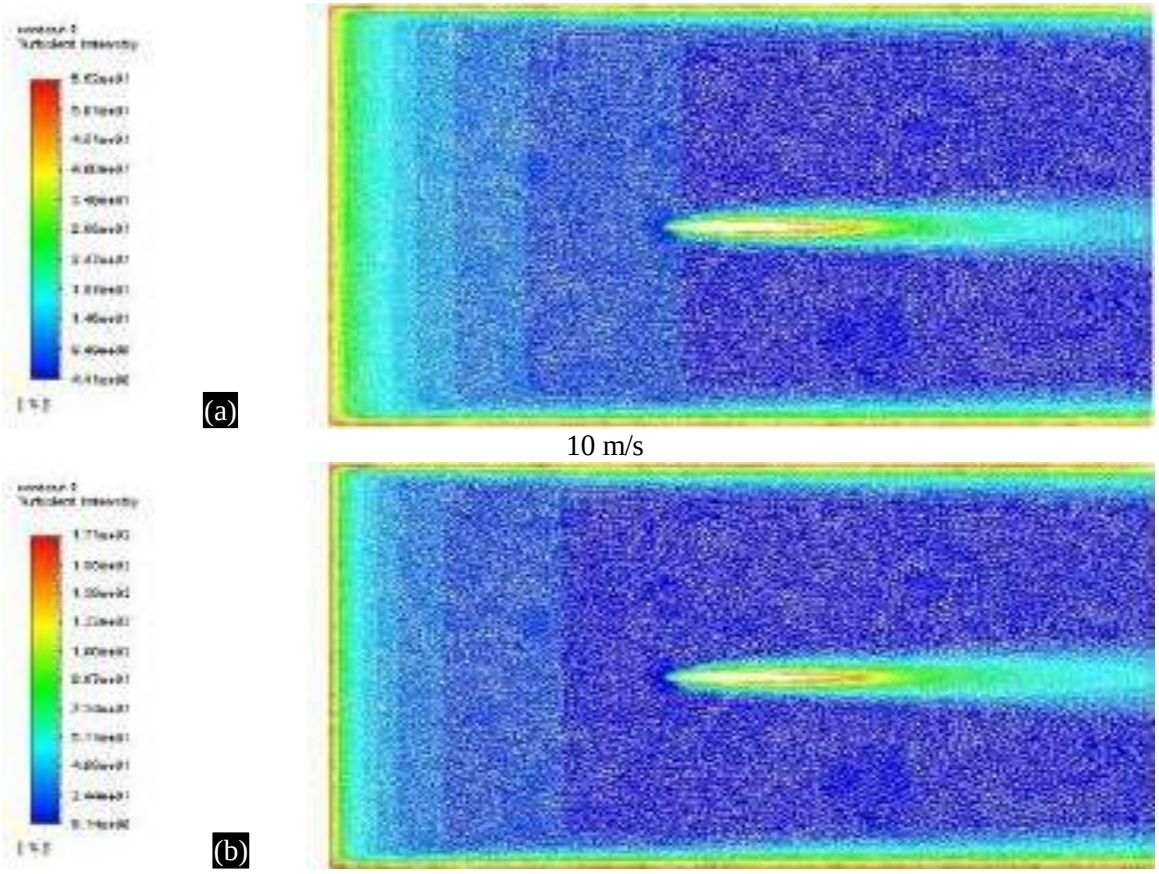

Figure 37. Turbulence contour at 0° angle of attack.

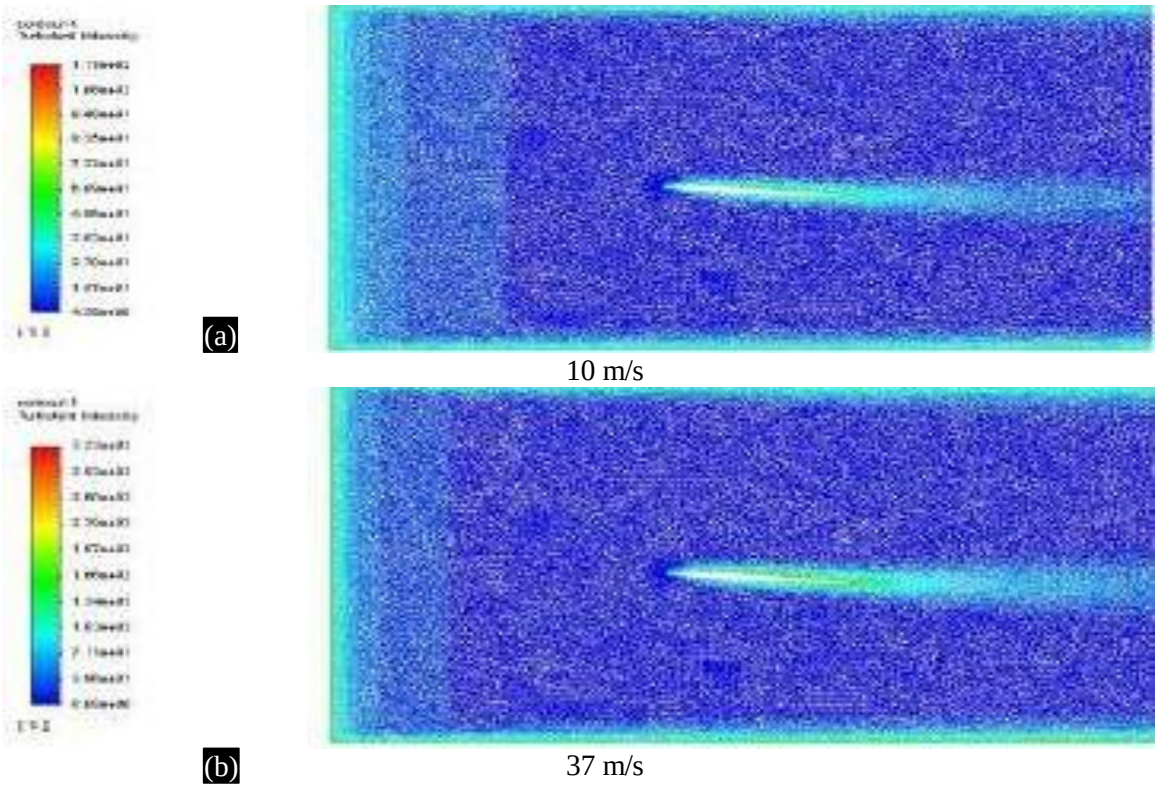

Figure 38. Turbulence contour at 4° angle of attack

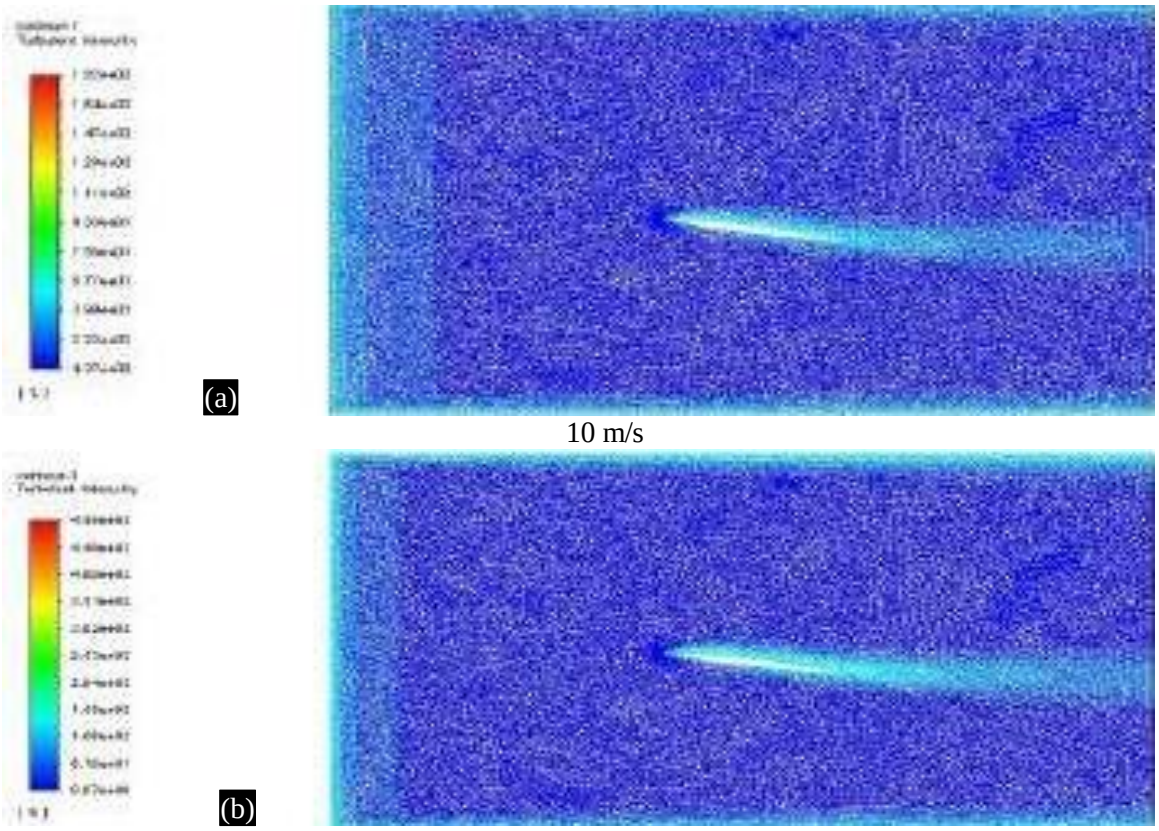

Figure 39. Turbulence contour at 8° angle of attack

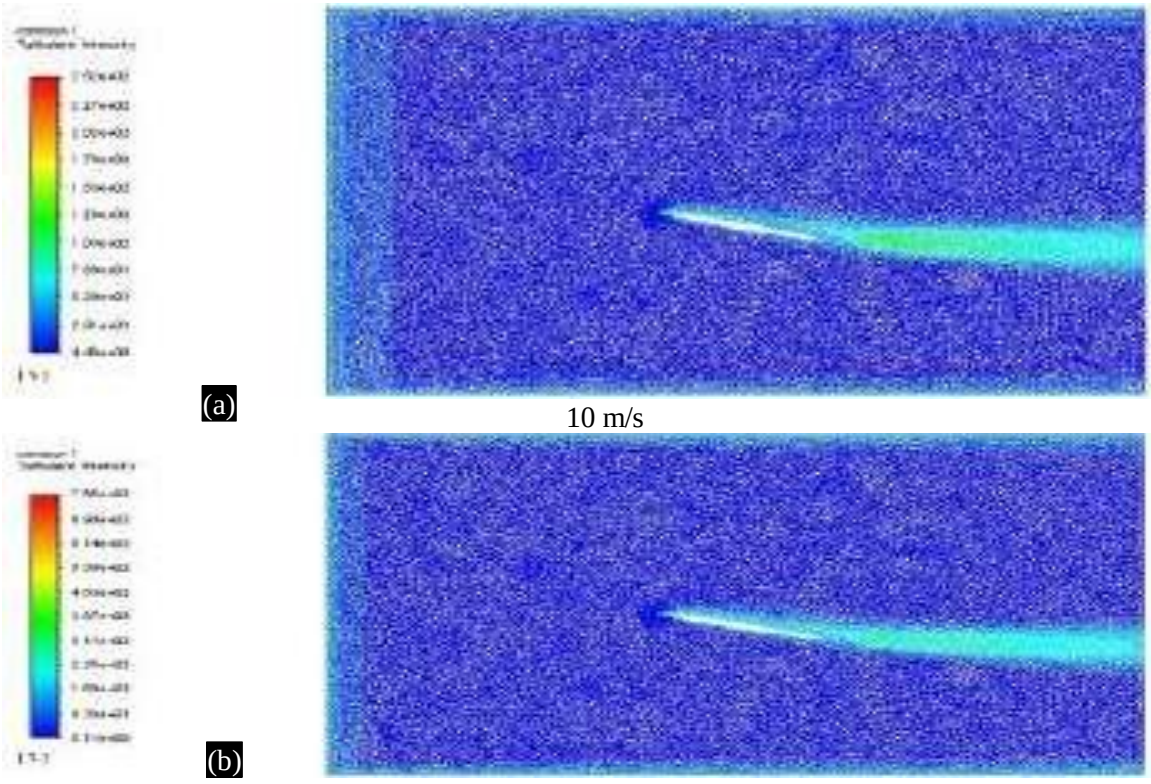

Figure 40. Turbulence contour at 12° angle of attack.

Figure 37 shows that the intensity of turbulence across the leaf (upper surface and lower surface) is equally very high. But as we increase the angle of attack (Figures 38-40), the turbulence value is decreased around the leaf and its value is higher in leading edge when compared to the trailing edge.

The changes in values of turbulence intensity may alter the flow pattern. The higher turbulence at the leading edge suggests changes in the boundary layer, the thin layer of air adjacent to the leaf surface.

By making few modifications on the upper and lower surface of this remodified custard apple leaf, we can alter the flow pattern without causing any changes in the boundary layer and thus reducing the flow disturbances.

CONCLUSION

In this study, we embarked on an extensive analysis of nine distinct leaf contours, namely Javaplum leaf, Sapota leaf, Custard apple leaf, Ixora live plant leaf, Mango leaf, Pumpkin ash leaf, Upas tree leaf, Curry leaf, and Adadhoda leaf. These leaves were subjected to rigorous scrutiny under various conditions, evaluating dynamic pressure, static pressure, turbulent intensity, and velocity at different angles of attack (0°, 4°, 8°, and 12°) using Ansys software with Carbon Fibre-reinforced Polymer as manufacturing material.

The primary objective of this initial phase was to compare and contrast the minimum and maximum values of these critical contours for each leaf, allowing us to calculate important aerodynamic parameters such as lift coefficient (C_l) and drag coefficient (C_d). As a result of this meticulous analysis, we were able to identify the top-performing leaves that consistently exhibited high C_l and C_d values under various conditions.

Following this rigorous selection process, the four leaves that demonstrated exceptional aerodynamic performance were singled out. These leaves were further scrutinized to assess only their C_l and C_d values. In doing so, we obtained definitive aerodynamic performance indicators that helped us pinpoint the leaves with the highest potential.

Subsequently, these four select leaves were integrated into specialized tool called the airfoil tool, where they were converted into airfoil profiles with a 15% thickness ratio based on a 100 mm chord length. Among these airfoil profiles, the custard apple leaf stood out by delivering remarkable lift performance and a superior lift-to-drag ratio.

From these findings, we can confidently conclude that the coordinates of the custard apple leaf represent a valuable foundation for the development of a high-performance airfoil. The NACA 23012 and the NACA 23015 airfoils has a maximum lift coefficient value of 0.3. Comparing these values with our remodified custard apple values, we can conclude that it produces enough lift. The Carbon Fibre-reinforced Polymer exhibits an excellent result with high strength to weight ratio, corrosion resistance and cost effective.

By further optimizing the leaf-inspired airfoils, we have the potential to create an exceptionally efficient and effective aerodynamic solution under complex fluid dynamic flow field. This study not only showcases the significance of biomimicry in airfoil design but also underscores the custard apple leaf's promising potential as a source of inspiration with less shear-thinning fluids leading to smoother and uniform pressure distribution around the foliage airfoil which leads to future advancements in aerodynamics and airfoil technology.

Funding

This research received no external funding.

REFERENCES

1. S. Kandwal and Dr. S. Singh, "Computational Fluid Dynamics Study of Fluid Flow and Aerodynamic Forces on an Airfoil", International Journal of Engineering and Technology (IJERT), ISSN2278-0181, Vol.1 Issue 7, September-2012.
2. Mehmet Numan Kaya, Ali Rıza Kök and Hüseyin Kurt, "Comparison of Aerodynamic Performances of Various Airfoils from Different Airfoil Families Using CFD", Necmettin erbakan University, Konya, Turkey, 2021.
3. Sundaram Rahulkumar, "Investigation of airfoil design and analysis", C.V Raman Global University, ISSN2321-9653, October 2022.
4. Karunakaran C.S, "Study of Flow Field over Fabricated Airfoil Models of NACA 23015 with its Kline-Fogleman Variant", ISSN 2277-3223 Vol 3, November 2013.
5. Shuji Otomo, Sabrina Henne, Karen Mulleners, Kiran Ramesh, Maria Viola, "An Unsteady Lift of a High Amplitude Airfoil", December 2020.
6. Mustafa Yilmaz, Hasan Koten, Erkan Cetikaya, Ziya Cosar, "A Comparative Analysis between NACA0012 and NACA4412", Marmara University, Istanbul, Turkey, December 2018.
7. Haixin Jiang, Dabo Xin, Hongfu Zhang, "Wind-tunnel study of the aerodynamic characteristics and mechanical response of the leaves of Betula platyphylla Sukaczev", Northeast Forestry University, 2021.
8. Burak Canakci, Ugur Cakir, Ayhan Aytac, "Determination of parameters affecting aerodynamics performance in S833 airfoil", November 2020.
9. F Rosa[1,2*], P Soetikno, IW Suweca[1] MA Meolyadi, "A new airfoil based on banana leaf midrib morphology for horizontal axis wind tunnel", IOP Conference Series Earth and Environmental Science, 2022 •iopscience.iop.org
10. Md. Shafiqul Islam[1], Md Alamgir Kabir[2], "A Review on Bio-inspired Airfoil Inspiration from Nature", International Journal of Science and Research (IJSR), ISSN 2319-7064, 2018.
11. Amit Kumar Saraf, Dr. Mahendra Pratap Singh, Dr. Tejsingh Chouhan, "A Review on Aerodynamic Behavior of Airfoil when Surface Modified", International Journal of Scientific & Engineering Research, Volume 7, Issue 3, 516 ISSN 2229-5518, March-2016.
12. Mr. Kaushik Devmurari[1] Mr. Tapan Barot[2] Prof. D. R. Shah[3], "A Review on Design and Aerodynamic Behavior of Airfoil", IJSRD - International Journal for Scientific Research & Development, Vol. 3, ISSN (online) 2321-0613, Issue 02, 2015.
13. Sanuja Jayatilake Branislav Titurus, "Nonlinear Aeroelastic Analysis of a Damped Elastic Airfoil System", University of Bristol, May 2022.
14. Wenbin Song & AndrewJ, "A Study of Shape Parameterization Methods of Airfoil Optimization", University of Southampton, high field,26 Jun 2012 https//doi.org/10.2514/6.2004-4482
15. T.C.Yap*, M.Z.Abdullah,Z.Husain, Z. Mohd Ripin, R. Ahmad, "The Effect of Turbulence Intensity on the Aerodynamic Performance of Airfoils",4th International Conference on Mechanical Engineering, December 26-28, 2001, Dhaka, Bangladesh/pp. IV 31-36,Section IV Fluid Mechanics 31
16. A.F.P. Ribeiro, A.M. Awruch, H.M. Gomes, "An Airfoil Optimization Technique for Wind Turbines",An airfoil optimization technique for wind turbines,December 2011, https//doi.org/10.1016/j.apm.2011.12.026
17. Slawomir Koziela and Leifur Leifssona, "Multi-level CFD-based Airfoil Shape Optimization with Automated Low-fidelity Model Selection", Engineering Optimization & Modeling Center, School of Science and Engineering, Reykjavik Uni., Menntavegur 1, 101 Reykjavik, Iceland,1 June 2013.https//doi.org/10.1016/j.procs.2013.05.254
18. Ankan Dash, "CFD Analysis of Wind Turbine Airfoil at Various Angles of Attack", IOSR Journal of Mechanical and Civil Engineering (IOSR-JMCE) e-ISSN 2278-1684, p-ISSN 2320-334X, Volume 13, Issue 4 Ver. II (Jul. - Aug. 2016), PP 18-24 www.iosrjournals.org
19. Mehmet Numan Kaya*1, Ali Rıza Kök1 and Hüseyin Kurt, "Comparison of Aerodynamic Performances of Various Airfoils from Different Airfoil Families Using CFD", 1Department of Mechanical Engineering, Necmettin Erbakan University, Konya, Turkey.

20. J. Morgado a,∗, R. Vizinho b, M.A.R. Silvestre a, J.C. Páscoa b, " XFOIL vs CFD Performance Predictions for High Lift Low Reynolds number Airfoils", Aerospace Science and Technology Volume 52, May 2016.
21. Stephane Moreau, Michel Roger, Vincent Jurdic, "Effect of Angle of Attack and Airfoil Shape on Turbulence-Interaction Noise", Stephane Moreau and Michel Roger**,** Session AA-26 Airfoil Noise, Published Online11 Nov 2012,https//doi.org/10.2514/6.2005-2973
22. W. Kyle Anderson¤ and Daryl L. Bonhaus, "Airfoil Design on Unstructured Grids for Turbulent Flows", Published Online17 May 2012, https//doi.org/10.2514/2.712
23. Muhao Chena, Jiacheng Liub, Robert E. Skelton, "Design and control of tensegrity morphing airfoils",31 January 2020,https//doi.org/10.1016/j.mechrescom.2020.103480
24. Jonathan M. Weaver-Rosen1 · Pedro B. C. Lea l2 · Darren J. Hartl2 · Richard J. Malak Jr, "Parametric optimization for morphing structures design application to morphing wings adapting to changing flight conditions", https//link.springer.com/journal/158
25. Tim Brek, Junk hook Kim, Phillips Joseph, "Mechanisms of Airfoil Noise near stall conditions", Phys. Rev. Fluids **4**, 123902 – Published 6 December 2019. https//openaccess.city.ac.uk/id/eprint/23398/1/
26. Vladimir Golube, "Recent Advances in Acoustics of Transitional Airfoils with Feedback-Loop Interactions A Review", Department of Aerospace Engineering, Embry-Riddle Aeronautical University, Daytona Beach, FL 32114, USA,25 January 2021**,** https//doi.org/10.3390/app11031057
27. Junkui CHENA, Zhijun WANGa, Juanting ZHANGb, Lianbo ZHANG, Guodong WU, "Numerical Simulation for Changes in Aerodynamic Characteristics along the Spanwise of "Diamond back" Wing" ,14 February 2015, https//doi.org/10.1016/j.proeng.2014.12.572
28. Rubel R. I. *1, Uddin M. K. 2, Islam M. Z. 3, Rokunuzzaman M, Comparison of Aerodynamics Characteristics of NACA 0015 and NACA 4415 Airfoil Blade", *Preprints* 2016, 2016100095. https//doi.org/10.20944/preprints201610.0095.v1
29. Mohamed Adel, "A Comparative Study for Different Shapes of Airfoils", Vol. 69 No. 1 Journal of Advance Research in Fluid Mechanics and Thermal Sciences, May (2020).
30. MR Ahmed T Takasaki, "Aerodynamics of a NACA4412 Airfoil in Ground Effect", Published Online2 May 2012, https//doi.org/10.2514/1.23872
31. Slawomir Koziela and Leifur Leifsson, "Multi-level CFD-based Airfoil Shape Optimization with Automated Low-fidelity Model Selection",Volume18, 2013, https//doi.org/10.1016/j.procs.2013.05.254
32. Karunakaran C.S," Study of Flow Field over Fabricated Airfoil Models of NACA 23015 with its Kline-fogleman Variant". Retrieved April 4, 2024, from https://www.ripublication.com/aasa/aasav3n2spl_11.pdf

